MECHANIK

RESEARCH REPORT

Some Contributions to the Homogenization of Macroscopically Isotropic Composites

Victor Salit

TECHNISCHE UNIVERSITÄT DARMSTADT

Volume 23

Some Contributions to the Homogenization of Macroscopically Isotropic Composites

Am Fachbereich Bauingenieurwesen und Geodäsie
der Technischen Universität Darmstadt
zur Erlangung des akademischen Grades eines
Doktor–Ingenieurs
(Dr.–Ing.)

genehmigte Dissertation
von

Victor Salit, M. Sc.
aus Ust'-Kamchatsk, Russland

Hauptreferent:	Prof. Dr.–Ing. habil. F. Gruttmann
Korreferent:	Prof. Dr.–Ing. habil. D. Gross
Tag der Einreichung:	04.05.2011
Tag der mündlichen Prüfung:	07.07.2011

Darmstadt
D17

Salit, Victor
Some Contributions to the Homogenization of Macroscopically Isotropic Composites
Forschungsbericht Mechanik, Technische Universität Darmstadt
Band 23

Herausgeber:
Studienbereich Mechanik
Technische Universität Darmstadt
Hochschulstraße 1
64289 Darmstadt
Germany

URN: urn:nbn:de:tuda-tuprints-26704
URL: http://tuprints.ulb.tu-darmstadt.de/2670/

ISBN 978-3-935868-23-5

Acknowledgements

This Doctor thesis is a result of my research activities at the chair of Solid Mechanics at the Technische Universität Darmstadt. It would however never be possible without the help and support of the professors, staff, colleagues, friends and my family.

In particular, I would like to express my endless gratitude to Professor Dr.-Ing. Dietmar Gross for his guidance, patience, trust and encouragement.

On the same note my gratitude is extended to Professor Dr.-Ing. Friedrich Gruttmann for his guidance and support, especially in the last phase of the research.

I also owe many thanks to Professor Dr.-Ing. Ralf Müller and Dr.-Ing. Jens Wackerfuß, who have always had the time to answer my questions and provide valuable suggestions.

I am grateful to Professor Dr. Jürgen Rödel for giving me a free access to his laboratory and allowing me not only to watch, but also to learn hands on, some of the processing steps in the preparation of the ceramic-metal composites.

I thank also Dr. Ludwig Weiler and Ms. Jami Winzer for guiding me in the laboratory and sharing their experimental results for the use in this work.

I am thankful to Dr. Geier from the Austrian Foundry Research Institute, Leoben, Austria, for providing the X-Ray tomography data of the composite samples and explaining the nature of the noise and scan anomalies.

I am indebted to our secretary, Ms. Angelika Priessnigg who has made many impossible things possible.

Many thanks go to my colleagues and friends for their support and great atmosphere inside and outside the institute.

Special thanks I extend to my family and parents.

Contents

Zusammenfassung

Eine der Techniken im Überlebensmechanismus in der Natur basiert auf Homogenisierung. Betrachtet man zwei Elemente bzw. Lebewesen einer Spezies, so sind diese (natürlich) nicht zu 100% identisch, weisen aber dennoch ähnliche makroskopische Eigenschaften auf. Man denke etwa an verschiedene Krabben der gleichen Art, die alle hohen Wasserdrücken standhalten können, obwohl in ihren Exoskeletten eine Vielzahl lokaler Unterschiede zu finden sind. Die Auswirkungen solcher lokaler Abweichungen und Defekte werden durch die Homogenisierung ausgeglichen.
Die Entwicklung von analytischen und numerischen Homogenisierungsmethoden ist eine hoch anspruchsvolle Aufgabe. Mathematisch gesehen ist die Homogenisierung eine Mittelung, die mittels integraler Gleichungen für denselben Effekt sorgt. Als Beispiel seien die Materialien Kupfer und Aluminium betrachtet, deren Kompressionsmoduln sich um etwa 80% unterscheiden. Die Kompressionsmoduln von Verbundwerkstoffen, die aus diesen beiden Materialien bei gleichem Volumenanteil bestehen, unterscheiden sich dagegen um höchstens 9% voneinander.
Bei Homogenisierungsüberlegungen ist zu beachten, dass in der Natur lediglich physikalische Defekte und Abweichungen vorliegen können, wohingegen in der mathematischen Betrachtung ein Defekt auch in Form von einer nichtzutreffenden Annahme oder nicht geeigneten Randbedingungen, oder auch in einem Fehler im Programmcode vorliegen kann. Sollten sich die Ergebnisse trotz derartiger Fehler innerhalb der theoretisch zulässigen Schranken (Voigt-Reuss) befinden, gibt es kein Mittel, um einen solchen Fehler zu ermitteln.
Die Homogenisierung ist daher nicht nur wegen der mathematischen Komplexität eine anspruchsvolle Aufgabe, sondern auch aufgrund der Tatsache, dass keine zuverlässige Methode existiert, die es erlaubt, die Modelle und ihre Ergebnisse zu validieren und zu verifizieren.
Im Kapitel 3 dieser Arbeit werden zunächst einige Grundlagen der Homogenisierungstheorie erläutert. Anschließend werden einige neue Erkenntnisse vorgestellt und diskutiert. Ein wichtiges Beispiel einer nichtzutreffenden Annahme ist das sogenannte Hill-Postulat (auch Hill-Bedingung), auf dem die moderne Homogenisierungstheorie basiert. Dieses Postulat setzt eine energetische Gleichheit zwischen der Mikro- und der Makroebene voraus.

Äquivalent zu dieser Bedingung ist die Aussage, dass keine Arbeit durch die Fluktuation der Spannungs- und Verzerrungsfelder geleistet wird bzw. verloren geht. Dies wird auch in der numerischen Betrachtung berücksichtigt, indem Randbedingungen (für die Homogenisierungsaufgabe) nur dann zugelassen werden, wenn sie die Hill-Bedingung erfüllen.

In der vorliegenden Arbeit wird gezeigt, dass die Hill-Bedingung dem Prinzip der minimalen potentiellen Energie widerspricht. Die bisher vernachlässigte Arbeit der Fluktuationen, entspricht einem Energieverlust und führt direkt zu einer so genannten strukturellen (materiellen) Dämpfung, die von der Dehnungsgeschwindigkeit unabhängig ist. Die Elastizitätskonstanten haben damit komplexe Werte, wobei der imaginäre Anteil als Verlustmodul bezeichnet wird. Damit erstellt man eine theoretische Brücke zwischen dem Werkstoffaufbau und der bisher fast 100 Jahre lang als reine mathematische Bequemlichkeit verwendeten komplexen Steifigkeiten, die bisher lediglich als mathematisch zweckmäßige Größen eingeführt und benutzt wurden.

Schließlich werden im Kapitel 4 einige numerische Beispiele für die zuvor vorgestellten Modelle und Methoden angegeben. Bei der numerischen Homogenisierung stellt die Abhängigkeit der Ergebnisse von der Modellgröße und den Randbedingungen das größte Zuverlässigkeitsproblem dar.

Ein im Jahr 1993 entwickeltes iteratives “Embedded Cell” -Verfahren, dass gemäss den Autoren diese Abhängigkeit löst, wird in dieser Arbeit erstmals analytisch geprüft. Dabei wird einerseits nachgewiesen, dass das Verfahren stets konvergiert, andererseits wird aufgezeigt, dass das Endergebnis im Allgemeinen einen nicht verschwindenen Fehler besitzt. Da dieser Fehler beschränkt ist, kann man das Verfahren als zuverlässig bezeichnen und mit einer gewissen Sicherheit verwenden.

Chapter 1

Introduction

In the nature there are probably not many materials that are not heterogeneous at least on one scale level. Here we refer to the term homogeneity in its broader sense, which includes the isotropy. In this setting, the isotropy is a directional homogeneity, to distinguish it from the spatial one. Thus, even a fully homogeneous (both spatially and directionally) metallic or ceramic sample is a microscopically heterogeneous mixture of single crystals. At least some of the macroscopic properties of this sample differ from those of its constituents - the single crystals.
This difference is even more pronounced in the composite materials, both the natural ones and the man-made. Natural composites are usually much more advanced than man-made, with different functional domains and several hierarchical levels. Typical examples are the bone, the teeth and, probably the most common structural composite in the nature, the exoskeleton of the crustaceans (crabs, lobsters, crayfish, shrimps, etc.) [1].
Typical man-made composites consist of small pieces of some stiff material, called the reinforcement, dispersed in and held together by some binding material, called the matrix. A good example of such material is the carbon fiber composite, Figure 1.1. There are also the composites in which the constituent phases form three-dimensional interpenetrating networks, like in the example depicted in Figure 1.2. In these composites, one can not categorize the phases into matrix and reinforcement (unless one or more constituents is a composite itself).

Interpenetrating composites are growing in popularity due to the greater flexibility in the choice of the constituents. The reason is the geometrical interlocking of the three-dimensional networks leading to an improved residual strength even in the case of complete interface debonding. This allows the use of such combinations as copper and graphite or copper and alumina, composites, which in both cases have inherently weak interfaces but a good combination of wear resistance and electrical conductivity.
One common feature of all the composites is that the macroscopic properties describe the

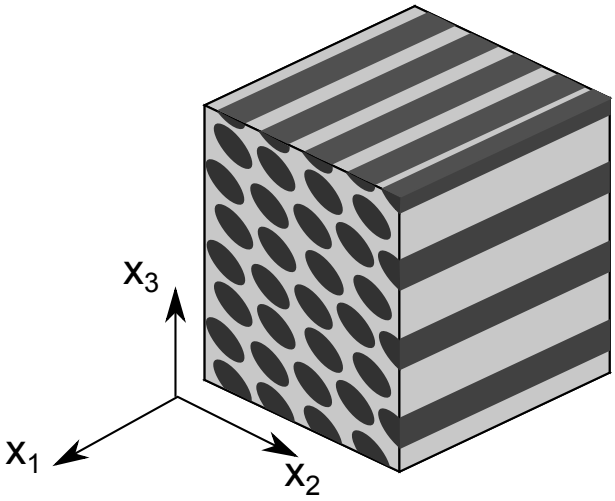

Figure 1.1: A model of a unidirectional fiber reinforced composite

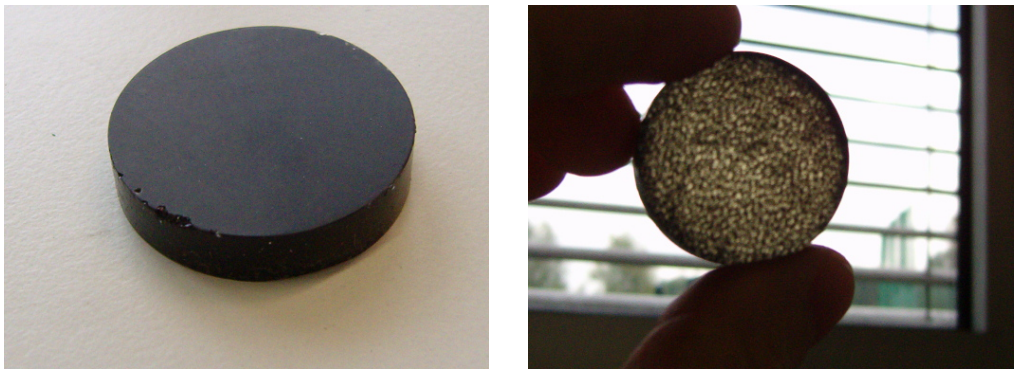

(a) The sample **(b)** with light background

Figure 1.2: A disk shaped sample with two interpenetrating phases: a polyurethane foam (the dark phase in (b)) filled with an epoxy resin (the clear phase in (b))

group response as opposed to that of a single component. As such, the macroscopic properties are less sensitive to the single local defects like the presence of a few pores, broken fibers or fibers misalignment. The resulting local variations are "averaged out". One can look at this as one of the survival mechanisms of the nature - given the almost vanishing probability to produce two exact copies, their properties must still be very similar for survival under the same conditions.

1.1 Current state of the research

The first attempts to relate the material's properties to its constitution were made already at the middle of 19^{th} century. Matthiessen [2], who measured electric properties of various

materials, noticed that the electric conductivity of some alloys at some concentrations follows a simple rule of mixtures (a volumetric average). It shall be noted, however, that this empiric result, stems from the low contrast between the properties of the tested materials. Some 15 years after the Matthiessen's experiments, Maxwell [3] includes a whole chapter devoted to the conduction through a heterogeneous media in his famous "Treatise on Electricity and Magnetism". There, he derives a model of dilute distribution of identical spherical particles inside a sphere of another material.
Other models were based on a simplified geometric representation of the polycrystal matter, like the chessboard pattern of Guertler, where the different crystals or phases are arranged as shown in Figure 1.3, for more details cf. [4, 5]. Guertler came to a conclusion

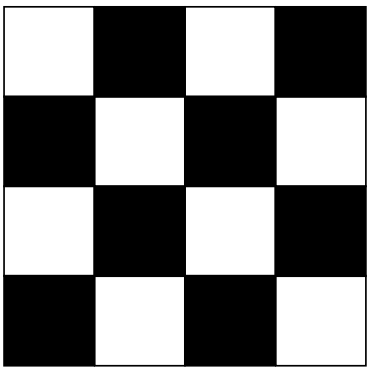

Figure 1.3: A chessboard model of the phases distribution

that simple mixture rules actually bound the effective properties. His model however does not allow any connectedness of the phases, which is not a very plausible assumption. Consequently, a very popular model proved to be the three-dimensional cross, Figure 1.4, explicitly drawn in Frey's work, [5], and implicitly considered in that of Lichtenecker, [6], which was the first model for composites with interpenetrating phases. This geometry was then adopted by Tuchinskii [7, 8] for the assessment of elastic and thermal constants of such composites and recently rediscovered at least two more times, [9] and [10].

The homogenization of elastic constants is based nowadays mainly on the following fundamental results and assumptions — the Voigt [11] and Reuss [12] mixing rules, which provide the absolute theoretical bounds for the effective stiffness tensor, the Hill micro-macro energy equivalence postulate [13], the variational principle of Hashin and Shtrikman, used to derive the bounds for the macroscopically isotropic composites [14, 15] and the Eshelby finding about the stress and strain inside an ellipsoidal inclusion/heterogeneity [16].
It is difficult to overestimate the importance of the Eshelby result, since the ellipsoidal shape covers a wide range of heterogeneities, from thin platelets to long fibers, and defects, from penny-shaped cracks to pores and channels. A range of models like the Dilute Distribution model (DD), the self-consistent model [17] and the Mori-Tanaka model [18] have their origin in Eshelby's result.

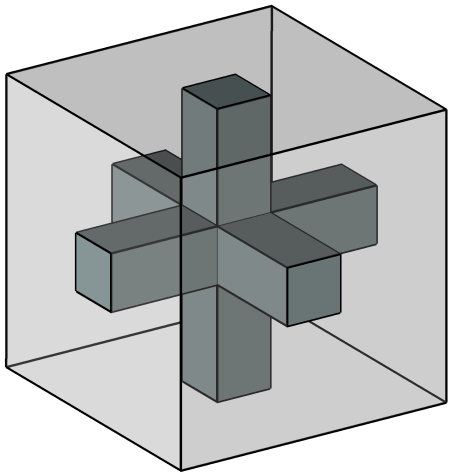

Figure 1.4: A three dimensional cross model with one of the phases made transparent

The DD model assumes no interaction between the embedded particles, in which case every particle is treated as if it was embedded in an infinite medium. The self-consistent method is similar to DD, but the medium is assumed to be the unknown homogenized one.

It is worth noting Bruggeman's work [19–21], who did not focus on one specific property, but rather systematically treated all possible material constants. Applying basically Maxwell's approach, i.e solution of fields inside and outside a single inhomogeneity, he was able to derive some interesting results applicable not only to dilute distribution, but also to non-dilute concentrations. His solution for bulk modulus for example can be transformed to that of Mori-Tanaka or the Hill self-consistent one just by changing indices of the constituents' constants. Unfortunately his expression for shear modulus is wrong due to an erroneous assumption regarding the displacement field.

Using the variational principle together with the statistical correlation functions for particular geometries of the embedded particles, higher-order bounds have been developed, [22–26]. These bounds, featuring two statistical parameters, are sharper then the Hashin-Shtrikman ones, [14, 15]. It is though not clear yet what exactly these parameters represent.

It is remarkable that all the bounds (Hashin-Shtrikman and higher-order) can be cast into an identical form $F^{U,L} = f(F_1, v_1, F_2, v_2, y^{U,L})$. Here F_i are some known constants of the constituent materials, v_i are their volume fractions and y is a function of the statistical parameters. Gibiansky [26] extracts the y parameter as an unknown function, i.e $y = Y(F_1, v_1, F_2, v_2, F^{U,L})$ and seeks bounds on it. Gibiansky claims that this 'Y'-transformation leads to simplified expressions.

There are two problems with this approach. The first one - no new information is ob-

tained by reforming an expression. The same way one could extract the volume fraction of one of the phases as an unknown and seek bounds on it. The second problem is that one immediately looses the intuitive link to the physics of the homogenization task. As a result, one needs to solve an optimization! problem to obtain some incomprehensible, badly twisted two-dimensional projection of boundary lines of otherwise very simple surfaces. A simple 3D plot of non-reformed expressions delivers much more information in a very comprehensible way.

At least until a complete solution of the homogenization problem will be derived, the analytical homogenization has its obvious limitations. For this reason the numerical homogenization is a very popular supplement. Essentially, numerical homogenization is a solution of simple boundary value problems with an objective of obtaining the effective response of the analyzed model. This allows a treatment of both the synthetic microstructures, like some random distribution of particles in a matrix, or idealized periodic unit cells, and the real ones, obtained by any three-dimensional imaging technique.

The main advantages of the numerical homogenization are the ability to treat various explicit geometries and, the automatic satisfaction of the continuity conditions at the material interfaces, namely the displacement continuity and the forces equilibrium. Whereas the main disadvantages are size and boundary-conditions dependence of the final results. This dependence stems from the fact that in most cases the treated geometries are smaller than the representative volume element (RVE), the size of which is not known a priori. Moreover, in some cases, even if the size of an RVE is known, it is prohibitively large. For more detailed discussion of the size effects, one is referred to the excellent introductory book of Zohdi & Wriggers [27], whereas the subject of boundary conditions effects was extensively studied by Huet [28] and Hazanov [29].

The numerical homogenization is a very broad field one with many different models and approaches. There are, however, two approaches that seem to be very interesting. The first one is the 'embedded cell method', developed by Dietrich et al [30], which is an iterative method that was described as providing results, which are independent of the already mentioned size and boundary conditions effects. An analytical proof of these properties, which is lacking in the original publication, is attempted in chapter 4 of the current work.

The second approach is the so-called FE^2, where one treats each Gauss point at the element level as being an RVE, which must be homogenized at each load increment. For details about this approach see [31]. Some 10-15 years ago this approach was very non-practical, however with recent advances in the parallel computing, it becomes a feasible approach not only for special clusters, but also for a common (though high-end) PC.

In some not so distant future, FE^2 will probably be one of the dominant techniques due to its inherent ability to explicitly incorporate for example the microstructural damage development, while macroscopically considering a complete structural or mechanical

detail.

1.2 Objectives and outline

Thinking of the homogenization task as of a puzzle with many missing pieces, the main objective of the current work is to bring together some pieces that were found till now and perhaps find new ones.
The thesis is structured in five chapters.
Chapter 2 is an abbreviated introduction of the continuum mechanics, necessary for the next chapters.
Chapter 3 is devoted to the analytical homogenization principles of the linear elasticity. Main concepts are explained and some are corrected. The Hill postulate is shown to contradict the minimum potential energy principle. A few new expressions are derived and explained. It is shown that the effective stiffness tensor of any heterogeneous mixture is a complex quantity with the imaginary part being the loss modulus, directly corresponding to the energy dissipation at the material interfaces.
Chapter 4 is devoted to the numerical homogenization methods. Main model types and homogenization strategies are explained and compared either with analytic results or with experimental data. An attempt is made at analytical proof of the 'embedded cell method' convergence. The slight disagreement between the proposed analytical proof and the numerical results is investigated and an explanation is proposed.
Chapter 5 gives a short summary.

1.3 Notation

An attempt has been made to use a consistent set of symbols and definitions throughout the whole text. In cases where this was not possible, a notation for the particular chapter has been additionally introduced.
In general, non-bold slanted Roman and Greek characters denote scalar quantities, vectors are denoted with an arrow, as in $\vec{n}$, tensors of rank 2 are denoted with bold Roman and Greek characters, whereas tensors of rank 4 with double-stroke Romans.

Symbols

For any quantity χ,

χ_0	initial value
χ^T	transpose
χ^{-1}	inverse
$\dot{\chi}$	time derivative
$\chi_{,i}$	spatial derivative with respect to x_i
$\det \chi$	determinant
$\operatorname{div} \chi$	divergence operator
$\langle \chi \rangle$	volumetric average

$\psi(\chi)$	a mapping, transformation
Ω	physical domain
$\partial\Omega$	domain boundary

Scalars

d	dissipation tensor in isotropic case
$\mathrm{d}V, \mathrm{d}v$	small volume element
G	shear modulus
J	Jacobian
K	bulk modulus
m	mass
p	pressure
Q	heat flux
W	work
X_i, x_i	cartesian coordinates of a point
t	time
U	strain energy density
$\tilde{U}$	complementary energy density

α	volumetric component of the isotropic Eshelby tensor
β	deviatoric component of the isotropic Eshelby tensor
δ_{ij}	Kronecker delta

ζ, η	3-point correlation functions
λ, μ	Lamé constants
ν	Poisson ratio
ρ	density
Π^{kin}	kinetic energy
Π^{int}	internal energy
V	total volume
V_i	i-th phase volume
v_i	i-th phase volume fraction

Vectors

$\vec{\mathrm{b}}$	body force
$\mathrm{d}\vec{\mathrm{a}}$	small area element
$\mathrm{d}\vec{\mathrm{f}}$	force vector
$\mathrm{d}\vec{\mathrm{X}}, \mathrm{d}\vec{\mathrm{x}}$	small line element
$\vec{\mathrm{n}}$	normal vector
$\vec{\mathrm{t}}$	stress vector
$\vec{\mathrm{u}}$	displacement vector
$\vec{\mathrm{X}}, \vec{\mathrm{x}}$	location vector

2^{nd} rank tensors

$\mathbf{A}$	Almansi strain tensor
$\mathbf{B}$	Left Cauchy-Green deformation tensor
$\mathbf{C}$	Right Cauchy-Green deformation tensor
$\boldsymbol{e}$	strain deviator
$\boldsymbol{\mathcal{E}}$	Green-Lagrange strain tensor
$\mathbf{F}$	deformation gradient
$\mathbf{H}$	displacement gradient
$\mathbf{I}$	second rank unit tensor
$\mathbf{P}$	nominal stress
$\mathbf{P}^T$	first Piola-Kirchhoff stress tensor
$\mathbf{P}^{sym}$	second Piola-Kirchhoff stress tensor
$\mathbf{R}$	rotation tensor
$\mathbf{U}$	right stretch tensor

$\mathbf{V}$ left stretch tensor

$\boldsymbol{\varepsilon}$ small strain tensor
$\boldsymbol{\varepsilon}^*$ eigenstrain
$\boldsymbol{\sigma}$ Cauchy stress tensor
$\boldsymbol{\tau}$ stress deviator

4^{th} rank tensors

$\mathbb{A}$ strain influence tensor
$\mathbb{B}$ stress influence tensor
$\mathbb{C}$ stiffness tensor
$[\mathbb{C}]$ stiffness tensor in matrix (Voigt) notation
$\mathbb{D}$ dissipation tensor
$\mathbb{I}$ fourth rank unit tensor
$\mathbb{S}$ compliance tensor
$[\mathbb{S}]$ compliance tensor in matrix (Voigt) notation
$\mathbb{E}$ Eshelby tensor

Chapter 2

Basic equations of Continuum Mechanics

The assessment, or prediction of the effective properties of a heterogeneous mixture is called "homogenization". However a discussion of the subject is impossible without the use of some definitions and concepts of the continuum mechanics. For this reason we start with a rather abbreviated restatement of the fundamentals of the continuum mechanics, directly applicable to this work. Reader, interested in a more complete treatment of the subject, is encouraged to consult textbooks like Fung's "A First Course In Continuum Mechanics" [32].

2.1 Kinematics of a deformable body

The motion, consisting of both the rigid body motion and the deformation (alteration of form or shape [33]), is probably the only observable phenomena when a deformable body is subjected to any possible loading. In (quasi)static problems we are mostly interested in the latter one. To draw any useful conclusion about the state of the analyzed body one must be able to quantify the deformation.

2.1.1 Deformation gradient

For that purpose we choose a convenient coordinate system (CS) and track the motion of the body in this CS through time. The state of the body at time $t = t_0$ is called the *initial configuration*. The snapshot at time $t = t^*$ is the *current configuration* and the body in its undeformed state is called the *reference configuration*. Sometimes the undeformed is also the initial one. Obviously, every particle of the body can be described

by its coordinates in the chosen CS. Let the material point P in the reference configuration have the coordinates (Cartesian CS)

$$\vec{\mathrm{X}} = [X_1, X_2, X_3]^T \tag{2.1}$$

and in the current configuration the coordinates

$$\vec{\mathrm{x}} = [x_1, x_2, x_3]^T \tag{2.2}$$

Let also the motion of the body be described by a continuous and single-valued function $\varphi(\mathbf{X}, t)$, which gives the locations of the material points as a function of their initial locations and the time, see Figure 2.1

$$\vec{\mathrm{x}} = \varphi(\vec{\mathrm{X}}, t) + c(t) \tag{2.3}$$

where the $c(t)$ is the rigid body translation and $\varphi(\vec{\mathrm{X}}, t)$ incorporates both the rigid body rotation and the deformation as defined in [33]. To avoid a possible discrepancy with the literature we'll refer to the $\varphi(\vec{\mathrm{X}}, t)$ as the *deformation*. In the absence of the rigid

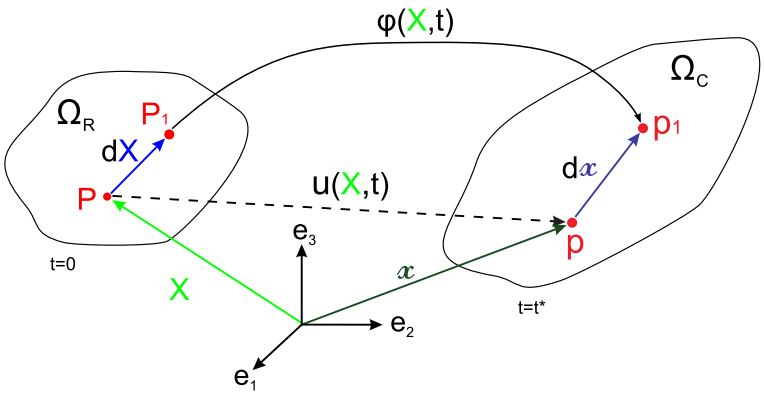

Figure 2.1: The reference and current configurations in the Cartesian CS

body translation, the difference between the current location and the initial one is the displacement $\vec{\mathrm{u}}(\vec{\mathrm{X}}, t)$

$$\vec{\mathrm{u}}(\vec{\mathrm{X}}, t) = \vec{\mathrm{x}} - \vec{\mathrm{X}} = \varphi(\vec{\mathrm{X}}, t) - \vec{\mathrm{X}} \tag{2.4}$$

Let's now consider the relative displacements of two non-coincident, three non-collinear and four non-coplanar, but closely spaced points at a time, Figure 2.2. Let denote the first point as $\vec{\mathrm{X}_0}$ in the reference configuration and $\vec{\mathrm{x}_0}$ in the current. Using the Taylor's

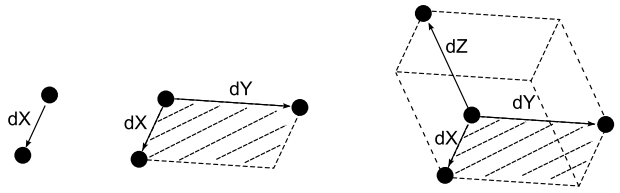

Figure 2.2: Two, three and four points defining vector, area and volume correspondingly

series, any other closely spaced point is given by

$$\vec{x} = \vec{x_0} + \left.\frac{\partial \varphi(\vec{X}, t)}{\partial \vec{X}}\right|_{\vec{X_0}} [\vec{X} - \vec{X_0}] + ... \tag{2.5}$$

Neglecting higher-order terms we get

$$\mathrm{d}\vec{x} = \mathbf{F}\mathrm{d}\vec{X} \tag{2.6}$$

where $\mathrm{d}\vec{x} = \vec{x} - \vec{x_0}$, $\mathrm{d}\vec{X} = \vec{X} - \vec{X_0}$ and

$$\mathbf{F} \triangleq \frac{\partial \varphi(\vec{X}, t)}{\partial \vec{X}} \tag{2.7}$$

is the 'deformation gradient'. Thus, the deformation gradient $\mathbf{F}$ transforms the infinitesimal line element $\mathrm{d}\vec{X}$ from the reference configuration into its image in the current configuration. Three non-coinciding points define two vectors $\mathrm{d}\vec{X}$ and $\mathrm{d}\vec{Y}$ with corresponding area $\mathrm{d}\vec{A} = \mathrm{d}\vec{X} \times \mathrm{d}\vec{Y}$ in the reference configuration and $\mathrm{d}\vec{x}$, $\mathrm{d}\vec{y}$ and $\mathrm{d}\vec{a} = \mathrm{d}\vec{x} \times \mathrm{d}\vec{y}$ in the current one. Whereas four non-coinciding points define three vectors $\mathrm{d}\vec{X}$, $\mathrm{d}\vec{Y}$ and $\mathrm{d}\vec{Z}$ with corresponding volume $\mathrm{d}V = \left(\mathrm{d}\vec{X} \times \mathrm{d}\vec{Y}\right) \cdot \mathrm{d}\vec{Z}$ in the reference configuration and $\mathrm{d}\vec{x}$, $\mathrm{d}\vec{y}$, $\mathrm{d}\vec{z}$ and $\mathrm{d}v = (\mathrm{d}\vec{x} \times \mathrm{d}\vec{y}) \cdot \mathrm{d}\vec{z}$ in the current one. These infinitesimal area and volume elements are then transformed through

$$\begin{aligned} \mathrm{d}\vec{a} &= J\mathbf{F}^{T-1}\mathrm{d}\vec{A} \\ \mathrm{d}v &= J\mathrm{d}V \end{aligned} \tag{2.8}$$

where J is the determinant of the deformation gradient, $J = \det \mathbf{F}$. Like any second order tensor, the deformation gradient can be multiplicatively decomposed into the rotation and scaling components using the polar decomposition theorem

$$\mathbf{F} = \mathbf{RU} = \mathbf{VR} \tag{2.9}$$

where $\mathbf{R}$ is the proper orthogonal rotation tensor, i.e

$$\mathbf{R}^{-1} = \mathbf{R}^T \text{ and } \det \mathbf{R} = 1 \tag{2.10}$$

$\mathbf{U}$ is the right stretch tensor and $\mathbf{V}$ is the left stretch tensor defined as

$$\begin{aligned} \mathbf{U} &= \sqrt{\mathbf{F}^T\mathbf{F}} \\ \mathbf{V} &= \sqrt{\mathbf{F}\mathbf{F}^T} \end{aligned} \tag{2.11}$$

This decomposition is useful to 'filter' the rigid body rotations out. The quantities inside the square root define the Cauchy-Green deformation tensors

$$\begin{aligned} \mathbf{C} &= \mathbf{U}^2 = \mathbf{F}^T\mathbf{F} \\ \mathbf{B} &= \mathbf{V}^2 = \mathbf{F}\mathbf{F}^T \end{aligned} \tag{2.12}$$

where $\mathbf{C}$ is the right Cauchy-Green deformation tensor and $\mathbf{B}$ is the left Cauchy-Green deformation tensor.

2.1.2 Strain

The deformation gradient and the Cauchy-Green deformation tensors can not be directly used as the deformation measures for two main reasons: first, we expect the measure to attain the zero value in the case of no deformation, second, it should be insensitive to rigid body rotations. Since in the case of no deformation the deformation gradient is the unity tensor $\mathbf{I}$ whose components are given by the Kronecker delta δ_{ij}, to meet the first condition it could be enough to subtract the unity tensor from the deformation gradient, i.e.

$$\mathbf{H} = \mathbf{F} - \mathbf{I} = \frac{\mathrm{d}\vec{\mathrm{x}} - \mathrm{d}\vec{\mathrm{X}}}{\mathrm{d}\vec{\mathrm{X}}} = \frac{\mathrm{d}\vec{\mathrm{u}}}{\mathrm{d}\vec{\mathrm{X}}} \tag{2.13}$$

This definition directly corresponds to the definition of the one-dimensional engineering strain $\frac{\Delta L}{L}$. However this definition still does not satisfy the second condition. In the case of rigid body rotation the deformation gradient is given by the rotation tensor $\mathbf{R}$ and consequently

$$\mathbf{H} = \mathbf{F} - \mathbf{I} = \mathbf{R} - \mathbf{I} \neq \mathbf{0} \tag{2.14}$$

Strain measures satisfying the both above conditions are for example the Green strain tensor $\boldsymbol{\mathcal{E}}$

$$\boldsymbol{\mathcal{E}} = \frac{1}{2}\frac{\mathrm{d}\vec{\mathrm{x}}^2 - \mathrm{d}\vec{\mathrm{X}}^2}{\mathrm{d}\vec{\mathrm{X}}^2} = \frac{1}{2}\left(\mathbf{F}^T\mathbf{F} - \mathbf{I}\right) = \frac{1}{2}\left(\mathbf{H} + \mathbf{H}^T + \mathbf{H}^T\mathbf{H}\right) \tag{2.15}$$

and the Almansi strain tensor $\mathbf{A}$

$$\mathbf{A} = \frac{1}{2}\left(\mathbf{I} - \mathbf{F}^{T-1}\mathbf{F}^{-1}\right) \tag{2.16}$$

In the case of small deformation gradients, all the strain tensors can be written as

$$\boldsymbol{\varepsilon} = \frac{1}{2}\left(\mathbf{H} + \mathbf{H}^T\right) \tag{2.17}$$

2.2 Stress

Unlike the deformation, stresses can not be directly observed. Stress is an abstraction used to describe the interaction between the material points and their surroundings within the continuous body. Note that a 'material point' is for itself an abstraction denoting a tiny volume consisting of some large amount of real material 'particles'. The interaction between this point and its surroundings occurs through the interface — an imagined closed surface surrounding the volume occupied by the point. If one removes this point from the interior of the body, to keep the surroundings in the previous equilibrium state, there must be a force applied on every single point of the surface. This force per unit area is the stress vector $\vec{\mathrm{t}}$

$$\vec{\mathrm{t}} = \frac{\mathrm{d}\vec{\mathrm{f}}}{\mathrm{d}a} \tag{2.18}$$

One might see an analogy to the definition of pressure in gases. In solids however, this 'pressure' has not only the normal to the surface component but also the tangential one. These components, written in Cartesian coordinates as σ_{ij} $(i, j = 1, 2, 3)$, form the Cauchy stress tensor $\boldsymbol{\sigma}$. Cauchy stress is often referred to as the physical or true stress [34] since it uniquely defines the stress vector at any point on a surface through the Cauchy's law

$$\vec{\mathrm{t}} = \vec{\mathrm{n}} \cdot \boldsymbol{\sigma} \tag{2.19}$$

Cauchy stress tensor is symmetric and is defined in the current configuration. Its counterpart in the reference configuration is the first Piola-Kirchhoff stress tensor $\mathbf{P}^T$, obtained through the equivalence of the force $d\vec{\mathrm{f}}$ in both configurations

$$\mathrm{d}\vec{\mathrm{f}} = \boldsymbol{\sigma}\mathrm{d}\vec{\mathrm{a}} = \mathbf{P}^T\mathrm{d}\vec{\mathrm{A}} \tag{2.20}$$

and the relation (2.8), resulting in

$$\mathbf{P}^T = J\boldsymbol{\sigma}\mathbf{F}^{-T} \tag{2.21}$$

Unlike the Cauchy stress, the first Piola-Kirchhoff stress tensor is not symmetric. Its transpose

$$\mathbf{P} = J\mathbf{F}^{-1}\boldsymbol{\sigma} \tag{2.22}$$

is the nominal stress. Note that some authors define these two tensors in the opposite way. This definition is consistent with the one given in [34]. Due to its lack of symmetry, the first Piola-Kirchhoff stress is not a convenient stress measure. However the second Piola-Kirchhoff stress, defined as

$$\mathbf{P}^{sym} = \mathbf{F}^{-1}\mathbf{P}^T = J\mathbf{F}^{-1}\boldsymbol{\sigma}\mathbf{F}^{-T} \tag{2.23}$$

is symmetric. In the case of small strains, all the above defined stress tensors coincide.

2.3 Conservation laws

Conservation laws (also balance laws) can all be written using a single template equation, also called the *master balance law*:

$$\frac{\mathrm{d}}{\mathrm{d}t}\mathcal{X} = \int_{\Omega} \frac{\partial \chi}{\partial t}\,\mathrm{d}v + \int_{\partial\Omega} \chi \dot{\vec{\mathrm{x}}}\cdot\vec{\mathrm{n}}\,\mathrm{d}a \tag{2.24}$$

where the net temporal change of some quantity Ψ is given by its production rate within the domain plus its flux through the boundaries of the domain.

2.3.1 Mass conservation

Applying this template to the material density field, a mass conservation law is obtained.

$$\frac{\mathrm{d}m}{\mathrm{d}t} = \int_{\Omega} \frac{\partial \rho}{\partial t}\,\mathrm{d}v + \int_{\partial\Omega} \rho \dot{\vec{\mathrm{x}}}\cdot\vec{\mathrm{n}}\,\mathrm{d}a \tag{2.25}$$

Given the assumption that no material $\Leftrightarrow$ energy conversion is taking place within the body and, no material is added through the boundaries (not always the case, even in solids), the mass conservation law simplifies to

$$\dot{m} = 0 \quad \Longrightarrow \quad m = \int_{\Omega_0} \rho_0\,\mathrm{d}v = \int_{\Omega} \rho\,\mathrm{d}v = \mathrm{Const} \tag{2.26}$$

and leads to the relationship $\rho_0 = J\rho$.

2.3.2 Linear momentum

The conservation of linear momentum is given by:

$$\frac{\mathrm{d}}{\mathrm{d}t}\int_{\Omega}\rho\,\dot{\vec{\mathrm{x}}}\,\mathrm{d}v = \int_{\Omega}\rho\vec{\mathrm{b}}\,\mathrm{d}v + \int_{\partial\Omega}\vec{\mathrm{t}}\cdot\vec{\mathrm{n}}\,\mathrm{d}a \tag{2.27}$$

where $\vec{\mathrm{b}}$ is the volume force and $\vec{\mathrm{t}}$ is the traction vector on the boundary, defined in (2.18). In the static case $\left(\ddot{\vec{\mathrm{x}}} = 0\right)$ the conservation of linear momentum is often referred to as the force equilibrium equation. Using the Gauss theorem and the Cauchy's law (2.19), the equilibrium equation can be written in its local form

$$\operatorname{div}\boldsymbol{\sigma} + \rho\vec{\mathrm{b}} = 0 \tag{2.28}$$

2.3.3 Angular momentum

The conservation of angular momentum (also moment of momentum) is obtained by the vectorial multiplication of the momentum terms with an arbitrary radius vector $\vec{\mathrm{x}}_0$:

$$\frac{\mathrm{d}}{\mathrm{d}t}\int_{\Omega}\rho\,(\vec{\mathrm{x}}_0\times\dot{\vec{\mathrm{x}}})\,\mathrm{d}v = \int_{\Omega}\rho\,(\vec{\mathrm{x}}_0\times\vec{\mathrm{b}})\,\mathrm{d}v + \int_{\partial\Omega}(\vec{\mathrm{x}}_0\times\vec{\mathrm{t}})\cdot\vec{\mathrm{n}}\,\mathrm{d}a \tag{2.29}$$

Assuming no point-moments or couple-stresses are present, the conservation of angular momentum implies the symmetry of the stress tensor, i.e. $\boldsymbol{\sigma} = \boldsymbol{\sigma}^T$.

2.3.4 Energy

The principle of energy conservation states that the total energy of any closed system must remain constant. The energy can not "disappear" or arise from nowhere. It implies that the energy can be converted from one form to another. From this point of view, the mass conservation is part of the energy conservation. However, since in a non-relativistic mechanics there is no mass to other energy-forms conversion, the mass conservation is separated as an independent law.
Given an interaction between a system and its environment, the energy of the system can be changed by adding/extracting heat through the boundaries or due to the work done either by the system on the environment or vice versa.

$$\Delta\text{system energy} = W + Q \tag{2.30}$$

where W is the work of the external forces

$$W = \int_{\Omega} \rho \vec{\mathrm{b}} \cdot \vec{\mathrm{u}} \, \mathrm{d}v + \int_{\partial\Omega} \vec{\mathrm{t}} \cdot \vec{\mathrm{u}} \, \mathrm{d}a \tag{2.31}$$

and Q is the absorbed heat.
The system energy consists of its kinetic part

$$\Pi^{\mathrm{kin}} = \frac{1}{2} \int_{\Omega} \rho \dot{\vec{\mathrm{x}}} \cdot \dot{\vec{\mathrm{x}}} \, \mathrm{d}v \tag{2.32}$$

and its internal part

$$\Pi^{\mathrm{int}} = \int_{\Omega} \rho \, e \, \mathrm{d}v \tag{2.33}$$

With regard to the mechanics of deformable bodies e is the strain energy density $U(\boldsymbol{\varepsilon})$

$$U \triangleq \int_{\Omega} \int_{0}^{\boldsymbol{\varepsilon}} \boldsymbol{\sigma} : d\boldsymbol{\varepsilon} \, \mathrm{d}v \tag{2.34}$$

which in a linear elastic case is given by

$$U \triangleq \frac{1}{2} \int_{\Omega} \boldsymbol{\sigma} : \boldsymbol{\varepsilon} \, \mathrm{d}v = \frac{1}{2} \int_{\Omega} \boldsymbol{\varepsilon} : \mathbb{C} : \boldsymbol{\varepsilon} \, \mathrm{d}v \tag{2.35}$$

and is also called the 'elastic potential'. $\mathbb{C}$ is the stiffness tensor, discussed in the next subsection.
It might be also useful to consider the complementary elastic potential $\tilde{U}(\boldsymbol{\sigma})$

$$\tilde{U} \triangleq \int_{\Omega} \int_{0}^{\boldsymbol{\sigma}} \boldsymbol{\varepsilon} : d\boldsymbol{\sigma} \, \mathrm{d}v \tag{2.36}$$

which in linear elastic case is equal to the elastic potential, i.e $\tilde{U} = U$.

2.4 Constitutive equations

The deformations and the stresses are mutually related quantities. The relationship between these is called the *constitutive law* or the *material law*. It is actually the mathematical way to express the identity of the material. Although the parameters (properties) of every material are unique, their material laws can be grouped into a number of common

types like *linear elastic*, *non-linear elastic*, *elasto-plastic*, *viscoelastic*, etc. Until stated otherwise, we limit our discussion to the **linear elastic** materials and linear part of the elasto-plastic ones, further restricting the consideration to infinitesimal strains.
As the name suggests, the relationship between the strains and stresses for this type of materials is linear and given by

$$\boldsymbol{\sigma} = \mathbb{C} : \boldsymbol{\varepsilon} \tag{2.37}$$

where $\mathbb{C}$ is the fourth rank tensor known as the *stiffness tensor*. This tensor is positive definite and consequently can be inverted to reverse the relationship (2.37):

$$\boldsymbol{\varepsilon} = \mathbb{S} : \boldsymbol{\sigma} \tag{2.38}$$

where $\mathbb{S} \equiv \mathbb{C}^{-1}$ is the *compliance tensor*. Ceramic materials are a good example for this type of constitutive law. Many metals, until the onset of the plastic flow, can be considered linear elastic as well.
The stiffness tensor $\mathbb{C}$ has 81 components c_{ijkl} (with i, j, k, l taking the values $1, 2, 3$). Due to the symmetries of the stress and strain tensors, the stiffness tensor is symmetric with respect to the corresponding indices (called the 'minor symmetries'), i.e

$$\begin{aligned} c_{ijkl} &= c_{jikl} \\ c_{ijkl} &= c_{ijlk} \end{aligned} \tag{2.39}$$

It follows that only 36 components have non-zero values in a most general case. These can be placed in a single matrix $[\mathbb{C}]$ (6×6) with components

$$\begin{bmatrix} C_{11} & C_{12} & C_{13} & C_{14} & C_{15} & C_{16} \\ C_{21} & C_{22} & C_{23} & C_{24} & C_{25} & C_{26} \\ C_{31} & C_{32} & C_{33} & C_{34} & C_{35} & C_{36} \\ C_{41} & C_{42} & C_{43} & C_{44} & C_{45} & C_{46} \\ C_{51} & C_{52} & C_{53} & C_{54} & C_{55} & C_{56} \\ C_{61} & C_{62} & C_{63} & C_{64} & C_{65} & C_{66} \end{bmatrix} \equiv \begin{bmatrix} c_{1111} & c_{1122} & c_{1133} & c_{1112} & c_{1123} & c_{1131} \\ c_{2211} & c_{2222} & c_{2233} & c_{2212} & c_{2223} & c_{2231} \\ c_{3311} & c_{3322} & c_{3333} & c_{3312} & c_{3323} & c_{3331} \\ c_{1211} & c_{1222} & c_{1233} & c_{1212} & c_{1223} & c_{1231} \\ c_{2311} & c_{2322} & c_{2333} & c_{2312} & c_{2323} & c_{2331} \\ c_{3111} & c_{3122} & c_{3133} & c_{3112} & c_{3123} & c_{3131} \end{bmatrix} \tag{2.40}$$

This form is known as the Voigt notation. In this form the Hooke's law, (2.37), is expressed as

$$\begin{bmatrix} \sigma_{11} \\ \sigma_{22} \\ \sigma_{33} \\ \sigma_{12} \\ \sigma_{23} \\ \sigma_{31} \end{bmatrix} = \begin{bmatrix} C_{11} & C_{12} & C_{13} & C_{14} & C_{15} & C_{16} \\ C_{21} & C_{22} & C_{23} & C_{24} & C_{25} & C_{26} \\ C_{31} & C_{32} & C_{33} & C_{34} & C_{35} & C_{36} \\ C_{41} & C_{42} & C_{43} & C_{44} & C_{45} & C_{46} \\ C_{51} & C_{52} & C_{53} & C_{54} & C_{55} & C_{56} \\ C_{61} & C_{62} & C_{63} & C_{64} & C_{65} & C_{66} \end{bmatrix} \begin{bmatrix} \varepsilon_{11} \\ \varepsilon_{22} \\ \varepsilon_{33} \\ 2\varepsilon_{12} \\ 2\varepsilon_{23} \\ 2\varepsilon_{31} \end{bmatrix} \tag{2.41}$$

In the linear elastic case, on account of the existence of the strain energy density $U(\boldsymbol{\varepsilon}_{ij})$, the stiffness tensor is also symmetric with respect to exchanging the first and the second index pairs (major symmetry), i.e

$$c_{ijkl} = c_{klij} \quad \text{or} \quad C_{mn} = C_{nm} \tag{2.42}$$

Consequently, in the most general linear elastic case there can only be 21 independent components of the stiffness tensor. The same is of course true for the compliance tensor s_{ijkl} and the compliance matrix S_{mn} as well.
Many materials possess however internal symmetries. These can be crystallographic planes in the case of single crystals, or other microstructural features. Such symmetries reduce the amount of non-zero entries of the stiffness tensor. Most important ones, at least with respect to the current work, are the orthotropic, transverse-isotropic and isotropic cases.

2.4.1 Orthotropy

In the orthotropic case, the material possesses three mutually orthogonal planes of symmetry. When aligned with the cartesian coordinate system, there are only 12 non-zero entries of which nine are independent (note the symmetry of the tensor).

$$\begin{bmatrix} C_{11} & C_{12} & C_{13} & 0 & 0 & 0 \\ C_{12} & C_{22} & C_{23} & 0 & 0 & 0 \\ C_{13} & C_{23} & C_{33} & 0 & 0 & 0 \\ 0 & 0 & 0 & C_{44} & 0 & 0 \\ 0 & 0 & 0 & 0 & C_{55} & 0 \\ 0 & 0 & 0 & 0 & 0 & C_{66} \end{bmatrix} \tag{2.43}$$

2.4.2 Transverse isotropy

In the transverse isotropic case, the material possesses a single plane of symmetry with its normal being also the axis of rotational symmetry. When aligned with the cartesian coordinate system, there are again only 12 non-zero entries. However, in this case the rotational symmetry makes the in-plane moduli equal. Taking, for instance, the x_3 axis

as rotational, we get

$$\begin{aligned} C_{11} &= C_{22} \\ C_{13} &= C_{23} \\ C_{44} &= \frac{1}{2}(C_{11} - C_{12}) \end{aligned} \tag{2.44}$$

consequently, only five entries remain independent.

2.4.3 Isotropy

In the isotropic case, the properties are invariant with respect to the rotation about any arbitrary axis. Any isotropic fourth-order tensor can always be represented as

$$c_{ijkl} = \lambda\delta_{ij}\delta_{kl} + \mu(\delta_{ik}\delta_{jl} + \delta_{il}\delta_{jk}) \tag{2.45}$$

where λ and μ are the Lamé constants. It follows that

$$\begin{aligned} C_{11} &= C_{22} = C_{33} = \lambda + 2\mu \\ C_{12} &= C_{23} = C_{13} = \lambda \\ C_{44} &= C_{55} = C_{66} = \mu \end{aligned} \tag{2.46}$$

The stress and strain can be decomposed into their volumetric and deviatoric parts,

$$\begin{aligned} \boldsymbol{\sigma} &= \frac{\operatorname{tr}\boldsymbol{\sigma}}{3}\mathbf{I} + \left(\boldsymbol{\sigma} - \frac{\operatorname{tr}\boldsymbol{\sigma}}{3}\mathbf{I}\right) \triangleq -p\mathbf{I} + \boldsymbol{\tau} \\ \boldsymbol{\varepsilon} &= \frac{\operatorname{tr}\boldsymbol{\varepsilon}}{3}\mathbf{I} + \left(\boldsymbol{\varepsilon} - \frac{\operatorname{tr}\boldsymbol{\varepsilon}}{3}\mathbf{I}\right) \triangleq \boldsymbol{\epsilon}\mathbf{I} + \mathbf{e} \end{aligned} \tag{2.47}$$

where $\mathbf{I}$ is the second order unit tensor, $-p$ is the hydrostatic pressure, $\boldsymbol{\tau}$ is the stress deviator, $3\boldsymbol{\epsilon}$ is the relative volumetric change (small strains) and $\mathbf{e}$ is the strain deviator. Consequently, it is convenient to split the Hooke's law as well. It is then given by

$$\boldsymbol{\sigma} = 3K\boldsymbol{\epsilon}\mathbf{I} + 2\mu\mathbf{e} \tag{2.48}$$

where K is the so called *bulk modulus* and μ is the *shear modulus*, often denoted by its engineering counterpart G. This pair, K and μ (G) will be extensively used throughout this work.

Chapter 3

Analytical homogenization

3.1 Basics

As already mentioned in the introduction, we are interested in effective elastic properties. More specifically, the effective stiffness tensor of the microscopically heterogeneous material for example. Moreover, unless explicitly mentioned, all the considered materials are assumed to be linearly elastic with constitutive behavior governed by the Hooke's law (2.37).

Of course, on the microscopic level the properties will vary spatially. Indeed, if one uses a small enough control volume, then at one point there might be a single homogeneous constituent material, while at another spatial location there might be a different homogeneous material. Yet at a third point there might happen two or more materials in the same control volume.

Let's now fix the control volume at some arbitrary location and incrementally increase its size and try to assess the properties of the resulting sample. At sizes much below the characteristic length of the microstructure, the properties of the volume will likely be constant for a while. At some size there will be already more than one material in the control volume and its properties will change. These will now be size dependent, since with every size change there will be a different mix of materials inside the volume.

There exists however a size, beyond which the properties become constant again. Even if the control volume moves to a different location, at this size its properties would not change. We say the sample of this size represents the macroscopic behavior of the material under consideration. The control volume of this size is consequently called an RVE — a Representative Volume Element. On the other hand, we assume the sample to be large enough to consider the RVE as a material point in the continuum sense.

This two-scales condition can be written as

$$L_{micro} \ll L_{RVE} \ll L_{macro} \tag{3.1}$$

where L_{micro} is the characteristic length of the microstructure, L_{macro} is the characteristic length of the macroscopic sample and L_{RVE} is the RVE size. Note however, that condition (3.1) is a necessary (for non-periodic microstructures) but not sufficient one. In some cases an RVE does not exist at all. An example could be a sample with macroscopic functional gradient of the mechanical properties. In such case the material is macroscopically inhomogeneous. There could also be a damage-born lack of an RVE. In the following we consider only materials for which either an RVE does exist, or the microstructure is periodic. In the latter case a unit cell is sufficient.

Homogenization is in some sense an averaging. Therefore, looking at the mechanical properties as stand-alone values, it might be tempting to assume that the effective macroscopic stiffness for example, is given by the volumetric average of the constituents' stiffness $\langle \mathbb{C} \rangle$, where the angled brackets denote a volumetric average

$$\langle \chi \rangle \triangleq \frac{1}{V} \int_{\Omega} \chi \, \mathrm{d}V \tag{3.2}$$

where χ is the averaged quantity and Ω is the domain of interest (here the RVE). In cases where the material consists of a number of discrete phases with piecewise constant properties, $\langle \mathbb{C} \rangle$ can be written as

$$\langle \mathbb{C} \rangle \triangleq \sum_i v_i \mathbb{C}_i \quad (i = 1, \ldots, n) \tag{3.3}$$

where i is the phase index, n is the total amount of different phases and v_i is the corresponding volume fraction

$$v_i \triangleq \frac{V_i}{V_{total}}; \quad \sum_i v_i = 1 \tag{3.4}$$

Equation (3.3) is known as the rule (or law) of mixtures. While being rather intuitively simple, this rule is far from being accurate or universal.

To properly derive the effective stiffness, one must consider the stiffness tensor as a map between the strain tensor and the stress tensor. Assuming now that for a microscopically heterogeneous material, macroscopic strains and stresses are given by their microscopic averages, the macroscopic stiffness $\mathbb{C}^{\mathrm{C}}$ is defined by

$$\langle \boldsymbol{\sigma} \rangle = \mathbb{C}^{\mathrm{C}} : \langle \boldsymbol{\varepsilon} \rangle \tag{3.5}$$

where the uppercase C in superscript denotes the "composite". Let's now introduce the local stress definition, (2.37), into the (3.5)

$$\langle \mathbb{C} : \boldsymbol{\varepsilon} \rangle = \mathbb{C}^{\mathrm{C}} : \langle \boldsymbol{\varepsilon} \rangle \tag{3.6}$$

and express the field quantities through their averages and fluctuations:

$$\chi \equiv \langle \chi \rangle + \tilde{\chi} \tag{3.7}$$

Having in mind that

$$\langle \Delta\chi \rangle \equiv 0 \tag{3.8}$$

the LHS of (3.6) simplifies to

$$\begin{aligned} \langle \mathbb{C} : \boldsymbol{\varepsilon} \rangle &= \langle (\langle \mathbb{C} \rangle + \tilde{\mathbb{C}}) : (\langle \boldsymbol{\varepsilon} \rangle + \tilde{\boldsymbol{\varepsilon}}) \rangle \\ &= \langle \langle \mathbb{C} \rangle : \langle \boldsymbol{\varepsilon} \rangle \rangle + \langle \langle \mathbb{C} \rangle : \tilde{\boldsymbol{\varepsilon}} \rangle + \langle \tilde{\mathbb{C}} : \langle \boldsymbol{\varepsilon} \rangle \rangle + \langle \tilde{\mathbb{C}} : \tilde{\boldsymbol{\varepsilon}} \rangle \\ &= \langle \mathbb{C} \rangle : \langle \boldsymbol{\varepsilon} \rangle + \langle \tilde{\mathbb{C}} : \tilde{\boldsymbol{\varepsilon}} \rangle \end{aligned} \tag{3.9}$$

Introducing (3.9) back into the (3.6) and applying $\langle \boldsymbol{\varepsilon} \rangle^{-1}$ to both sides, we finally obtain the following relationship

$$\mathbb{C}^{\mathrm{C}} = \langle \mathbb{C} \rangle + \langle \tilde{\mathbb{C}} : \tilde{\boldsymbol{\varepsilon}} \rangle : \langle \boldsymbol{\varepsilon} \rangle^{-1} \tag{3.10}$$

i.e, in general, $\mathbb{C}^{\mathrm{C}} \neq \langle \mathbb{C} \rangle$.

3.1.1 Mean strain theorem

The strain field within the elastic body is given by the symmetric part of the displacement field gradient (small deformations)

$$\boldsymbol{\varepsilon} = \frac{1}{2} \left(u_{i,j} + u_{j,i} \right) \tag{3.11}$$

Consequently, in case the displacement field is continuously linear

$$\vec{\mathrm{u}}^{0} = \boldsymbol{\varepsilon}^{0} \cdot \vec{\mathrm{x}} \tag{3.12}$$

the strain field is constant and is given by

$$\boldsymbol{\varepsilon} = \boldsymbol{\varepsilon}^{0} \tag{3.13}$$

Of course a continuously linear displacement field can only occur in a homogeneous material with constant properties. In a heterogeneous material, the strain field is probably

intractable in a most general case. However, the average strain can still be expressed as an average displacement gradient, by introducing (3.11) into (3.2)

$$\langle \boldsymbol{\varepsilon} \rangle = \frac{1}{2V} \int_{\Omega} (u_{i,j} + u_{j,i}) \, \mathrm{d}V \tag{3.14}$$

Note that since the displacement field is not continuously differentiable, the RHS of the above equation must actually be written as a sum over regions with constant properties, i.e

$$\langle \boldsymbol{\varepsilon} \rangle = \frac{1}{2V} \sum_{k=1}^{n} \left(\int_{\Omega_k} (u_{i,j} + u_{j,i}) \, \mathrm{d}V \right) \tag{3.15}$$

where Ω_k is the k^{th} region with constant properties.
The displacement gradient is still an unknown field, but using the divergence theorem, it can be expressed through the boundary displacements

$$\begin{aligned} \frac{1}{2V} \sum_{k=1}^{l} \left(\int_{\Omega_k} (u_{i,j} + u_{j,i}) \, \mathrm{d}V \right) &= \sum_{k=1}^{l} \left(\int_{\partial\Omega_k} u_i n_j \, \mathrm{d}A \right) + \sum_{l=1}^{m} \left(\int_{S} \left(u_i^+ - u_i^- \right) n_j \, \mathrm{d}A \right) \\ &= \int_{\partial\Omega} u_i n_j \, \mathrm{d}A + \int_{I} \left(u_i^+ - u_i^- \right) n_j \, \mathrm{d}A \end{aligned} \tag{3.16}$$

where we have used the symmetry of the displacement gradient and the fact that for the same interface $n_j^+ = -n_j^-$. I denotes material interface. The sums can be dropped out since the integration is independent of the actual geometry and various regions can be virtually rearranged to form a single integration domain. Thus, equation (3.14) can be written as

$$\langle \boldsymbol{\varepsilon} \rangle = \int_{\partial\Omega} u_i n_j \, \mathrm{d}A + \int_{S} \left(u_i^+ - u_i^- \right) n_j \, \mathrm{d}A \tag{3.17}$$

If the interfaces are perfect, the displacement field is continuous and the last integral is identically zero. In this case the mean strain is given by the boundary displacements only. Consequently, given a uniform macroscopic strain $\boldsymbol{\varepsilon}^0$, prescribed through the linear boundary displacements (3.12), the average value of the resulting strain field is equal the prescribed macroscopic value

$$\langle \boldsymbol{\varepsilon} \rangle = \boldsymbol{\varepsilon}^0 \tag{3.18}$$

3.1.2 Mean stress theorem

The derivation of the mean stress theorem is similar to the mean strain theorem. In the definition of the stress average

$$\langle \sigma_{ij} \rangle = \frac{1}{V} \int_{\Omega} \sigma_{ij} \, \mathrm{d}V \tag{3.19}$$

a following substitution

$$\sigma_{ij} = \sigma_{ik}\delta_{jk} = \sigma_{ik}n_{j,k} = \left(\sigma_{ik}n_j\right)_{,k} - \sigma_{ik,k}n_j \tag{3.20}$$

is made (double index implies summation). Assuming no volume forces are present (or negligible), the equilibrium condition (2.28) reduces to $\sigma_{ik,k} = 0$. Consequently, the definition (3.19) transforms into

$$\langle \boldsymbol{\sigma} \rangle = \frac{1}{V} \int_{\Omega} \left(\sigma_{ik}n_j\right)_{,k} \, \mathrm{d}V \tag{3.21}$$

Applying now the divergence theorem, one obtains the relationship between the mean stress and the forces on the sample boundary

$$\langle \sigma_{ij} \rangle = \frac{1}{V} \int_{\partial\Omega} t_i n_j \, \mathrm{d}A \tag{3.22}$$

Note that $t^+ - t^-$ is zero at the interface in any case since either the interface is bonded and the forces are in equilibrium, or the interfaces are separated and the forces vanish at free surfaces.
Applying now a macroscopic stress $\boldsymbol{\sigma}^0$ through the constant tractions

$$\vec{\mathrm{t}}^0 = \vec{\mathrm{n}} \cdot \boldsymbol{\sigma}^0 \tag{3.23}$$

one obtains the mean stress theorem — given a uniform macroscopic stress $\boldsymbol{\sigma}^0$, prescribed through the constant tractions (3.23), the average value of the resulting stress field is equal the prescribed macroscopic value

$$\langle \boldsymbol{\sigma} \rangle = \boldsymbol{\sigma}^0 \tag{3.24}$$

3.1.3 Hill energy condition

Hill [13] has required an equivalence of the microscopic and macroscopic definitions of the mean strain energy density

$$\langle U \rangle = \frac{1}{2}\langle \boldsymbol{\sigma} : \boldsymbol{\varepsilon} \rangle = \frac{1}{2}\langle \boldsymbol{\sigma} \rangle : \langle \boldsymbol{\varepsilon} \rangle = \frac{1}{2}\langle \boldsymbol{\varepsilon} \rangle : \mathbb{C}^{\mathrm{C}} : \langle \boldsymbol{\varepsilon} \rangle \tag{3.25}$$

This condition, expressed as

$$\langle \boldsymbol{\sigma} : \boldsymbol{\varepsilon} \rangle = \langle \boldsymbol{\sigma} \rangle : \langle \boldsymbol{\varepsilon} \rangle \tag{3.26}$$

has subsequently been termed the Hill energy condition and is often used as a necessary homogenization condition.
It will be shown, in subsections 3.3.1 and 3.4.2.1 that this condition leads to the absolute bounds on effective properties and thus provides no new information.

3.1.4 Influence tensors

Limiting the treatment to the problems of linear elasticity only, allows one to express the microscopic strain and stress fields as the linear functions of the prescribed ones, i.e.

$$\begin{aligned} \boldsymbol{\varepsilon} &= \mathbb{A} : \boldsymbol{\varepsilon}^0 \qquad \text{for} \qquad \vec{\mathrm{u}}^0 = \boldsymbol{\varepsilon}^0 \cdot \vec{\mathrm{x}} \\ \boldsymbol{\sigma} &= \mathbb{B} : \boldsymbol{\sigma}^0 \qquad \text{for} \qquad \vec{\mathrm{t}}^0 = \vec{\mathrm{n}} \cdot \boldsymbol{\sigma}^0 \end{aligned} \tag{3.27}$$

where $\mathbb{A}$ and $\mathbb{B}$ are forth-order *influence tensors*. These tensors are location dependent and in general not symmetric. Using however the mean strain and mean stress theorems it is easy to show that their spatial average is the unit tensor

$$\langle \mathbb{A} \rangle = \langle \mathbb{B} \rangle = \mathbb{I} \tag{3.28}$$

Introducing the influence tensor, say $\mathbb{A}$, into the Hook's law for heterogeneous materials (3.5), and applying the mean strain theorem, one obtains

$$\langle \boldsymbol{\sigma} \rangle = \langle \mathbb{C} : \mathbb{A} : \boldsymbol{\varepsilon}^0 \rangle = \langle \mathbb{C} : \mathbb{A} \rangle : \langle \boldsymbol{\varepsilon} \rangle \tag{3.29}$$

Comparing the RHS of the (3.29) with the RHS of the (3.5), it immediately follows that

$$\mathbb{C}^{\mathrm{C}} = \langle \mathbb{C} : \mathbb{A} \rangle \tag{3.30}$$

Similarly, the effective compliance tensor is given by

$$\mathbb{S}^{\mathrm{C}} = \langle \mathbb{S} : \mathbb{B} \rangle \tag{3.31}$$

In other words, the effective material constant can by represented as a weighted sum of the individual phases' properties, where the weights are given by the volume fractions multiplied with the influence tensors. For this reason, the influence tensors are, sometimes, also called the 'concentration' tensors. However, the term 'influence' seems to better resemble the definition, (3.27), as the internal fields are influenced by the boundary conditions through these tensors. It means also that the influence tensors must implicitely include the morphological information of the microstructure.

3.1.5 Eshelby tensor

In many practical cases, composites consist of a matrix phase and separate 'instances' of another phase(s) embedded in it. We will refer to these 'instances' as *inhomogeneities*. They can be either particles of any form and size, or fibers and they can be randomly distributed or form a pattern. In any case, the embedded phase is always surrounded by the matrix phase. This means the loads, applied on the boundaries of the sample, are guided to the inhomogeneities inside the sample by the matrix (with or without the interaction effects with other inhomogeneities on the way).
In the case of a single ellipsoidal inclusion with constant eigenstrain $\boldsymbol{\varepsilon}^*$, embedded in an infinite, stress and strain free isotropic homogeneous matrix, Figure 3.1, Eshelby [16] has found that the total strains and likewise the stresses are constant inside it. The total

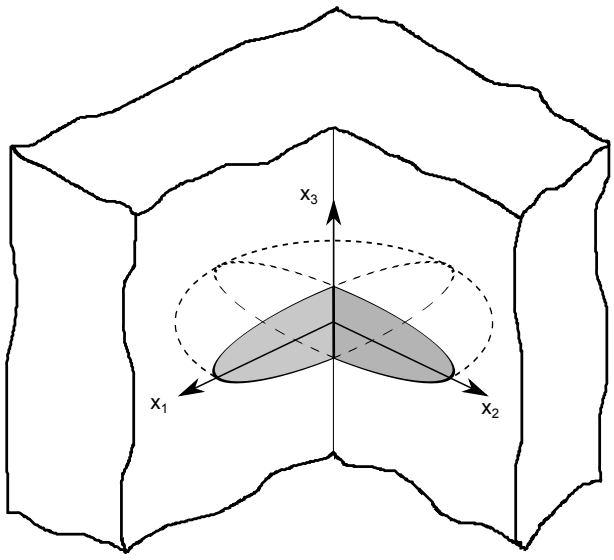

Figure 3.1: A single ellipsoidal inclusion in an infinite elastic medium

strain inside the inclusion is given by

$$\boldsymbol{\varepsilon} = \boldsymbol{\varepsilon}^e + \boldsymbol{\varepsilon}^* = \mathbb{E} : \boldsymbol{\varepsilon}^* = \text{const} \tag{3.32}$$

where $\boldsymbol{\varepsilon}^e$ is the elastic part of the strain field and $\mathbb{E}$ is a fourth-order *Eshelby tensor*. For a spherical inclusion inside an isotropic matrix this tensor is given by

$$E_{ijkl} = \alpha\frac{1}{3}\delta_{ij}\delta_{kl} + \beta\left(I_{ijkl} - \frac{1}{3}\delta_{ij}\delta_{kl}\right) \tag{3.33}$$

where α and β are the volumetric and deviatoric components, given by

$$\alpha = \frac{1+\nu}{3(1-\nu)} = \frac{3K}{3K+4\mu} \tag{3.34}$$

and

$$\beta = \frac{2(4-5\nu)}{15(1-\nu)} = \frac{6(K+2\mu)}{5(3K+4\mu)} \tag{3.35}$$

such that the volumetric and deviatoric strains are expressed as

$$\varepsilon_{kk} = \alpha\varepsilon^*_{kk}, \qquad e_{ij} = \beta e^*_{ij} \tag{3.36}$$

inside the inclusion domain.
Using the concept of equivalent eigenstrain, explained in [16], the Eshelby result can by applied to inhomogeneity as well. The equivalent eigenstrain is given by

$$\boldsymbol{\varepsilon}^* = -\mathbb{C}_0^{-1}[\mathbb{C} - \mathbb{C}_0]\boldsymbol{\varepsilon} \tag{3.37}$$

where $\mathbb{C}_0$ is an arbitrary homogeneous comparison material (cf. [35]). In case of an ellipsoidal domain, this eigenstrain can be rewritten using the Eshelby tensor as

$$\boldsymbol{\varepsilon}^* = -[\mathbb{E} + (\mathbb{C}_I - \mathbb{C}_M)^{-1} : \mathbb{C}_M]^{-1} : \boldsymbol{\varepsilon}_0 \tag{3.38}$$

with subscript I denoting the inhomogeneity and M the matrix material.
While a single inhomogeneity is of little practical importance, the Eshelby tensor serves as a fundament of many analytical homogenization models.

3.2 Selected analytic homogenization models

3.2.1 Voigt model

The Voigt model, [11], is derived using the assumption of a (spatially) constant strain $\boldsymbol{\varepsilon} = \boldsymbol{\varepsilon}^0$ inside the composite, in which case the influence tensor $\mathbb{A}$ is identically a unit tensor. By substitution of a unit tensor into equation (3.30), the effective stiffness is then

a volumetric average of the constituents' stiffnesses

$$\mathbb{C}^{\mathrm{C}} = \langle \mathbb{C} \rangle \tag{3.39}$$

Note that the above assumption leads to the violation of the stress equilibrium at the interfaces. This can be easily demonstrated with a simple bilayer model with a straight interface. At the first step, we allow the interface to be completely debonded and apply a unidirectional strain, say, parallel to the interface. In case the Poisson's ratios of both materials are non-zeroes, the free surfaces at the interface will move in the direction, perpendicular to the applied displacement, Figure 3.2.

Obviously, the local strain field in the vicinity of the interface differs from the global one

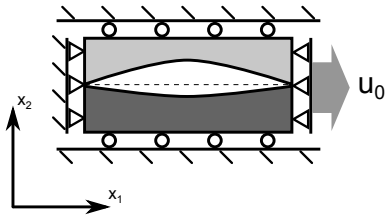

Figure 3.2: A bilayer strip loaded longitudinally. For illustration purposes the Poisson ratios are positive.

and thus the overall strain field is not constant. To make it constant, one must apply a stress, normal to the free surface, Figure 3.3, in the amount

$$\sigma_{22}^{i} = C_{12}^{i} \varepsilon_{11} \tag{3.40}$$

where the upper index i denotes the different materials. It immediately follows that for

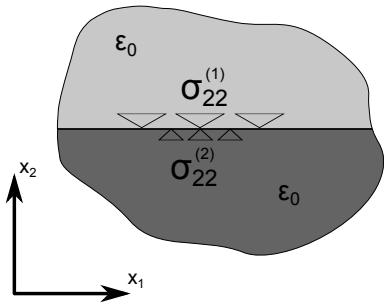

Figure 3.3: Local stresses needed to 'stitch' the interface.

any material pair, if the difference of the off-diagonal components of the stiffness tensors is not zero, i.e $C_{12}^{1} - C_{12}^{2} \neq 0$, there must be different 'amounts' of stress, applied to the interface to keep the strain field constant.

3.2.2 Reuss model

The Reuss model, [12], is derived using the assumption of a constant stress $\boldsymbol{\sigma} = \boldsymbol{\sigma}^0$ inside the sample, in which case the influence tensor $\mathbb{B}$ is identically a unit tensor. By substitution of a unit tensor into equation (3.31), the effective compliance is then a volumetric average of the constituents' compliancies

$$\mathbb{S}^{\mathrm{C}} = \langle \mathbb{S} \rangle \tag{3.41}$$

Note that the above assumption leads to the kinematic incompatibility at the interfaces. This can be again easily demonstrated with a simple bilayer model with a straight interface. This time, we apply a stress field perpendicular to the interface and allow the materials to slide relative to each other. In case the Poisson's ratio of both materials are again non-zeroes, layers will contract (or expand) in the perpendicular direction Figure 3.4. The amount of the displacement will be different if the difference of the off-diagonal components of the compliance tensors is not zero, i.e $S^1_{12} - S^2_{12} \neq 0$. To remove the displacement

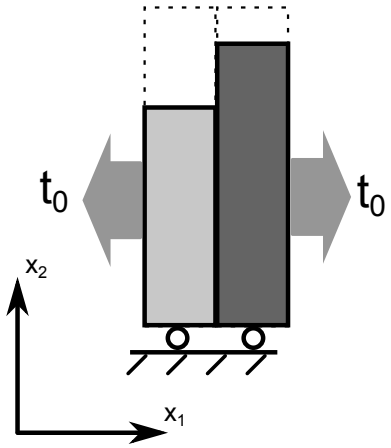

Figure 3.4: A bilayer strip loaded across the interface. For illustration purposes the Poisson ratios are positive.

jump at the interface, one must apply a stress at the interface, Figure 3.5, in which case the overall stress field is no longer constant. In other words, a constant stress field requires a displacement jump at the interface (tangent to it).

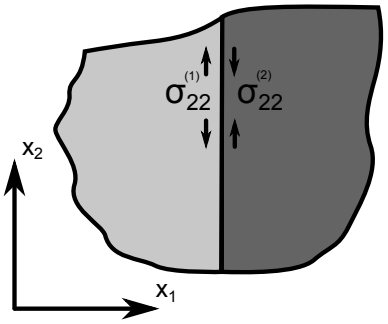

Figure 3.5: Local stresses needed to cancel the displacement jump.

3.2.3 Dilute Distribution

The dilute distribution model (DD) is derived from the solution of the strain and stress fields for a single inhomogeneity. It is assumed that in case the distance between any two inhomogeneities is much larger than their characteristic size, there is no interaction between them, Figure 3.6.

Probably the first account of such approach is given in Maxwell's treatise [3]. He

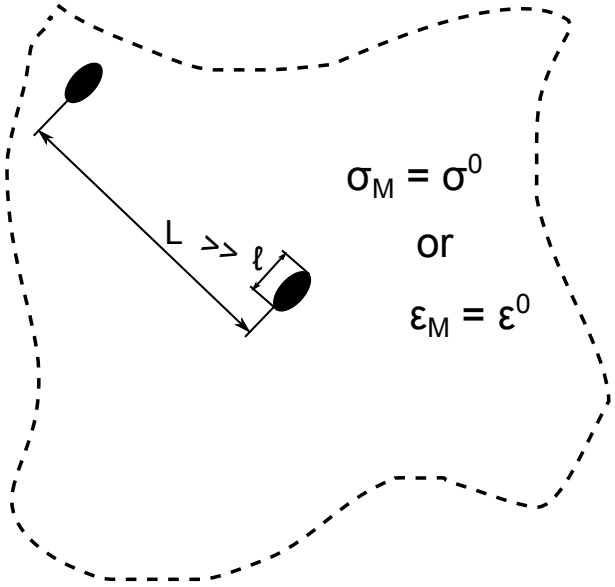

Figure 3.6: Inhomogeneities at a very low concentration

considers the specific resistivity of a single spherical heterogeneity embedded inside a sphere of another material.

Bruggeman [21] considered the mechanical properties of a spherical inhomogeneity by solving the hydrostatic compression problem and a shear problem of a spherical composite. The solution of the shear problem contains however an error.

An alternative way is to use the Eshelby tensor (3.38), in which case the solution applies to a general ellipsoid shape. Using the subscripts 'M' for matrix and 'I' for the reinforcement,

the effective stiffness takes the form

$$\mathbb{C}^{\mathrm{C}} = v_M \mathbb{C}_M : \mathbb{A}_M + v_I \mathbb{C}_I : \mathbb{A}_I \tag{3.42}$$

introducing now the property (3.28) into (3.42), the effective stiffness can be written as a function of the inhomogeneity influence tensor

$$\mathbb{C}^{\mathrm{C}} = \mathbb{C}_M + v_I \left(\mathbb{C}_I - \mathbb{C}_M\right) : \mathbb{A}_I \tag{3.43}$$

which for a single inhomogeneity is given by

$$\mathbb{A}_I = [\mathbb{I} + \mathbb{E} : \mathbb{C}_M^{-1} : (\mathbb{C}_I - \mathbb{C}_M)]^{-1} \tag{3.44}$$

In case the inhomogeneities are of spherical shape and uniformly distributed within the matrix, such that the composite is macroscopically isotropic, its effective stiffness tensor simplifies to

$$\begin{aligned} K_{dd}^{\mathrm{C}} &= K_M + v_I \frac{(K_I - K_M)K_M}{K_M + \alpha(K_I - K_M)} \\ G_{dd}^{\mathrm{C}} &= G_M + v_I \frac{(G_I - G_M)G_M}{G_M + \beta(G_I - G_M)} \end{aligned} \tag{3.45}$$

where α and β are the components of the isotropic Eshelby tensor, given in (3.34) and (3.35) correspondingly.

3.2.4 Mori-Tanaka model

Mori & Tanaka [18], have assumed that if the concentration of the reinforcement phase is not dilute, then the strain and stress fields surrounding the inhomogeneity at some distance are the average matrix strain $\langle \boldsymbol{\varepsilon} \rangle$ and stress $\langle \boldsymbol{\sigma} \rangle$, Figure 3.7. In this case the influence tensor of the inclusion is given by

$$\mathbb{A}_I = [\mathbb{I} + v_M \mathbb{E} : \mathbb{C}_M^{-1} : (\mathbb{C}_I - \mathbb{C}_M)]^{-1} \tag{3.46}$$

In case of an isotropic composite with spherical inhomogeneities, this model yields

$$\begin{aligned} K_{MT}^{\mathrm{C}} &= K_M + v_I \frac{(K_I - K_M)K_M}{K_M + \alpha(1 - v_I)(K_I - K_M)} \\ G_{MT}^{\mathrm{C}} &= G_M + v_I \frac{(G_I - G_M)G_M}{G_M + \beta(1 - v_I)(G_I - G_M)} \end{aligned} \tag{3.47}$$

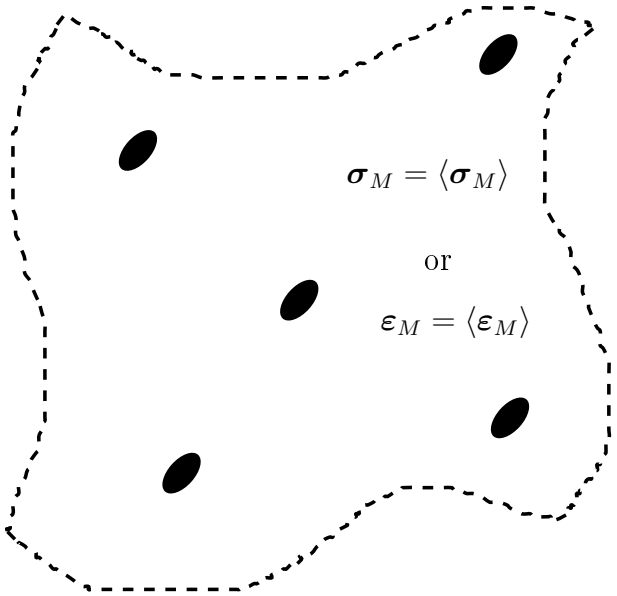

Figure 3.7: The stress and strain fields in the Mori-Tanaka model

It shall be noted that this model is sometimes interpreted as being valid for small volume fractions only, see Gross & Seelig [35]. This conclusion is based on the thought that a defect can 'see' a homogeneous stress or strain field only for small values of v_I. However, a look at the MT representation of the average defect strain

$$\langle \boldsymbol{\varepsilon} \rangle_I = \mathbb{A}_I : \langle \boldsymbol{\varepsilon} \rangle_M \tag{3.48}$$

may suggest a slightly different interpretation. Since the influence tensor $\mathbb{A}_I$ appears as a constant factor, otherwise the RHS would be $\langle \mathbb{A}_I : \boldsymbol{\varepsilon} \rangle_M$, it can be thought of as 'all the defects are identical'. It means that in general, the MT method valid for all values of v_I, however if the defect is not a sphere, all the defects must additionally be identically oriented.

3.2.5 Self-consistent approach

The self-consistent method, originally derived for aggregates of crystals was applied by Hill to the particle reinforced composite materials [17]. This method accounts for the interaction between the inhomogeneities by looking at the inhomogeneity as being embedded not in the matrix material, but rather in the homogenized composite. The strain and stress fields that it 'sees' are then the effective macroscopic fields. This leads to the

following system of equations (in case of spherical inclusions)

$$\begin{gathered}\frac{3}{3K_{SC}+4G_{SC}}=\frac{3v_1}{3K_1+4G_{SC}}+\frac{3v_2}{3K_2+4G_{SC}}\\ \left(\frac{3v_1K_1}{3K_1+4G_{SC}}+\frac{3v_2K_2}{3K_2+4G_{SC}}\right)+5\left(\frac{v_1G_2}{G_{SC}-G_2}+\frac{v_2G_1}{G_{SC}-G_1}\right)+2=0\end{gathered}\tag{3.49}$$

Note that the expressions are symmetric with regard to the index change. Citing Hill: "However, this does not imply that the matrix phase also is treated as particulate in this theory, through a kind of conceptual fragmentation. It simply means that the same overall moduli are predicted for another composite in which the roles of the phases are reversed: that is, where the first phase forms a coherent matrix and the second phase is distributed as inclusions shaped and oriented as before, both in their original concentrations."
The main problem of this approach is that an inhomogeneity, placed inside an equivalent homogenized material, stiffens (weakens) it. Consequently, at low concentrations, the model is over (under) predicting and vice versa — it oscillates about some mid value.
The expression for the bulk modulus, first line in (3.49), is identical to the Bruggeman's equation (27), [21]. However the composite, considered by Bruggeman is different. Bruggeman has thought of an homogeneous medium in which one embeds spheres of two different materials, see Figure 3.8. The spheres can be of different sizes, but they must fill the original homogeneous material till its volume fraction is reduced to zero and the spheres are separated by thickness-less membranes. Basically, Bruggeman model is a perfect

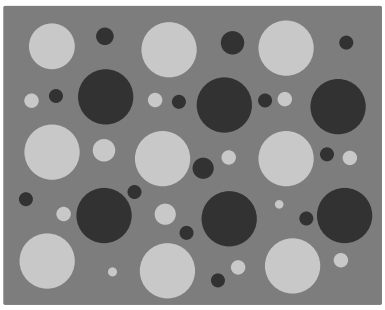

Figure 3.8: Bruggeman model of spheres aggregate [21]

closed-cell foam of zero volume fraction, whose cells are filled with two different materials. Consequently, it can be used as such for a three material composites. By changing the G_{SC} to G_M the bulk modulus of the composite is given by

$$K^{\mathrm{C}}=\frac{(K_2+\frac{4}{3}G_M)K_1v_1+(K_1+\frac{4}{3}G_M)K_2v_2}{(K_2v_1+K_1v_2+\frac{4}{3}G_M)}\tag{3.50}$$

As an example, one can think of a matrix with reinforcement and pores. The only restriction is that the volume fraction of the matrix must be small compared to that of the

reinforcement and the pores together. Note that when the cell walls are very thin, the matrix can contribute to the overall stiffness only through the shear stiffness.
Another observation is that for the matrix, one can choose a material of one of the embedded particles. In this case the composite is a matrix of one material with embedded spheres of the other. In equation (3.50) the index M must be changed to either 1 or 2 and one obtains expression identical to the Mori-Tanaka model.

3.3 Bounds on effective response

The material phases in the majority of the real composites are distributed in a random fashion. Consequently, to exactly describe the morphology, one needs an infinite set of correlation functions which statistically characterize the sample [36]. Moreover, it is also assumed that since the macroscopic properties depend on the morphology, "For general random media, the complexity of the microstructure prevents one from obtaining the effective properties of the system exactly." [37]. It follows that in general case, only the bounds on the effective properties can be stated with rigor.
The above claim is somewhat arguable, since there exist no proof rejecting the existence of a finite set of morphological descriptors. Nevertheless, the bounds are very valuable and useful tools. Rigorous bounds can always be used as "sanity check" for new theories or numerical models.

3.3.1 Absolute upper and lower bounds

The minimum potential energy principle states that of all kinematically admissible strain fields $\hat{\boldsymbol{\varepsilon}}$, the true strain field $\boldsymbol{\varepsilon}$ will render the potential energy a minimum.

$$U(\hat{\boldsymbol{\varepsilon}}) = \frac{1}{2}\int_{\Omega} \hat{\boldsymbol{\varepsilon}} : \mathbb{C} : \hat{\boldsymbol{\varepsilon}}\, \mathrm{d}V = \frac{V}{2}\langle \hat{\boldsymbol{\varepsilon}} : \mathbb{C} : \hat{\boldsymbol{\varepsilon}} \rangle > \frac{V}{2}\langle \boldsymbol{\varepsilon} : \mathbb{C} : \boldsymbol{\varepsilon} \rangle = U(\boldsymbol{\varepsilon}) \tag{3.51}$$

Let's now consider a constant strain field, i.e $\boldsymbol{\varepsilon}^0$. A constant strain field is a true field ($\boldsymbol{\varepsilon} = \boldsymbol{\varepsilon}^0$) if and only if the stiffness is also constant, $\mathbb{C} = \mathbb{C}^{\mathrm{C}}$, otherwise it is only a kinematically admissible field, $\hat{\boldsymbol{\varepsilon}} = \boldsymbol{\varepsilon}^0$, thus

$$\langle \boldsymbol{\varepsilon}^0 : \mathbb{C}(\vec{\mathrm{x}}) : \boldsymbol{\varepsilon}^0 \rangle > \langle \boldsymbol{\varepsilon}^0 : \mathbb{C}^{\mathrm{C}} : \boldsymbol{\varepsilon}^0 \rangle \tag{3.52}$$

or

$$\boldsymbol{\varepsilon}^0 : \langle \mathbb{C}(\vec{\mathrm{x}}) \rangle : \boldsymbol{\varepsilon}^0 > \boldsymbol{\varepsilon}^0 : \mathbb{C}^{\mathrm{C}} : \boldsymbol{\varepsilon}^0 \tag{3.53}$$

Consequently, the Voigt stiffness estimate, obtained with the assumption of a constant strain field is the absolute upper bound.
Likewise, an application of the minimum complementary potential energy principle, which states that of all statically admissible stress fields $\hat{\boldsymbol{\sigma}}$, the true stress field will render the complementary energy a minimum, leads to the upper bound on the compliance tensor

$$\boldsymbol{\sigma}^0 : \langle \mathbb{S}(\vec{\mathrm{x}}) \rangle : \boldsymbol{\sigma}^0 > \boldsymbol{\sigma}^0 : \mathbb{S}^{\mathrm{C}} : \boldsymbol{\sigma}^0 \tag{3.54}$$

which is given by the Reuss estimate. Hence, in the sense of the respective energy quantities, the effective macroscopic stiffness is always bounded by the Voigt and Reuss estimates, i.e

$$\langle \mathbb{C} \rangle > \mathbb{C}^{\mathrm{C}} > \langle \mathbb{C}^{-1} \rangle^{-1} \tag{3.55}$$

For this reason they are often termed the Voigt and Reuss bounds.
The Hill condition, (3.26), requires an equivalence of the microscopic and macroscopic definitions of the mean strain energy density, see 3.1.3. For the sake of the reader's convenience, it is presented here again:

$$\langle \boldsymbol{\sigma} : \boldsymbol{\varepsilon} \rangle = \langle \boldsymbol{\sigma} \rangle : \langle \boldsymbol{\varepsilon} \rangle \tag{3.56}$$

or

$$\langle \boldsymbol{\varepsilon} : \mathbb{C}(x) : \boldsymbol{\varepsilon} \rangle = \langle \boldsymbol{\varepsilon} \rangle : \mathbb{C}^{\mathrm{C}} : \langle \boldsymbol{\varepsilon} \rangle \tag{3.57a}$$

$$\langle \boldsymbol{\sigma} : \mathbb{S}(x) : \boldsymbol{\sigma} \rangle = \langle \boldsymbol{\sigma} \rangle : \mathbb{S}^{\mathrm{C}} : \langle \boldsymbol{\sigma} \rangle \tag{3.57b}$$

By the way of application of either the constant strain field, or the constant stress field, it is immediately clear that the Hill condition contradicts the above minimum energy principles, (3.53) and (3.54).
In general, to relate the macroscopic and microscopic energy quantities, one must consider the field fluctuation terms as well

$$\langle \boldsymbol{\sigma} : \boldsymbol{\varepsilon} \rangle = \langle \boldsymbol{\sigma} \rangle \langle \boldsymbol{\varepsilon} \rangle + \langle \tilde{\boldsymbol{\sigma}} : \tilde{\boldsymbol{\varepsilon}} \rangle \tag{3.58}$$

(the derivation is similar to equation (3.9)).
The Hill condition is often interpreted as saying that for RVE the average work of the field fluctuations must vanish. Moreover, the boundary conditions are judged for they applicability for the homogenization task by their compliance to the Hill condition. Thus the linear displacement, constant traction and their combinations are 'appropriate' ones, since they nullify the last term of (3.58) on the boundaries by definition.
Using the strain and stress influence tensors, defined in (3.27), and mean strain and mean

stress theorems, equation (3.58) can be rewritten as

$$\langle \mathbb{B}^T : \mathbb{A} \rangle = \mathbb{I} + \langle (\mathbb{B} - \mathbb{I})^T : (\mathbb{A} - \mathbb{I}) \rangle \tag{3.59}$$

which means that the last term can vanish inside the heterogeneous material only if either of the influence tensors is a unit tensor, leading back to the Voigt and Reuss results.
For a correct interpretation of the equation (3.58), we first determine the sign of its last term. Using the effective stiffness tensor of a two-component composite, defined through the influence tensors (3.30), the inequalities (3.53) and (3.54) can be written as

$$\begin{aligned} \mathbb{C}_1 : \mathbb{A}_1 v_1 + \mathbb{C}_2 : \mathbb{A}_2 v_2 &< \mathbb{C}_1 v_1 + \mathbb{C}_2 v_2 \\ \mathbb{S}_1 : \mathbb{B}_1 v_1 + \mathbb{S}_2 : \mathbb{B}_2 v_2 &< \mathbb{S}_1 v_1 + \mathbb{S}_2 v_2 \end{aligned} \tag{3.60}$$

where we have dropped the constant strain and stress tensors on both sides to reduce the visual clutter.
Since $v_1 + v_2 = 1$ and $\langle \mathbb{A} \rangle = \langle \mathbb{B} \rangle = \mathbb{I}$, we have

$$\begin{aligned} \mathbb{C}_1 : \mathbb{A}_1 v_1 + \mathbb{C}_2 : (\mathbb{I} - \mathbb{A}_1 v_1) &< \mathbb{C}_1 v_1 + \mathbb{C}_2 (1 - v_1) \\ \mathbb{C}_1 : (\mathbb{I} - \mathbb{A}_2 v_2) + \mathbb{C}_2 : \mathbb{A}_2 v_2 &< \mathbb{C}_1 (1 - v_2) + \mathbb{C}_2 v_2 \\ \mathbb{S}_1 : \mathbb{B}_1 v_1 + \mathbb{S}_2 : (\mathbb{I} - \mathbb{B}_1 v_1) &< \mathbb{S}_1 v_1 + \mathbb{S}_2 (1 - v_1) \\ \mathbb{S}_1 : (\mathbb{I} - \mathbb{B}_2 v_2) + \mathbb{S}_2 : \mathbb{B}_2 v_2 &< \mathbb{S}_1 (1 - v_2) + \mathbb{S}_2 v_2 \end{aligned} \tag{3.61}$$

After a simple rearrangement, the above inequalities can be simplified to

$$\begin{aligned} (\mathbb{C}_1 - \mathbb{C}_2) : \mathbb{A}_1 &< (\mathbb{C}_1 - \mathbb{C}_2) \\ (\mathbb{C}_2 - \mathbb{C}_1) : \mathbb{A}_2 &< (\mathbb{C}_2 - \mathbb{C}_1) \\ (\mathbb{S}_1 - \mathbb{S}_2) : \mathbb{B}_1 &< (\mathbb{S}_1 - \mathbb{S}_2) \\ (\mathbb{S}_2 - \mathbb{S}_1) : \mathbb{B}_2 &< (\mathbb{S}_2 - \mathbb{S}_1) \end{aligned} \tag{3.62}$$

and we finally get

$$\begin{aligned} (\mathbb{A}_1 - \mathbb{I});\ (\mathbb{B}_2 - \mathbb{I}) \quad &\begin{cases} \text{negative} & \forall \quad \mathbb{C}_1 > \mathbb{C}_2 \\ \text{positive} & \forall \quad \mathbb{C}_1 < \mathbb{C}_2 \end{cases} \\ (\mathbb{A}_2 - \mathbb{I});\ (\mathbb{B}_1 - \mathbb{I}) \quad &\begin{cases} \text{positive} & \forall \quad \mathbb{C}_1 > \mathbb{C}_2 \\ \text{negative} & \forall \quad \mathbb{C}_1 < \mathbb{C}_2 \end{cases} \end{aligned} \tag{3.63}$$

from which follows that $\langle \tilde{\boldsymbol{\sigma}} : \tilde{\boldsymbol{\varepsilon}} \rangle$ is a negative quantity. Thus the last term of the equation is the loss, energy 'dissipated' through the interfaces. Equation (3.58) then reads: "The microscopically stored energy of the heterogeneous mixture equals the externally added

energy minus the energy, 'wasted' through the interfaces adjustment".

$$U_{micro} = U_{macro} - U_D \tag{3.64}$$

It shall be noted that this 'dissipation' is an associative term and must not be confused with the thermodynamic one, since no thermodynamic process takes place during the mathematical homogenization.

3.3.2 Hashin-Shtrikman bounds

The Hashin-Shtrikman bounds [15] were derived using the variational principle applied to an elastic potential that includes the so called *stress polarization tensor*. After quite elaborate derivation, they arrive at the following expressions for the bulk and shear moduli of a macroscopically homogeneous composite consisting of two different phases:

$$\begin{aligned}
K_{HS1} &= K_1 + \frac{v_2}{(K_2 - K_1)^{-1} + 3v_1(3K_1 + 4G_1)^{-1}} \\
K_{HS2} &= K_2 + \frac{v_1}{(K_1 - K_2)^{-1} + 3v_2(3K_2 + 4G_2)^{-1}} \\
G_{HS1} &= G_1 + \frac{v_2}{(G_2 - G_1)^{-1} + \frac{6v_1(K_1+2G_1)}{5G_1(3K_1+4G_1)}} \\
G_{HS2} &= G_2 + \frac{v_1}{(G_1 - G_2)^{-1} + \frac{6v_2(K_2+2G_2)}{5G_2(3K_2+4G_2)}}
\end{aligned} \tag{3.65}$$

where the K_{HS1} and G_{HS1} are the upper bounds in case $K_1 > K_2$; $G_1 > G_2$ and lower bounds in case $K_1 < K_2$; $G_1 < G_2$.
Remarks:

- Both moduli of one material must be greater than both moduli of the other material. Otherwise these bounds fail. This restriction was later removed by Walpole [38] in his multiphase generalization.
- In case the shear moduli of the consituents are equal - the bounds for bulk moduli coincide and provide an exact solution. This is not so for bounds on shear moduli when the bulk moduli of the constituents are equal.
- The expressions for bulk moduli are proven to be bounds, whereas the expressions for shear moduli are assumed to be bounds.
- These bounds are the tightest possible if no structural information is known (i.e. only the constituents' properties and their volume fractions are considered).

- These bounds are an exact solution for a 'spherical composite' - a single spherical particle inside a spherical shell of another material (see for example Hill [13]) and for a composite consisting of a matrix with spherical particles embedded in it ([15]).
- In case of a closed-cell foam, the particles are actually voids, $K, G = 0$, the lower bound does not exist and the upper bound is an exact solution.

3.3.3 Higher order bounds

One of the positive features of bounds in addition to their usefulness, described at the beginning of the section, is the fact that the bounds can be improved. Since the effective properties depend on the microstructure, to improve the existing bounds one have to include successively more and more morphological information. A popular choice is the n-point correlation function of penetrable spheres randomly distributed in some volume. The n-point correlation function is defined as the probability to find n random non-coinciding points in the same phase. Thus a 1-point correlation function is equivalent to the volume fraction of a particular phase and the one-point bounds are the Voigt-Reuss ones. Similarly, the 2-point correlation function is the probability function $S_2(r)$ that gives the probability to find two points, separated by the distance r in the same phase. The two-point bounds are the Hashin-Shtrikman ones.
The three-point bounds were derived by Beran and Molyneux [22] for the effective bulk modulus and by McCoy [23] for the shear modulus of two-phase composites. In a simplified form [24] these bounds are given by

$$\begin{aligned} K_U^{\mathrm{C}} &= \langle K \rangle - \frac{3v_1v_2\left(K_1 - K_2\right)^2}{3\langle \tilde{K} \rangle + 4\langle G \rangle_\zeta} \\ K_L^{\mathrm{C}} &= \left[\langle 1/K \rangle - \frac{4v_1v_2\left(1/K_1 - 1/K_2\right)^2}{4\langle 1/\tilde{K} \rangle + 3\langle G \rangle_\zeta} \right]^{-1} \\ G_U^{\mathrm{C}} &= \langle G \rangle - \frac{6v_1v_2\left(G_1 - G_2\right)^2}{6\langle \tilde{G} \rangle + \Theta} \\ G_L^{\mathrm{C}} &= \left[\langle 1/G \rangle - \frac{v_1v_2\left(1/G_1 - 1/G_2\right)^2}{\langle 1/\tilde{G} \rangle + 6\Xi} \right]^{-1} \end{aligned} \tag{3.66}$$

with

$$\begin{aligned} \Theta &\equiv \frac{10\langle G \rangle^2 \langle K \rangle_\zeta + 5\langle G \rangle \langle 3G + 2K \rangle \langle G \rangle_\zeta + \langle 3K + G \rangle^2 \langle G \rangle_\eta}{\langle K + 2G \rangle^2} \\ \Xi &\equiv \frac{10\langle K \rangle^2 \langle 1/K \rangle_\zeta + 5\langle G \rangle \langle 3G + 2K \rangle \langle 1/G \rangle_\zeta + \langle 3K + G \rangle^2 \langle 1/G \rangle_\eta}{\langle 9K + 8G \rangle^2} \end{aligned} \tag{3.67}$$

where

$$\begin{aligned} \langle\chi\rangle &\equiv v_1\chi_1 + v_2\chi_2 \\ \langle\chi\rangle_\zeta &\equiv \zeta_1\chi_1 + \zeta_2\chi_2 \\ \langle\chi\rangle_\eta &\equiv \eta_1\chi_1 + \eta_2\chi_2 \end{aligned} \tag{3.68}$$

χ represents any property and tilde above it denotes the interchanging of the subscripts 1 and 2 i.e. $\langle\tilde{\chi}\rangle \equiv v_1\chi_2 + v_2\chi_1$. The ζ_i and η_i are geometric parameters, given by

$$\begin{aligned} \zeta_1 = 1 - \zeta_2 &= \frac{9}{2v_1v_2}\int_0^\infty dr\int_0^\infty ds\int_{-1}^1 du\frac{Q_1(r,s,\Lambda)}{rs}P_2(\Lambda) \\ \eta_1 = 1 - \eta_2 &= \frac{5\zeta_1}{21} + \frac{150}{7v_1v_2}\int_0^\infty dr\int_0^\infty ds\int_{-1}^1 du\frac{Q_1(r,s,\Lambda)}{rs}P_4(\Lambda) \end{aligned} \tag{3.69}$$

$P_2(\Lambda)$ and $P_4(\Lambda)$ are Legendre polynomials and $Q_1(r,s,\Lambda)$ is the probability of a triangle with sides of length r and s at angle $\cos^{-1}(\Lambda)$ having all three vertices lie in the material 1 when placed randomly in the composite.

Of course, one can derive fourth-order bounds and even higher. In the given form there are no exact analytical values for the parameters η and ζ and they must be integrated numerically. For details about the involved complexity, one can consult Helte, [39].

It should be noted that the above bounds for shear modulus are not the tightest ones. These were subsequently improved by Milton and Phan-Thien [40], Lado and Torquato [25] and Gibiansky and Torquato [26].

3.3.4 Remarks on HS and higher-order bounds

Hashin-Shtrikman and the higher-order bounds can all be written as

$$\chi^{\mathrm{C}} = v_1\chi_1 + v_2\chi_2 - \frac{v_1v_2\left(\chi_1-\chi_2\right)^2}{v_1\chi_2 + v_2\chi_1 + y} \tag{3.70}$$

for any property χ. This template can be recast into a form given by the use of the influence tensors, for example equation (3.30):

$$\chi^{\mathrm{C}} = \frac{(\chi_2+y)}{v_1\chi_2 + v_2\chi_1 + y}v_1\chi_1 + \frac{(\chi_1+y)}{v_1\chi_2 + v_2\chi_1 + y}v_2\chi_2 \tag{3.71}$$

The y expressions for various bounds are collected in Tables 3.1 and 3.2. Here, 'GT' corresponds to the 3^{rd}-order bounds from Gibiansky and Torquato [26]. The phases are assumed to be well-ordered, i.e $(K_1 - K_2)(G_1 - G_2) > 0$.

Table 3.1: 'y' expressions for the HS bounds

	K^{C}	G^{C}
y_U	$\frac{4}{3}G_1$	$\frac{9K_1G_1+8G_1^2}{6K_1+12G_1}$
y_L	$\frac{4}{3}G_2$	$\frac{9K_2G_2+8G_2^2}{6K_2+12G_2}$

Table 3.2: 'y' expressions for the GT bounds

	K^{C}	G^{C}
y_U	$\frac{4}{3}(\zeta_1 G_1 + \zeta_2 G_2)$	$\frac{48\langle G\rangle_\eta\langle K\rangle_\zeta+56\langle G\rangle_\eta\langle G\rangle_\zeta+15\langle G\rangle_\zeta\langle K\rangle_\zeta}{80\langle G\rangle_\eta+42\langle K\rangle_\zeta+4\langle G\rangle_\zeta}$
y_L	$\frac{4}{3}\left[\frac{\zeta_1}{G_1}+\frac{\zeta_2}{G_2}\right]^{-1}$	$\frac{48\langle G^{-1}\rangle_\zeta+56\langle K^{-1}\rangle_\zeta+15\langle G^{-1}\rangle_\eta}{80\langle G^{-1}\rangle_\zeta\langle K^{-1}\rangle_\zeta+42\langle G^{-1}\rangle_\eta\langle G^{-1}\rangle_\zeta+4\langle G^{-1}\rangle_\eta\langle K^{-1}\rangle_\zeta}$

Note that the 3^{rd}-order bounds coincide with the H-S bounds for $\eta,\ \zeta = 0,\ 1$. Moreover, both of the 3^{rd}-order bounds coincide with each other for the same parameters, which means that the H-S bounds are actually exact solutions for these values — the limiting cases with respect to ζ, η. Figure 3.9 shows the bounding shear modulus surfaces of the Alumina-Copper homogeneous isotropic composites for the case $v_1 = v_2 = 0.5$. The edges of such surfaces appear also in [26], in a rather incomprehensible two dimensional twisted projection. Hashin-Shtrikman bounds correspond to a very particular composite, the uniform random assembly of coated spherical particles of different sizes. In other words a closed-cell foam filled with another material. All the cells must have a spherical shape, be randomly and uniformly distributed and be closed. In the case of the upper H-S bound the stiff phase is the matrix and the compliant phase is fully disconnected. This situation correspond to the $\eta_1 = 1,\ \zeta_1 = 1;\ \eta_2 = 0,\ \zeta_2 = 0$, whereas in case of the lower H-S bound, the opposite is true. Figure 3.10 depicts the bulk modulus of a perfect closed-cell Alumina foam evaluated with the finite element model, Figure 4.27a, and compared to the H-S solution (the upper bound). The details of the numerical homogenization procedure are discussed in section 4.4. The second material is assumed to have zero-valued properties (voids), in which case the foam properties are given by

$$\begin{aligned} K_{foam} &= \frac{(1-v_2)G_1K_1}{v_2K_1+G_1} \\ G_{foam} &= \frac{(9K_1+8G_1)(1-v_2)G_1}{6(K_1+2G_1)v_2+9K_1+8G_1} \end{aligned} \tag{3.72}$$

where v_2 is the volume fraction of voids. Note that since the cells are all closed, there is no percolation of voids and loss of load bearing capacity, associated with it. It immediately

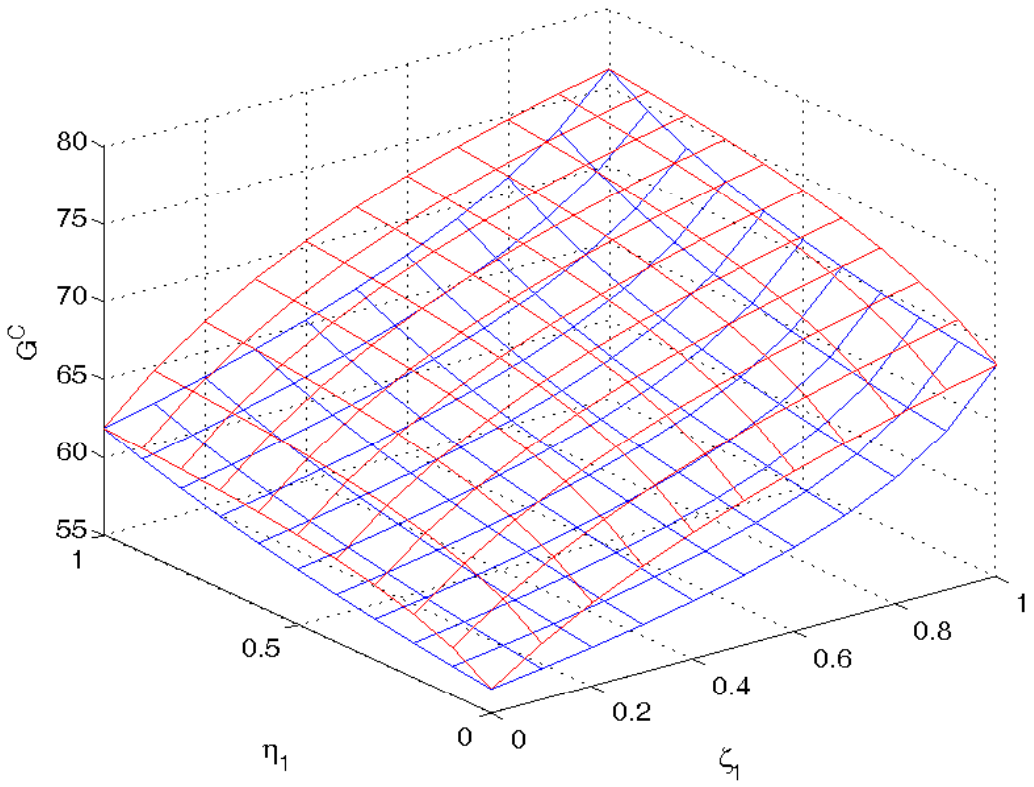

Figure 3.9: 3^{rd} order shear modulus bounds, $K_1 = 216.6\ [GPa]$, $G_1 = 162.5\ [GPa]$, $K_2 = 67.7\ [GPa]$, $G_2 = 25.9\ [GPa]$; $v_1 = v_2 = 0.5$

follows that the parameters ζ, η must be associated with terms like 'connectedness' and 'matricity' of the phases. An interesting observation in this regard is that in the expression of the bulk modulus, the parameter 'y' is a function of shear modulus only. Moreover, at the limits, appears the shear modulus of the matrix phase.
It must be stressed, however, that it is actually a misconception to refer to H-S expressions as bounds for isotropic materials. If this was the case, one of the following claims would be true:

- A foam with all of its cells closed is less isotropic than a foam with some of its cells open. Consequently, there exist a unique microstructure wich is the only truly isotropic, or,
- By incorporation of more and more correlation functions one can make the bounds so 'sharp' that they coincide at a unique isotropic value.

Clearly, this is not so. A closed-cell foam can be as isotropic as an open-cell foam even though the stiffness tensor of the first one attains the H-S bounds, while the second one

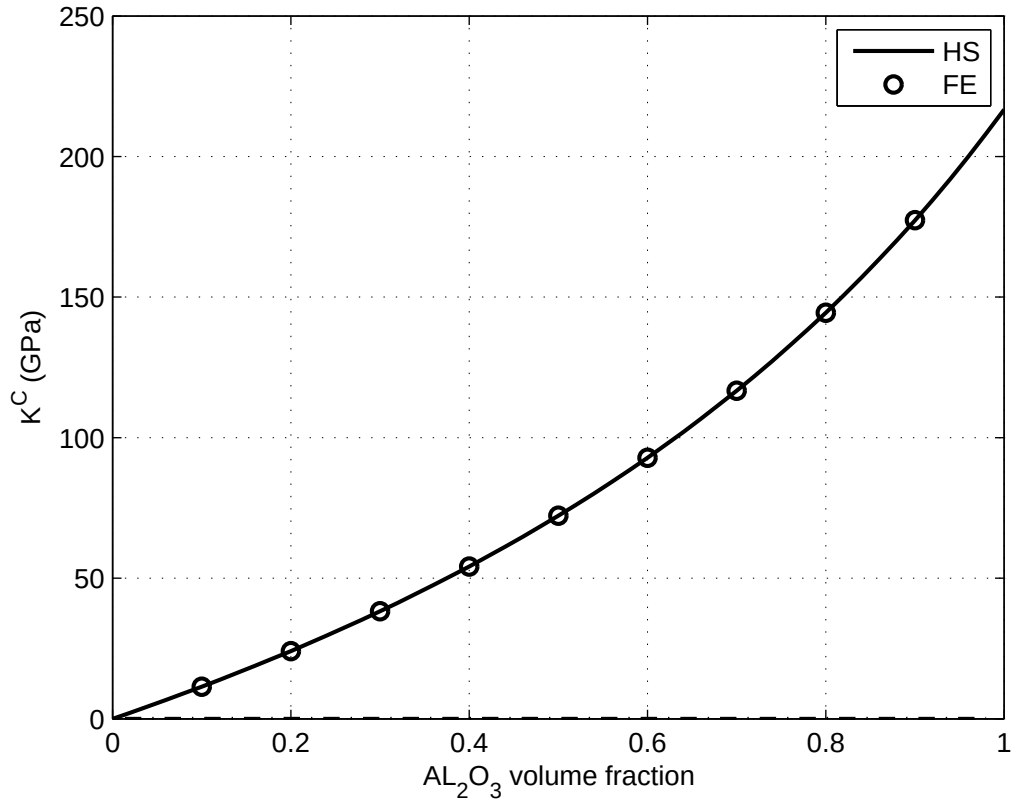

Figure 3.10: The Bulk modulus of the perfect closed-cell Alumina foam, $K_1 = 216.6\ [GPa],\ G_1 = 162.5\ [GPa],\ K_2 = G_2 = 0$

is always inside. Consequently, there is no unique isotropic value or microstructure, but an infinite number of equally isotropic ones. It is as much a misconception to refer to the microstructures, attaining any of these or other bounds, as 'optimal' (see for example [26]) without an explicit mention of the parameter(s) with regard to which these microstructures are optimal.

At this point it is not yet clear whether the y_U and y_L, given in the tables 3.1 and 3.2 are themselves bounds or limiting cases with respect to other parameters. It is possible, however, to approximate the effective properties by using say an arithmetic or a geometric mean y:

$$\begin{aligned} y_a &= \frac{y_U + y_L}{2} \\ y_g &= \sqrt{y_U y_L} \end{aligned} \tag{3.73}$$

in which case the maximum inaccuracy will be limited to about half the difference.

Regardless of the actual meaning of the ζ and η parameters, we can assume that these are equal to 0.5 for an absolutely symmetric composite with interpenetrating phases.

A final remark —- the HS proof that the bounds for bulk modulus are the tightest, is based on the fact that their expression coincides with an exact solution. The shear modulus was

not considered to be proven since at their time there was no exact solution for the shear modulus of a composite with spherical inclusions. This solution was given later by Mori & Tanaka [18]. This solution, following the Hashin & Shtrikman argument, is the missing proof for the shear modulus bounds.
It is however important to reiterate that setting a variation of a multivariate function with respect to some parameter to zero, delivers a local extremum and not a bound. Since the varied function in our case (the strain energy density) is monotonous, as has been noted by HS, the local minimum is also a global one —- an end point (or line) of the energy surface.

3.4 Homogeneous isotropic mixture with interpenetrating phases

Methods, described in the previous section, are based on a particular assumption regarding the microstructure - it is a 'matrix & reinforcement' composite. The reinforcement can be either in the form of particles or whiskers or fibers. In either case their shapes can be approximated by an ellipsoid, which allows the application of the Eshelby tensor.
Such treatment excludes however an important class of composite materials - composites with more than one connected phase, see the Figure 1.2 in the introduction. Figure 3.11 depicts a similar composite though instead of plastics, the constituents are alumina foam infiltrated with copper. These composites are quite common, since even the particulate

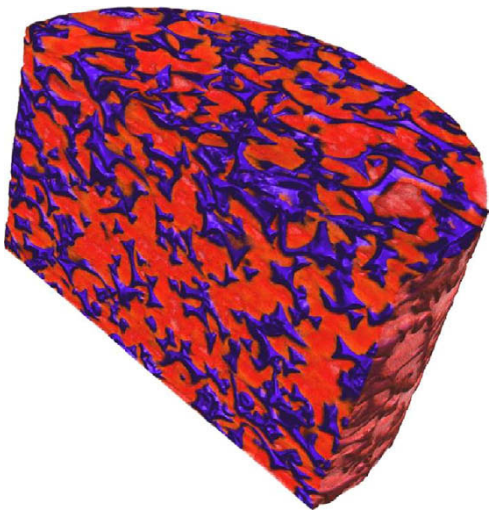

Figure 3.11: A pseudocolor image of the Al2O3-Cu interpenetrating composite (computerized tomography, courtesy of Dr. Geier, Austrian Foundry Research Institute in Leoben); blue color denotes copper

matter above certain concentration creates connected clusters and networks. This fact

has been appreciated already more than 100 years ago in connection with the problem of effective electrical conductivity of what was then called 'binary aggregates'. Lichtenecker [4, 6, 41] has derived some formulas based on the slicing technique.
The technique consists of slicing the microstructure into many thin slices and considering either infinite conductivity surface between two slices, or infinite resistance. These two conditions ultimately lead to a combination of mixing rules, like Voigt and Reuss (though in case of electromagnetic properties, these were known under other names).
Figure 3.12, was the first geometric model to actually possess three-dimensional connectivity of both phases. This was considered an especially important case of a mixture with "gleichberechtigten" phases ("having same rights", German). We shall say (morphologically) equivalent phases. This model was first considered by Lichtenecker [6], then by Frey [5] and later was reused by Tuchinskii [7] to assess the mechanical properties of such composites.

The 3D cross geometry, proved to be a popular model and was subsequently rediscov-

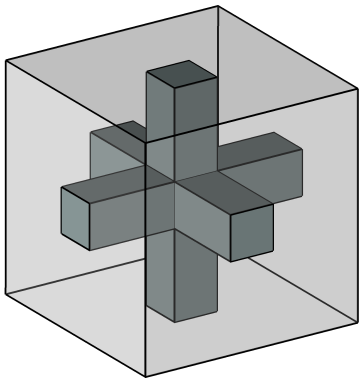

Figure 3.12: Lichtenecker-Frey model of the interpenetrating composite

ered at least two more times, [9] and [10]. Unlike Lichtenecker, the latter authors however slice the composite along the material interfaces only, Figure 3.13, leading to coarser, less general approximations. For a more detailed discussion of this approach, including the correction of some misprints, appearing in [7], see Poniznik et al., [42].

The homogenization procedure using a mix of Voigt and Reuss equations, is also quite a popular method for other geometries as well, see [43]. However, the final result depends on the particular 'slicing' combination. This dependence led Tuchinsky to designate two of the possible slicing combinations as bounds for this model, whereas Lichtenecker considered four lines as being bounds (in two dimesions) — one for each direction and then exchanging the phases with each other — a 'quadruple'. Using his intuition, Lichtenecker

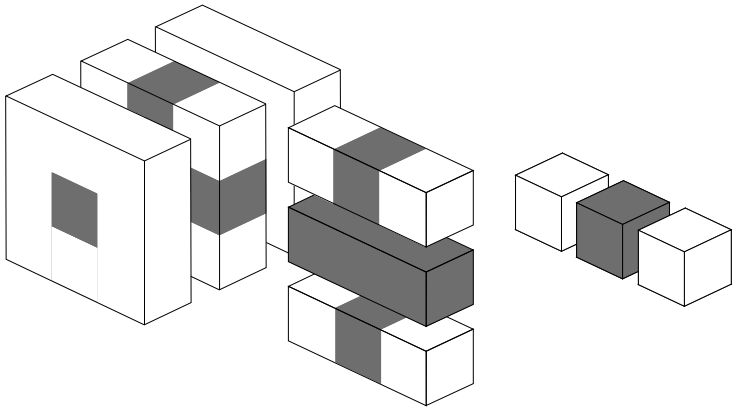

Figure 3.13: Hierarchical slicing of the model along the material interfaces

[6] devised an elegant averaging formula for the composites with equivalent phases

$$\chi^{\mathrm{C}} = \chi_1^{v_1} \chi_2^{v_2} \tag{3.74}$$

where χ stands for any material constant. This formula is basically a generalized geometric mean, which proved to match many experimental results of various material constants like the dielectric ones, the light refraction indices, thermal conductivities and even temperature-dependent electric resistivities, see discussion in [41]. Lichtenecker concluded that the agreement of the experimental results with his formula means that the constituent phases are equivalent in the tested sample. A recent comparative study of various mixing rules has revealed that the Lichtenecker's formula gave the best results in 13 out of 20 cases in determination of the interstellar dust properties, [44]

3.4.1 Voigt-Reuss statistical mix

A little bit more rigorous way of building the 'mixed' model is to consider a complete statistical sample.
Consider two particular types of composite materials, namely a unidirectional fiber-reinforced composite, Figure 3.14a, and a layered one, Figure 3.14b, with homogeneous layers. Any direction-dependent property in these two cases can be approximated by the Voigt equation along the fibers or in the layers plane and by the Reuss equation otherwise (as in a one-dimensional springs model). Hence, the Properties of the chosen composites, in their main material axes, are either $[K_V K_R K_R]$ for the fiber reinforced composite, or $[K_R K_V K_V]$ for the layered plate. The approximation error in the case of K_V is positive, i.e. the value is 'stiffer' than should be, whereas in the case of K_R - negative, i.e. the value is 'softer' than should be. A note of caution —- Voigt equation, commonly applied

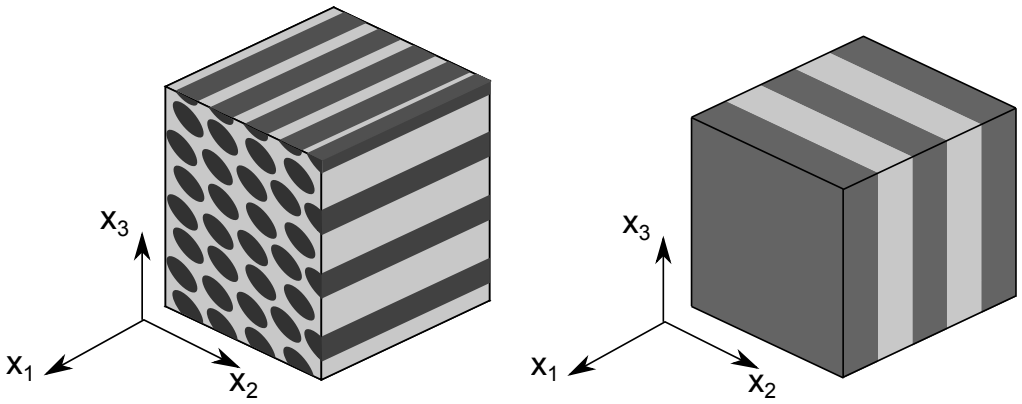

(a) UD composite **(b)** layered plate

Figure 3.14: Composites associated with the spring stiffness model

to the Young's modulus, is actually not an upper bound (cf. [13]).
Imagine now a homogeneous isotropic material, consisting of the described composite pieces, dispersed uniformly with random orientations. Obviously, for any given spatial direction, one can find pairs of pieces, which are oriented perpendicular to each other. An application of the Voigt/Reuss procedure again on such pair will cancel, at least to some extent, the discussed above approximation errors. However, to guarantee the existence of such pairs for any spatial direction, the sample must be large enough — it must be a representative volume element.
We proceed with a cubic sample, partitioned into eight equal sub-volumes, Figure 3.15. Each sub-volume is assumed to have a constant density (phase concentration), equal to the macroscopic one, but is allowed to be anisotropic. Since the described above two

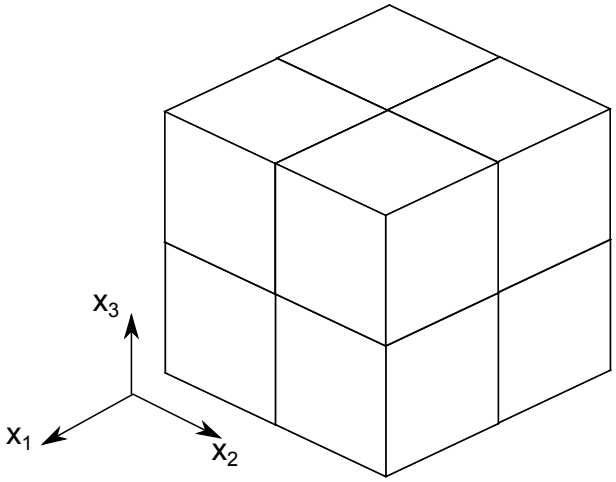

Figure 3.15: Statistical homogenization unit cell

transverse isotropic composites are the only ones approaching the Voigt-Reuss bounds, we restrict our sample to be composed of such microstructures only. To resemble the 3D-cross model, we also restrict the orientation of each sub-volume microstructure to the

three cartesian main axes. Even with this restriction, the total amount of different combinations is $3^8 = 6561$, which is almost too much for a manual computation. Though it's a trivial task for a pc. Let's slice the unit cell as in Figure 3.16 and enumerate the sub-volumes. According to the above method, the homogenized properties of this model

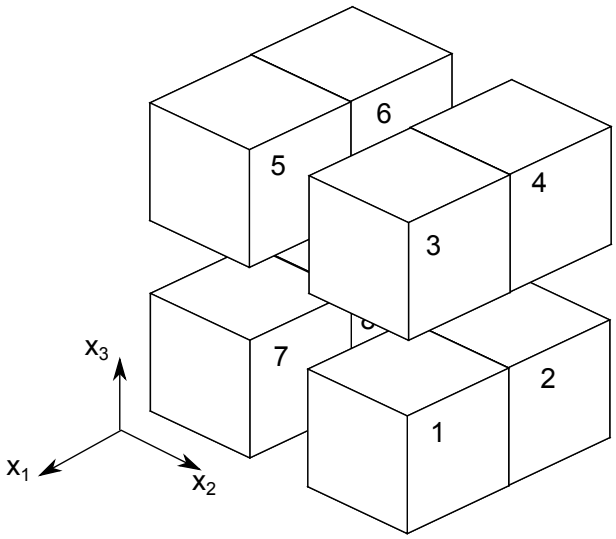

Figure 3.16: A sliced unit-cell

are given by

$$\begin{aligned} \chi_{x1} &= Voigt(Reuss(1,2); Reuss(3,4); Reuss(5,6); Reuss(7,8)) \\ \chi_{x2,x3} &= Reuss(Voigt(1,2,3,4); Voigt(5,6,7,8)) \end{aligned} \tag{3.75}$$

where 'Voigt' and 'Reuss' are the corresponding homogenization procedures.
Since χ stands for any property, we choose it to be the bulk modulus. This allows us to compare the results to the Hashin-Shtrikman bounds. Figure 3.17 illustrates the results for the both cell geometries with $\frac{K_1}{K_2} = 10$ and $\frac{G_1}{G_2} = 100$. The difference between the lines, corresponding to equations (3.75), is small for both microstructures. There are also only two lines per model instead of four. This is the result of considering all the possible combinations — the phases are equivalent. Moreover, all the results are inside the Hashin-Shtrikman bounds, as expected from an isotropic composite with interpenetrating phases. Yet another set of properties shows a different picture, Figure 3.18. The difference between the lines is still small, but these are not inside the Hashin-Shtrikman bounds anymore. This is due to the fact that the bulk and the shear moduli are not independent quantities, even for isotropic materials. Consequently, the above statistical procedure, as well as the Lichtenecker's and others' formulas should not be used for the approximation of the tensorial properties. Note also that the HS bounds can not be converted to the scalar ones by, say, assuming $G_i = 0$ since in that case both HS bounds coincide with the Reuss bound.

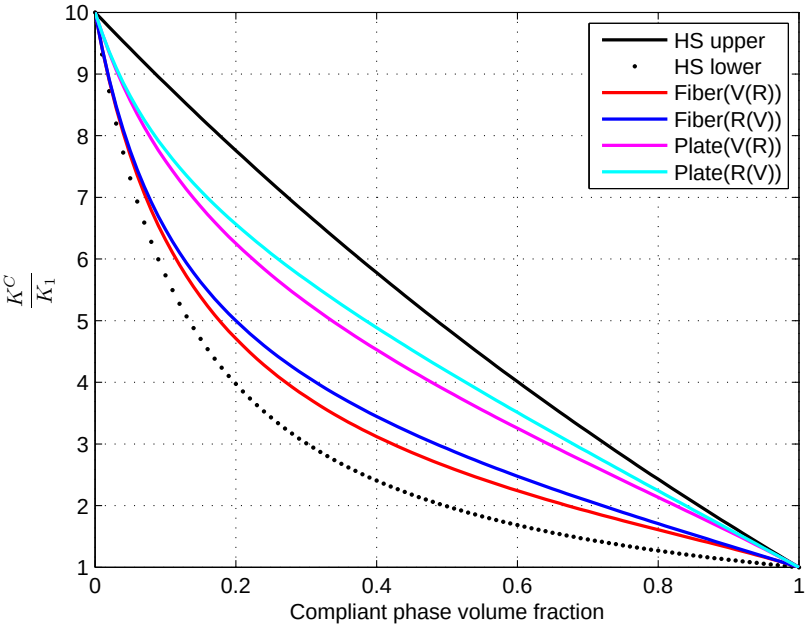

Figure 3.17: The mixed Voigt-Reuss procedure results for $\frac{K_1}{K_2} = 10$ and $\frac{G_1}{G_2} = 100$ compared to the Hashin-Strikman bounds; 'Fiber' corresponds to the cell in Figure 3.14a and 'Plate' corresponds to the cell in Figure 3.14b

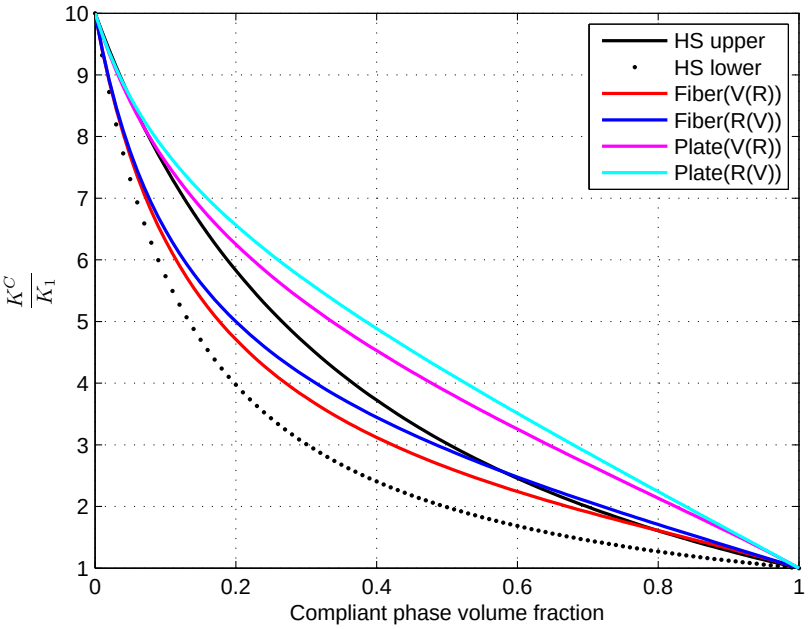

Figure 3.18: The mixed Voigt-Reuss procedure results for $\frac{K_1}{K_2} = 10$ and $\frac{G_1}{G_2} = 10$ compared to the Hashin-Strikman bounds; 'Fiber' corrsponds to Figure 3.14a and 'Plate' corresponds to Figure 3.14b

3.4.2 Influence tensor approach

The discussed in previous subsections approach, is not suitable for the assessment of the effective tensorial properties. Moreover, even for scalar (vectorial) properties like the various conductivities, the validity of the above approach is questionable.
Instead, we shall try to derive the solution using the micromechanical concepts. Let's consider a microscopically heterogeneous solid, consisting of two discrete phases. We make no additional assumptions as to its microstructure. However we do require it to be macroscopically isotropic. We also consider at this point only scalar properties and continue using K as the placeholder for any material constant.
Equations (3.28) in their scalar form are given by the following system of equations

$$\begin{aligned} v_1 a_1 + v_2 a_2 &= 1 \\ v_1 b_1 + v_2 b_2 &= 1 \end{aligned} \tag{3.76}$$

Note that these are two independent equations with four independent unknowns. Note also that influence tensors fully identify the material response and do include an information about the microstructure.
To the above system we can add the homogeneity requirement, expressed through the equivalence of the effective property and reciprocal one.

$$v_1 a_1 \chi_1 + v_2 a_2 \chi_2 = \left(\frac{v_1 b_1}{\chi_1} + \frac{v_2 b_2}{\chi_2} \right)^{-1} \tag{3.77}$$

We need a fourth equation to complete the system. This is yet another opportunity to show that the Hill condition leads to the Voigt and Reuss bounds.

3.4.2.1 Hill condition

The Hill condition, (3.59), in this case is expressed as

$$b_1 a_1 v_1 + b_2 a_2 v_2 = 1 \tag{3.78}$$

since the system contains a polynom of a second degree, it produces two solution branches (this and the following results were obtained using the Mathematica® symbolic math package [45]).

$$\left.\begin{aligned} a_1 = 1 \qquad b_1 &= \frac{\chi_2}{\chi_1 v_1 + \chi_2 v_2} \\ a_2 = 1 \qquad b_2 &= \frac{\chi_1}{\chi_1 v_1 + \chi_2 v_2} \end{aligned}\right\} \quad \text{Branch I} \tag{3.79}$$

and

$$\left.\begin{aligned} a_1 &= \frac{\chi_2}{\chi_1 v_2 + \chi_2 v_1} & b_1 &= 1 \\ a_2 &= \frac{\chi_1}{\chi_1 v_2 + \chi_2 v_1} & b_2 &= 1 \end{aligned}\right\} \quad \text{Branch II} \tag{3.80}$$

The first branch corresponds to the Voigt bound, whereas the second branch to the Reuss bound. QED.

3.4.2.2 Morphological equivalence condition

Using the fact that the influence tensors (by their definition, equation (3.27)), implicitly contain an information about the microstructure, one can formulate the following equivalence condition:

$$a_1 b_1 = a_2 b_2 \tag{3.81}$$

The resulting solution is given again by two branches:

$$\left.\begin{aligned} a_1 &= \frac{\sqrt{\chi_2}}{v_1\sqrt{\chi_2} + v_2\sqrt{\chi_1}} & b_1 &= \frac{\sqrt{\chi_1}}{v_1\sqrt{\chi_1} + v_2\sqrt{\chi_2}} \\ a_2 &= \frac{\sqrt{\chi_1}}{v_2\sqrt{\chi_1} + v_1\sqrt{\chi_2}} & b_2 &= \frac{\sqrt{\chi_2}}{v_2\sqrt{\chi_2} + v_1\sqrt{\chi_1}} \end{aligned}\right\} \quad \text{Branch I} \tag{3.82}$$

and

$$\left.\begin{aligned} a_1 &= \frac{\sqrt{\chi_2}}{v_1\sqrt{\chi_2} - v_2\sqrt{\chi_1}} & b_1 &= \frac{\sqrt{\chi_1}}{v_1\sqrt{\chi_1} - v_2\sqrt{\chi_2}} \\ a_2 &= \frac{\sqrt{\chi_1}}{v_2\sqrt{\chi_1} - v_1\sqrt{\chi_2}} & b_2 &= \frac{\sqrt{\chi_2}}{v_2\sqrt{\chi_2} - v_1\sqrt{\chi_1}} \end{aligned}\right\} \quad \text{Branch II} \tag{3.83}$$

However in this case the second solution branch is not physical since the influence tensors must be finite and well defined for all volume fractions.
The first branch leads to the following expression

$$\chi^{\mathrm{C}} = \frac{v_1\chi_1\sqrt{\chi_2} + v_2\chi_2\sqrt{\chi_1}}{v_2\sqrt{\chi_1} + v_1\sqrt{\chi_2}} \tag{3.84}$$

Figure 3.19 illustrates the difference between the above solution and the Lichtenecker's averaging (3.74). This difference is only significant for a large contrast between the constituents' properties. Like the Lichtenecker's formula, equation (3.84) is also a guess. Both approximations predict zero resulting constant when one of the constituents has a zero-valued constant. Thus, these expressions could be used for properties like the viscosity, but not for stiffness.

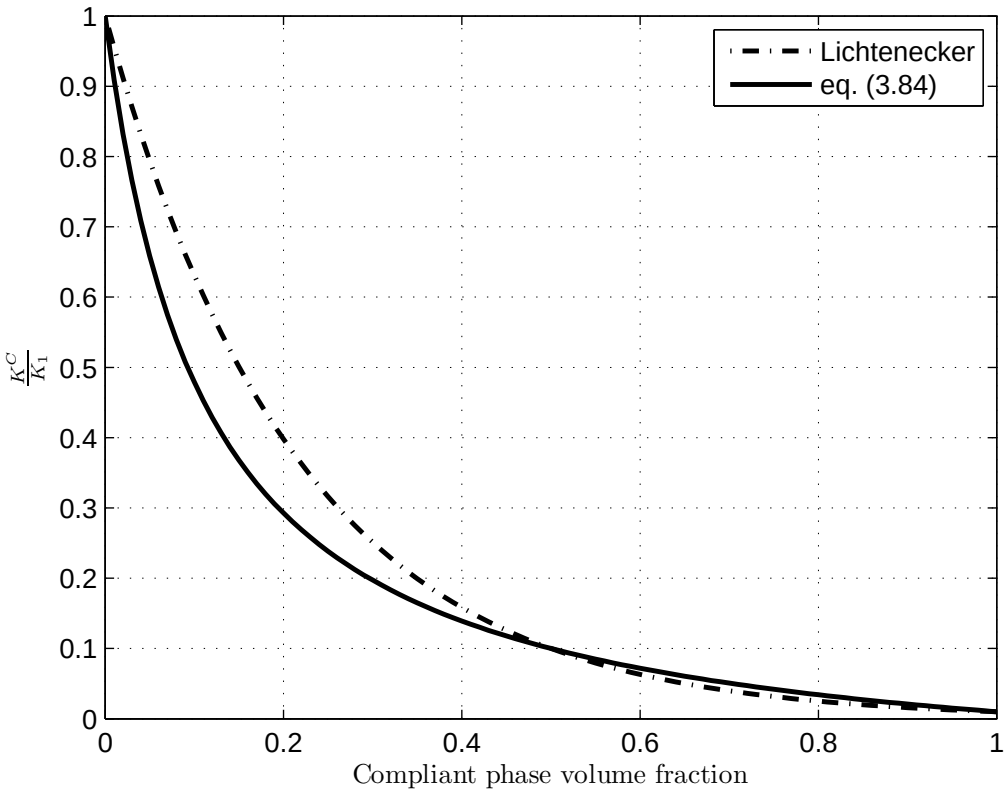

Figure 3.19: The Lichtenecker's approximation vs. equation (3.84) for a material contrast $\frac{K_1}{K_2} = 100$

3.4.2.3 Energy balance

It was shown in subsection 3.3.1 that the complete energy balance must include a dissipation term,

$$b_1 a_1 v_1 + b_2 a_2 v_2 = 1 - d \tag{3.85}$$

where $0 < d < 1$ is the scalar equivalent of the $\mathbf{D} \triangleq -\langle(\mathbb{B} - \mathbb{I}) : (\mathbb{A} - \mathbb{I})\rangle$.
We now have a system of four algebraic equations and five unknowns. The advantage of this representation over others is that the complete solution depends on a single, experi-

mentally measurable parameter. This solution is given by

$$\begin{aligned} a_1 &= \frac{v_1(2\chi_2 + (1-d)(\chi_1-\chi_2)v_2) \pm \sqrt{\Psi}}{2v_1(\chi_1 v_2 + \chi_2 v_1)} \\ a_2 &= \frac{v_2(2\chi_1 - (1-d)(\chi_1-\chi_2)v_1) \mp \sqrt{\Psi}}{2v_2(\chi_1 v_2 + \chi_2 v_1)} \\ b_1 &= \frac{v_1(2\chi_1 - (1-d)(\chi_1-\chi_2)v_2) \pm \sqrt{\Psi}}{2v_1(\chi_1 v_2 + \chi_2 v_1)} \\ b_2 &= \frac{v_2(2\chi_2 + (1-d)(\chi_1-\chi_2)v_1) \mp \sqrt{\Psi}}{2v_2(\chi_1 v_2 + \chi_2 v_1)} \end{aligned} \tag{3.86}$$

where Ψ is given by

$$\Psi = (1-d)^2(\chi_1-\chi_2)^2 v_1^2 v_2^2 - 4d\chi_1\chi_2 v_1 v_2 \tag{3.87}$$

Note that depending on the value of d, Ψ can be either positive, negative or a zero. For a negative Ψ, the resulting effective property χ^{C} has two complex conjugate values, whereas for a positive Ψ, χ^{C} has two real values.
The effective material constant is given by

$$\chi^{\mathrm{C}} = \frac{2\chi_1\chi_2 + (1-d)(\chi_1-\chi_2)^2 v_1 v_2 \pm (\chi_1-\chi_2)\sqrt{\Psi}}{2(\chi_1 v_2 + \chi_2 v_1)} \tag{3.88}$$

Since for any single set of parameters the resulting effective material constant must be unique, Ψ must be always non-positive. Thus, all material constants of heterogeneous materials, for which there exist a potential, are complex in most general case. Since the influence tensors are complex, the corresponding stress and strain fields are complex as well.
Complex material constants are a known 'phenomenon' in electromagnetics, vibration theory and viscoelasticity, with the imaginary part being associated with energy losses or damping.
The imaginary term in equation (3.88) must be positive, which becomes clear when considering equations of damped motion. Usually, a damper is assumed to be viscous, i.e the damping coefficient is velocity dependent and the force equilibrium of a mass on a linear spring with viscous damper is given by

$$\mathcal{M}\ddot{u} = -\mathcal{K}u - \mathcal{C}\dot{u} \tag{3.89}$$

where $\mathcal{M}$ is the oscillating mass, $\mathcal{C}$ is the velocity-dependent damping coefficient and $\mathcal{K}$ is the spring constant. Note that the damping force has the same sign as the spring force.

Let now consider an equation of motion of one-dimensional forced oscillations.

$$\mathcal{M}\ddot{u} + \mathcal{C}\dot{u} + \mathcal{K}u = \mathcal{F}e^{i\omega t} \tag{3.90}$$

It is known, that there exists also a frequency or velocity independent damping - 'internal' / 'material' / 'structural' / 'hysteretic' damping. It was also found that the structural damping is a function of the stiffness as opposed to the viscous one. In the absence of the viscous term, the equation (3.90) was consequently modified to

$$\mathcal{M}\ddot{u} + \frac{\mathcal{K}g}{\omega}\dot{u} + \mathcal{K}u = \mathcal{F}e^{i\omega t} \tag{3.91}$$

where g is a small dimensionless constant. Since ω is not known a priory, two further models were developed, one by Küssner (see in [46]) —-

$$\mathcal{M}\ddot{u} + \mathcal{K}\left(\cos g + i \sin g\right) u = \mathcal{F}e^{i\omega t} \tag{3.92}$$

and another one by Kassner (see in [46]) —-

$$\mathcal{M}\ddot{u} + \mathcal{K}(1 + ig)u = \mathcal{F}e^{i\omega t} \tag{3.93}$$

For small g the difference between the two is negligible and both equations were successfully used for treatment of aeroelastic flutter. For more detailed historical review, discussion of the subject and corresponding references see [46].
In a most general case the LHS of equation of motion should include both the viscous and the structural damping. That the complex stiffness contributes to the damping term, one can see by applying the steady-state solution of the form

$$u = xe^{i\omega t} \tag{3.94}$$

in which case we have

$$(-\mathcal{M}\omega^2 + \mathcal{K} + i(C\omega + \mathcal{K}_{Im}))x = \mathcal{F} \tag{3.95}$$

Considering again equation (3.89) with complex stiffness clarifies the sign of its imaginary component — it must be positive, otherwise the structural damping would accelerate the motion instead of decelerating it.
It seems also that the solution (3.88) is a bridge between the material constitution and the experimentally observed behavior, providing a basis to otherwise phenomenological model of Kassner.
Comparing the real part of the obtained effective constant K with the general equation, obtained from considering the higher-order bounds, (3.71), the dissipation parameter d

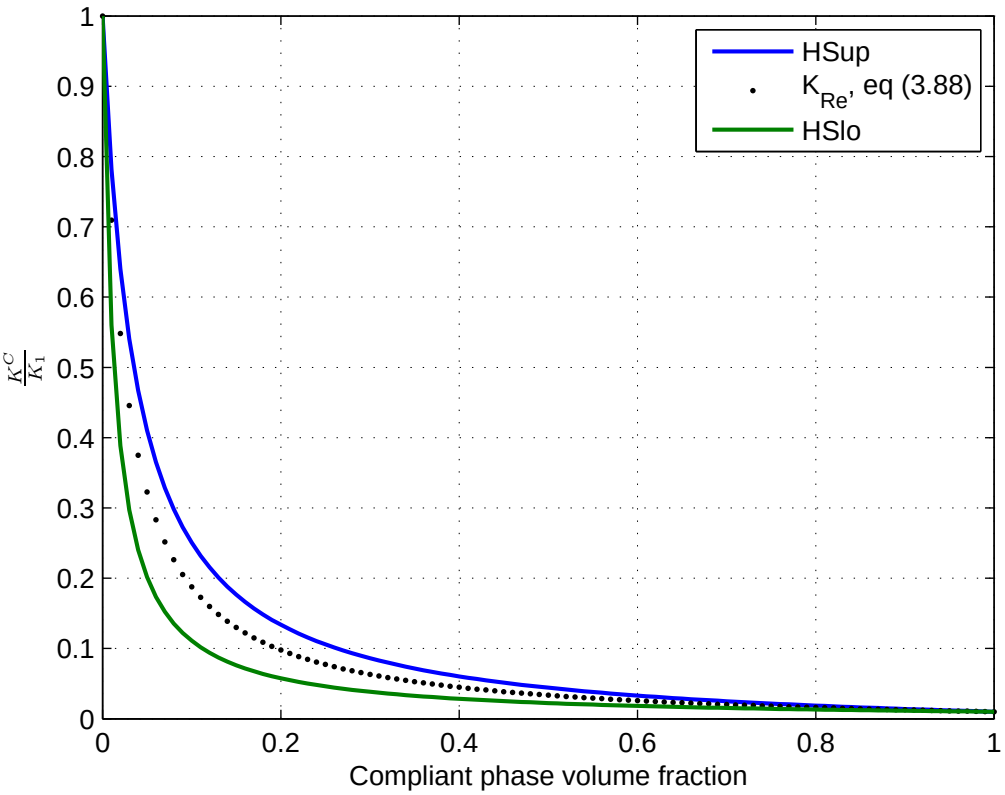

Figure 3.20: The real part of the effective bulk modulus of the interpenetrating phase composite

takes a particularly simple form

$$d = \frac{\chi_1 v_2 + \chi_2 v_1 - y}{\chi_1 v_2 + \chi_2 v_1 + y} \tag{3.96}$$

where y is a function of the microstructural morphology.
As an example we consider expression from Table 3.2 for the upper bound of y for the bulk modulus

$$\frac{4}{3}(\zeta_1 G_1 + \zeta_2 G_2) \tag{3.97}$$

It was concluded in subsection 3.3.4 that the geometric parameter ζ expresses the 'matricity' or the 'connectedness' of the phases. Figure 3.20 depicts the effective bulk modulus of a composite with interpenetrating equivalent phases ($\zeta_1 = \zeta_2 = 0.5$) for a material pair with $\frac{G_1}{G_2} = 10$ and $\frac{K_1}{K_2} = 100$

Chapter 4

Numerical homogenization

Unlike the analytical homogenization, which seeks the conjectures on the effective properties by making assumptions regarding the strain and stress fields, the numerical homogenization is necessarily a solution of a boundary value problem. The problem is set up as a sample with an explicit microstructure, either real or synthetic, and a series of loadings applied to the boundaries of the sample. This problem set up mimics actually various material testing procedures and is often referred to as a virtual or numerical testing.
In the presented work the numerical homogenization methods are divided into two categories: (i) a direct homogenization, where the results of a single solution are considered to be final and (ii) an iterative homogenization, where the results of a single solution are used as a starting point for the next iteration

4.1 Methods

4.1.1 Direct homogenization

The easiest test, both in the laboratory and numerically is the tensile one. It can be displacement or force controlled. In the laboratory the boundary conditions are of the mixed type - two (opposite) sides of the specimen are clamped and the others are free if the specimen is a rod. If the specimen is a plate, there can be four clamped and two free faces. In the numerical set up there are no feasibility limitations on the types of boundary conditions.

4.1.1.1 Displacement controlled loading

Looking at the Hook's law in the Voigt notation (2.41), it is immediately clear that in order to obtain the full stiffness matrix, one has to solve the following six homogeneous load cases (three dimensions):

$$\underset{LC\ 1}{\begin{bmatrix}\varepsilon\\0\\0\\0\\0\\0\end{bmatrix}};\quad \underset{LC\ 2}{\begin{bmatrix}0\\\varepsilon\\0\\0\\0\\0\end{bmatrix}};\quad \underset{LC\ 3}{\begin{bmatrix}0\\0\\\varepsilon\\0\\0\\0\end{bmatrix}};\quad \underset{LC\ 4}{\begin{bmatrix}0\\0\\0\\2\varepsilon\\0\\0\end{bmatrix}};\quad \underset{LC\ 5}{\begin{bmatrix}0\\0\\0\\0\\2\varepsilon\\0\end{bmatrix}};\quad \underset{LC\ 6}{\begin{bmatrix}0\\0\\0\\0\\0\\2\varepsilon\end{bmatrix}} \tag{4.1}$$

where the first three are uniaxial tensile strains and the last three are shear ones.
The corresponding displacements are

$$\underset{LC\ 1}{\begin{bmatrix}u&0&0\\0&0&0\\0&0&0\end{bmatrix}};\ \underset{LC\ 2}{\begin{bmatrix}0&0&0\\0&u&0\\0&0&0\end{bmatrix}};\ \underset{LC\ 3}{\begin{bmatrix}0&0&0\\0&0&0\\0&0&u\end{bmatrix}};\ \underset{LC\ 4}{\begin{bmatrix}0&u&0\\u&0&0\\0&0&0\end{bmatrix}};\ \underset{LC\ 5}{\begin{bmatrix}0&0&0\\0&0&u\\0&u&0\end{bmatrix}};\ \underset{LC\ 6}{\begin{bmatrix}0&0&u\\0&0&0\\u&0&0\end{bmatrix}} \tag{4.2}$$

where $u = \mathrm{d}X\varepsilon$ and $\mathrm{d}X$ is the distance along the sample edge.
These load cases constitute the kinematic uniform boundary conditions (KUBC). The resulting average stress is obtained as the total corresponding reaction force divided by the sample face area

$$\langle\sigma_i\rangle = \frac{\sum f_i}{\frac{n_B}{A}} \tag{4.3}$$

where n_B are the boundary nodes, or by averaging the element stresses

$$\langle\sigma_i\rangle = \frac{\sum\limits_e \sigma_e V_e}{\sum\limits_e V_e} \tag{4.4}$$

4.1.1.2 Force controlled loading

In a case of the force controlled loading, one has to apply the following static uniform boundary conditions (SUBC):

$$\underset{LC\ 1}{\begin{bmatrix}\sigma\\0\\0\\0\\0\\0\end{bmatrix}};\quad \underset{LC\ 2}{\begin{bmatrix}0\\\sigma\\0\\0\\0\\0\end{bmatrix}};\quad \underset{LC\ 3}{\begin{bmatrix}0\\0\\\sigma\\0\\0\\0\end{bmatrix}};\quad \underset{LC\ 4}{\begin{bmatrix}0\\0\\0\\\sigma\\0\\0\end{bmatrix}};\quad \underset{LC\ 5}{\begin{bmatrix}0\\0\\0\\0\\\sigma\\0\end{bmatrix}};\quad \underset{LC\ 6}{\begin{bmatrix}0\\0\\0\\0\\0\\\sigma\end{bmatrix}} \tag{4.5}$$

where the first three are uniaxial tensile stresses and the last three are shear ones.
The corresponding loads are

$$\underset{LC\ 1}{\begin{bmatrix}f&0&0\\0&0&0\\0&0&0\end{bmatrix}};\ \underset{LC\ 2}{\begin{bmatrix}0&0&0\\0&f&0\\0&0&0\end{bmatrix}};\ \underset{LC\ 3}{\begin{bmatrix}0&0&0\\0&0&0\\0&0&f\end{bmatrix}};\ \underset{LC\ 4}{\begin{bmatrix}0&f&0\\f&0&0\\0&0&0\end{bmatrix}};\ \underset{LC\ 5}{\begin{bmatrix}0&0&0\\0&0&f\\0&f&0\end{bmatrix}};\ \underset{LC\ 6}{\begin{bmatrix}0&0&f\\0&0&0\\f&0&0\end{bmatrix}} \tag{4.6}$$

Note however that in case of force controlled loading one has additionally to constrain the rigid body motion.

4.1.1.3 Periodic boundary conditions

Sometimes, the analyzed microstructure is periodic in one, two, or three dimensions. In this case a single periodic unit cell can represent the whole material. The boundary conditions, however, must assure the periodic deformation of the boundaries regardless of the applied load. Hence, the term "periodic BC" means actually a periodic coupling of degrees of freedom on corresponding nodes of the opposite boundaries in addition to other loads or displacements. Using the notation, defined in chapter 2 and using the geometry in Figure 4.1 the periodicity condition can be written as

$$\vec{\mathrm{x}}^{+} - \vec{\mathrm{x}}^{-} = \mathbf{F}(\vec{\mathrm{X}}^{+} - \vec{\mathrm{X}}^{-}) \tag{4.7}$$

or, equivalently as

$$\vec{\mathrm{u}}^{+} - \vec{\mathrm{u}}^{-} = (\mathbf{F} - \mathbf{I})(\vec{\mathrm{X}}^{+} - \vec{\mathrm{X}}^{-}) = \mathrm{d}\vec{\mathrm{u}} \tag{4.8}$$

Note that this equation must be applied pair-wise to all the nodes on the corresponding boundaries. In practice, instead of prescribing the same $\mathrm{d}\vec{\mathrm{u}}$ value at each constraint equation, it is convenient to define a so-called dummy node outside the sample volume

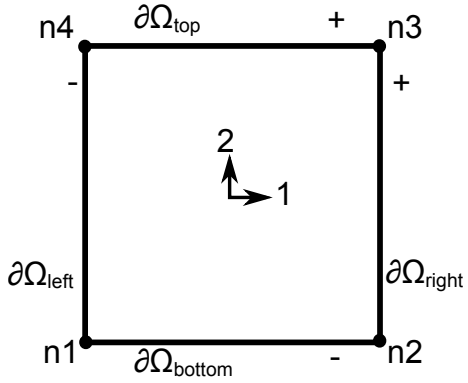

Figure 4.1: A 2D periodic unit cell

Figure 4.2 and tie the displacements of the boundary nodes to that dummy node (see for example [47])

$$\vec{u}^{+} - \vec{u}^{-} = \vec{u}_{di} \tag{4.9}$$

Alternatively, one can use nodes on the sample boundaries (two per coupling direction)

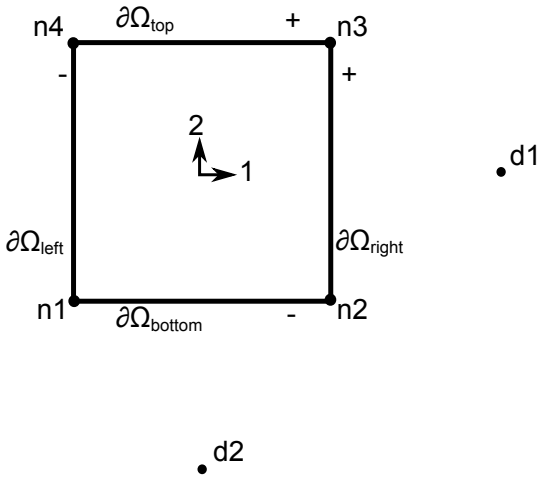

Figure 4.2: Dummy nodes - a practical way of applying PBC

as master nodes and couple the rest to these master nodes (see for example [31])

$$\vec{u}^{+} - \vec{u}^{-} = \vec{u}_{2,4} - \vec{u}_{1} \tag{4.10}$$

It has been noted that periodic boundary conditions deliver better homogenization results than the prescribed displacements or the prescribed tractions, even in the case of non-periodic microstructure. However the periodic coupling requires a mapped mesh on the boundaries, which is not always possible.

4.2 Model types

The analyzed microstructure can be either a simulated one (synthetic), which does not really exist, but its geometric features represent the real one, or a reconstructed one. In the latter case the geometry is reconstructed from the three-dimensional scan of a sample.

4.2.1 Synthetic microstructure

4.2.1.1 Simple random model

This is the simplest model possible. A cubic volume is meshed with $N \times N \times N$ brick elements. All the elements have the attributes of material number one. A set of k unique random integers ($k = v \times N^3$) is chosen from a range $[1, N^3]$, where v is the volume fraction of the second phase. Material properties of the element k_i are changed to those corresponding to material number two. The resulting sample distribution for $v = 0.2$ is shown in Figure 4.3. This model simulates a composite with granular inclusions/clusters at $v <$ percolationthreshold and percolating clusters otherwise.

While this model seems to be overly simplistic, it is actually very flexible. One can for

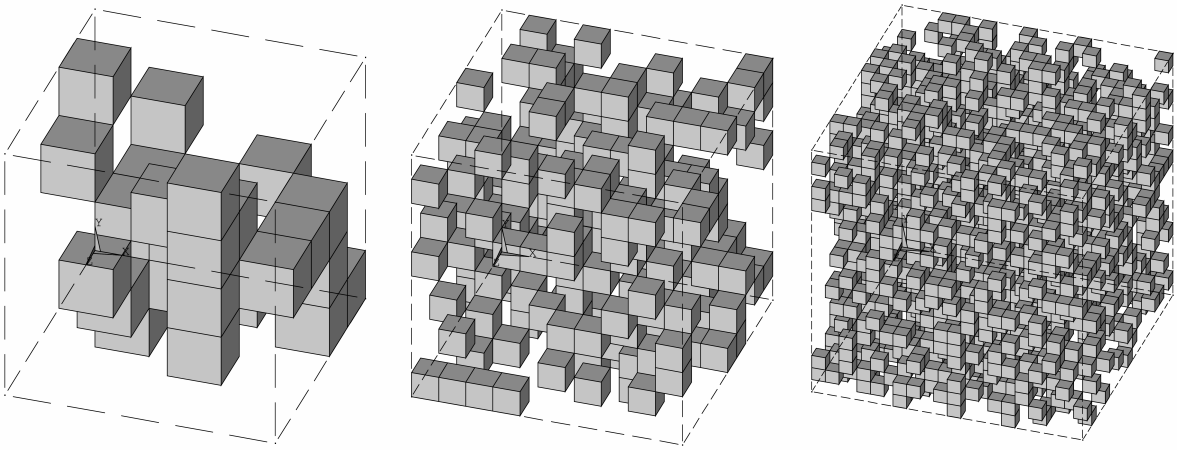

Figure 4.3: Randomly chosen elements with $v = 0.2$ for 5, 10 and 20 elements per edge samples

example use different random distributions to simulate phase gradients, see for example Mishnaevsky [43]. With volume fraction above the percolation threshold, for a cubic lattice - about 30%, one obtains interpenetrating phases.

This model can be used to assess all the thermomechanical properties of the composite like the stiffness, thermal conductivity, thermal expansion coefficient. The usefulness of this model can be illustrated by the direct comparison with the results of a real microstructure (foam based composite, subsection 4.2.2), Figure 4.4.

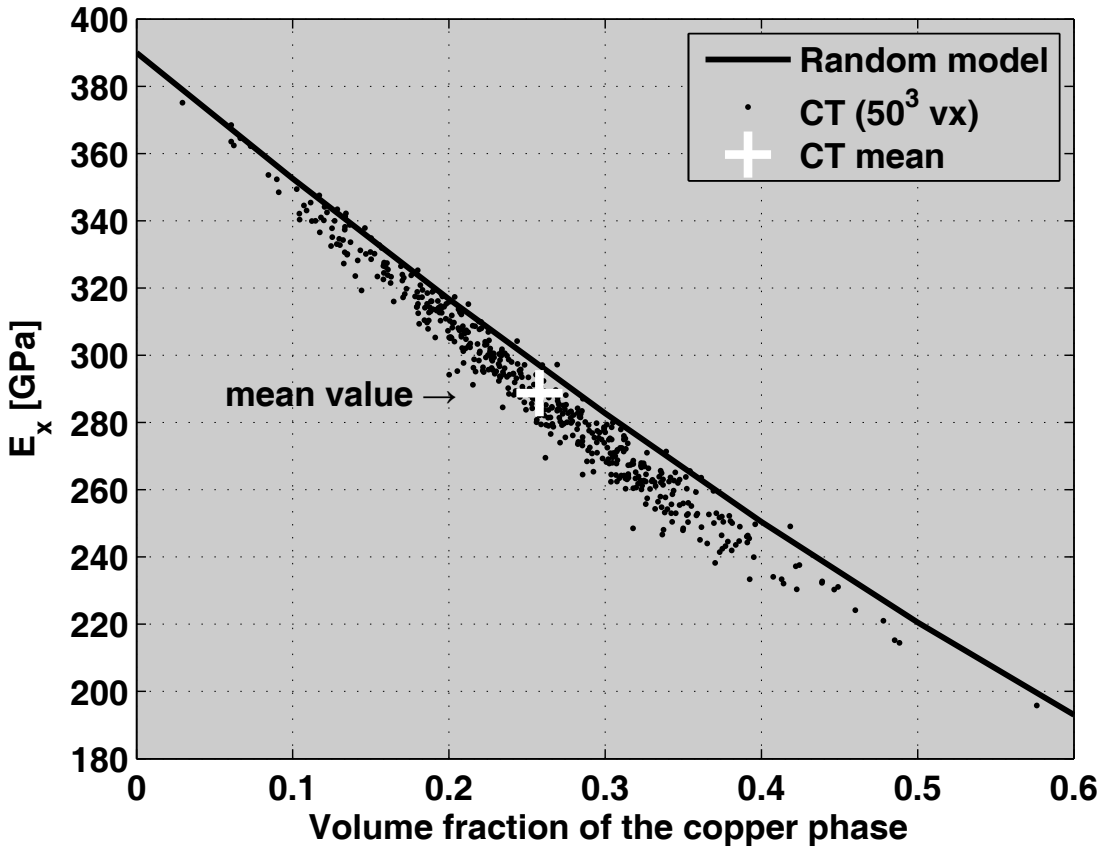

Figure 4.4: Young's modulus of a simple random model vs real composite microstructure, obtained via X-Ray computer Tomography

4.2.1.2 Random network model

Below the percolation limit, the simple random model represents a particle reinforced composite. If the goal is to obtain interpenetrating microstructure at low volume fractions, the procedure must be slightly modified.
A set of m ($m < k$) unique random integers is chosen and the corresponding elements' properties are changed (initial "seed"). Then, for each seed element i ($i \in [1, m]$), a random Cartesian direction is chosen and j elements adjacent to seed(i) are changed in the chosen direction (j is the length of the random branch). The seed(i) is replaced with the last element of the new branch. These steps are repeated until the desired volume fraction is reached. The resulting sample network for $m = 5$, $j = 6$ and $v = 0.1$ is shown in Figure 4.5. This model simulates a fiber-reinforced composite at $v <$ percolationthreshold and interpenetrating networks otherwise. Note that the percolation threshold of this model is lower than that of the previous one.

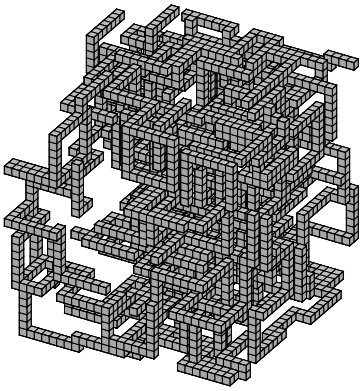

Figure 4.5: Randomly built network with seed = 5 and branch length = 6 elements for $v = 0.1$; 30 elements per edge samples

4.2.1.3 Periodic unit cell

Many geometries are either periodic in one or more spatial directions or can be considered as such. Common examples are crystal lattices, honeycombs, unidirectional fiber reinforced composites, some laminates, foams and others. For these geometries the RVE can be reduced to a single periodic unit cell.
With regard to the interpenetrating composites, the simplest periodic model so far is the three-dimensional cross Figure 4.6, described in the introduction and in section 3.4.

The advantage of this model is the fact that the step of building the geometry can be

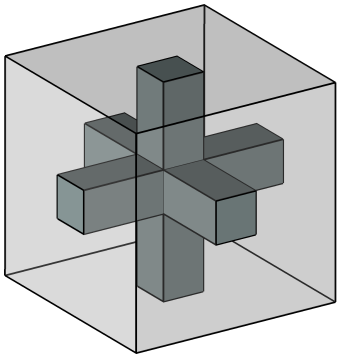

Figure 4.6: The 3D cross geometric representation of the interpenetrating composite

eliminated. To build the model, one can use the same procedure as described in subsection 4.2.1.1, however, instead of modifying random elements, one has to modify particular ones. Its inherent drawback - one can not simulate an isotropic composite using this geometry. It is orthotropic by definition.
A much better model is obtained using a tetrahedron instead of a cross geometry. It can also be inscribed in the cube Figure 4.7 and it is also the only one who's dual is also a

tetrahedron, Figure 4.8. This means that the composite cell is absolutely symmetric with regard to phase interchange.

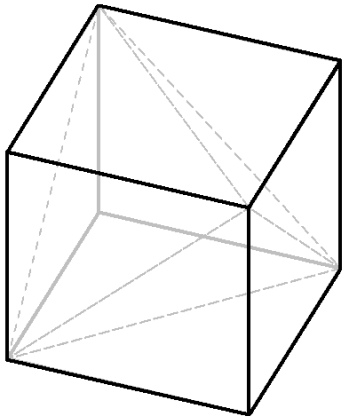

Figure 4.7: The cubic cell with an inscribed tetrahedron

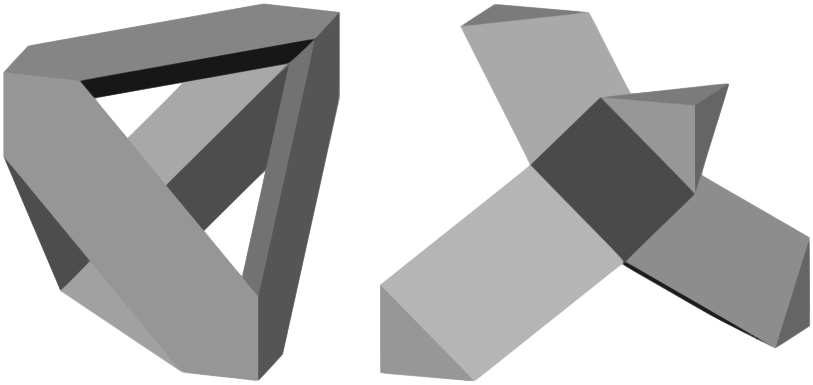

(a) Phase 1 **(b)** Phase 2

Figure 4.8: Complementary tetrahedral networks

This cell is not periodic with regard to its geometry, however it represents a one-eights of the symmetric and periodic unit cell depicted in the Figure 4.9. Since the faces of the basic cell are also the symmetry planes of the master cell, the material symmetries and thus also the properties of these cells are identical.
Note that this unit cell has four planes with hexahedral symmetry and another four planes with cubic symmetry. Consequently, it is a much better approximation for the isotropic composite with symmetric interpenetrating phases. Figure 4.10 illustrates the agreement between the results of the tetrahedral unit cell for an alumina-copper material pair with the analytical approximation, (3.88) with the dissipation parameter d from (3.96) for $\zeta_1 = \zeta_2 = 0.5$.

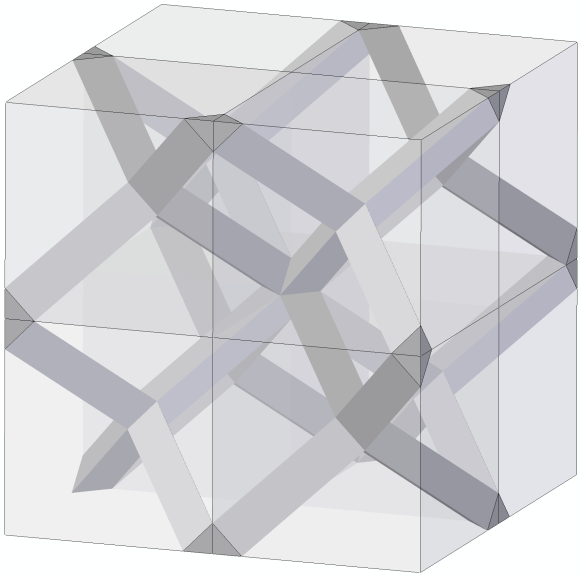

Figure 4.9: The periodic master cell formed from eight basic tetrahedrons

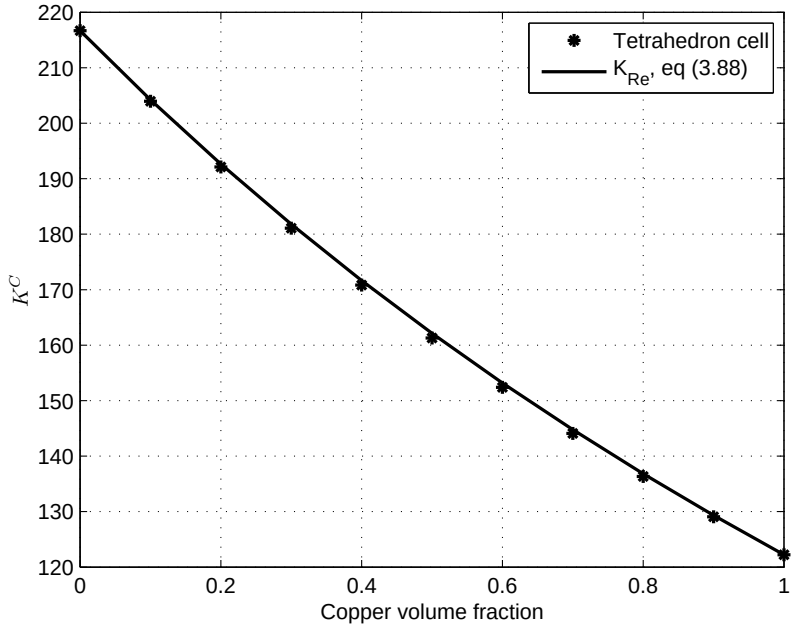

Figure 4.10: A comparison of the tetrahedral unit cell results with the analytical approximation, (3.88)

4.2.2 "Real" microstructure

The real microstructure is a reconstructed three-dimensional image of the sample, obtained in a series of scans. The scans are performed using X-Ray Computer Tomography (CT) technology.

4.2.2.1 Samples

For our purposes we use the CT scans of samples produced in the materials science department of the TUD in the framework of the KMM network of excellence. All the samples were produced using the *lost preform* technique. In a general outline this technique consists of the following steps:

- preparation of the ceramic emulsion (slurry)
- choosing a polymeric or organic preform (place holder)
- slip casting the ceramic emulsion into the voids of the preform
- drying the sample
- burning the preform out and subsequently sintering the ceramics
- infiltrating the sintered ceramic sample with molten metal
- cooling to the room temperature

To form the interpenetrating network three different preform types were used

- polymeric foam
- felt (both polymeric and natural)
- starch (rice and corn)

Figure 4.11 shows the typical microstructures, obtained from the CT scan (the upper) and with the High Resolution Scanning Electron Microscope (HRSEM, lower two).
For more details see for example Prielipp et al [48], Hoffman et al [49] or Studart et al [50].
The composite samples were subsequently cut into small disks of ~ 5.5 [mm] diameter and ~ 4.5 [mm] height and scanned at the Austrian Foundry Research Institute, Leoben, Austria.

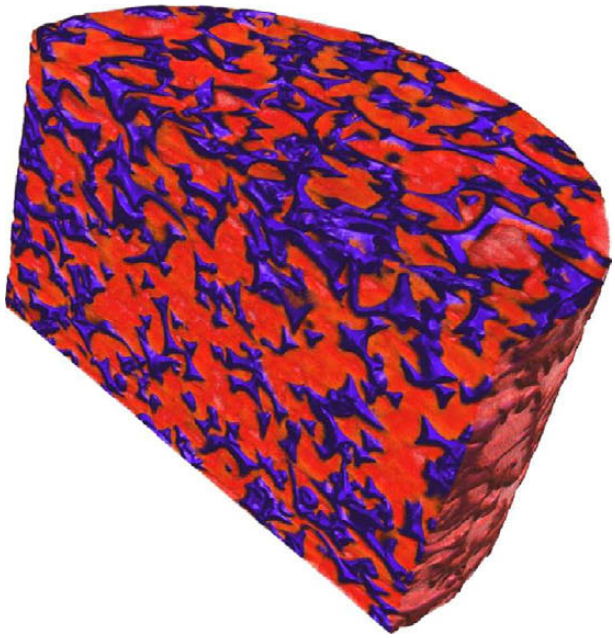

(a) CT scan of foam based composite

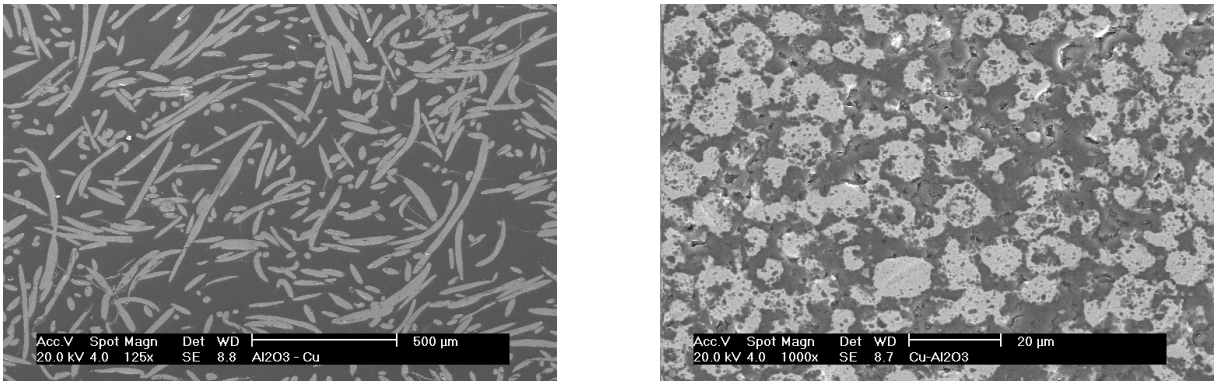

(b) HRSEM micrograph of felt based (left) and starch based (right) composites

Figure 4.11: The three types of the microstructure as function of the preform, (the HRSEM pictures are courtesy of J. Winzer, NAW, Materialwissenschaften, TU Darmstadt)

4.2.2.2 Image data

The obtained raw data is organized as a three-dimensional matrix with intensity values sorted by coordinates (first x, then y and finally z). The distance between two points is the resolution of the scan. In case of the foam-based samples it was about 10 μm, whereas the other types where scanned with the resolution of 4.85 μm.
Figure 4.12 depicts some typical CT slices of the various composite samples. The ceramic phase is the darker one. Note the noise around the sample, non-uniform light intensity inside the samples and structural defects like incomplete metal infiltration, or, the opposite, metal drops. The structural defects are a consequence of the imperfect manufacturing process and can be cropped out, unless the influence of such defects is the main purpose

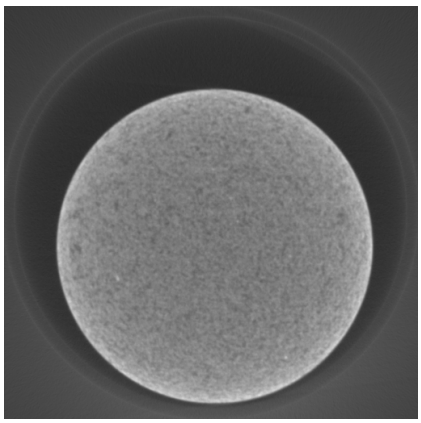

(a) Starch 30%

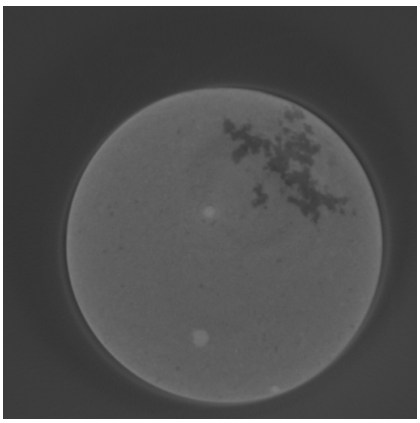

(b) Starch 60%

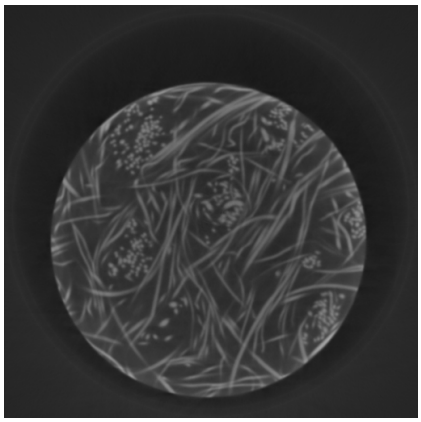

(c) Felt 25%

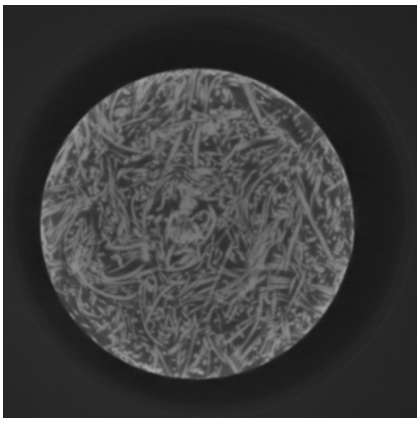

(d) Felt 50%

Figure 4.12: Typical axial slice

of the analysis. The noise and non-uniform intensity, however, are scan artifacts that may prevent a reliable image reconstruction. The image reconstruction is based on the separation of the phases using the intensity values. The noise and the non-uniform intensity may alter the reconstructed microstructure.

4.2.2.3 Noise

The noise around the sample appears to be uniform and is assumed to remain uniform inside the sample with negligible effect on the structural information (given a sufficient signal to noise ratio).

4.2.2.4 Non-uniform intensity

Viewing only the sample region in Figure 4.12, one can notice that the image intensity possesses an axial symmetry. The center of the sample appears darker than its edge. This artifact is the so-called 'beam hardening' effect [51], caused by the thickness dependent absorption of the polychromatic beam. Using this axial symmetry, the following generic correction algorithm was developed:

Algorithm 1 Removal of the beam-hardening effect

1. Trace the boundary of the sample and compute the center and the radius.
2. Divide the axial slice into N discs of thickness dR.
3. For each disc compute its mean luminance intensity $\bar{I}_i$ and store it as a function of the corresponding radius R_i.
4. Smooth the resulting radial intensity function using appropriate spline.
5. Find an inverse intensity function I^{-1} such that $I(R_i)I^{-1}(R_i) = \text{Const}$.
6. Multiply each pixel (voxel) value of the i-th disc with the corresponding value of the inverse intensity function.

This algorithm was implemented in Matlab®[52] using the image processing and spline toolboxes. The amount of discs is chosen to be equal to the sample radius (rounded to the lowest integer) with width of two pixels. Figure 4.13 depicts a typical mean radial intensity distribution and its smoothing spline. Basically, algorithm 1 can not be used for images with large structural defects. In these cases one can however apply a correction function from a 'good' slice, since the beam hardening effect is not a function of the axial location. The result of this correction scheme is shown in the Figure 4.14.

4.2.2.5 Segmentation

To finally separate the phases, one must choose an appropriate threshold value. Knowing the volume fractions of the tested sample it is possible to adjust the threshold to the corresponding value. However, this is not always possible. The experimentally measured values, correspond to the volumetric average of a much bigger sample than that which was scanned. This average includes also all the existing defects like the incomplete metal infiltration or bubbles. The small CT sample does not necessarily represent the bigger one, from which it was cut. Moreover, to remove some of the scan artifacts, one must choose a homogeneous region, which definitely does not represent the original sample.

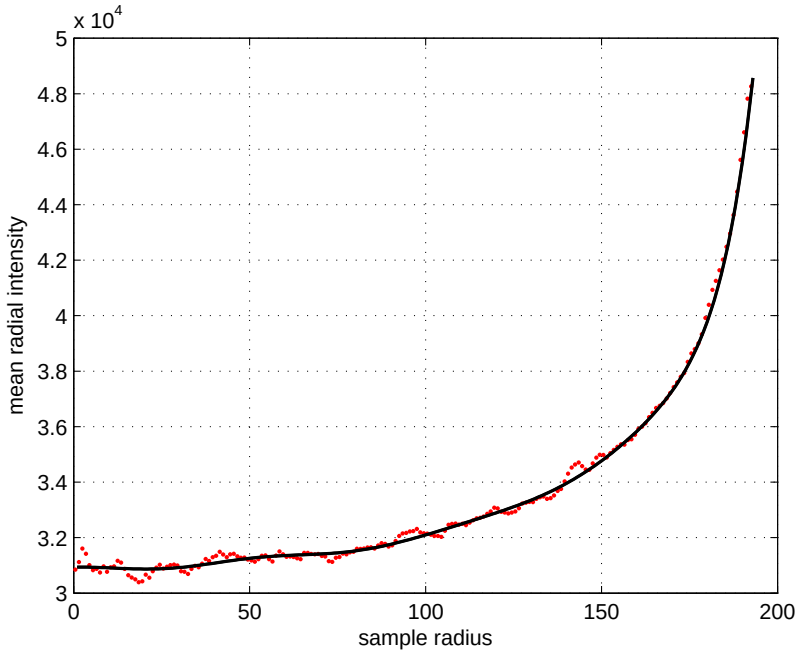

Figure 4.13: A typical radial intensity distribution, red dots, and the smoothing spline, black line

For the above reasons, the threshold in our case is determined by the built-in Matlab function "graythresh" from the image processing toolbox. This function chooses the threshold that "minimizes the intraclass variance of the black and white pixels" [52]. The result is shown in Figure 4.15. Using this threshold, one can binarize the image and directly translate it to finite element model. This is the so called *voxel-based approach*, where one voxel (volume element, as derived from pixel - picture element) corresponds to one finite element. Figure 4.16 shows the metallic phase of the felt-based composite reconstructed in Matlab Figure 4.15b, represented as finite elements. This approach is straight forward and simple, but has two inherent drawbacks. The first drawback is that it leads to stepwise interfaces between the two materials, see e.g. Figure 4.16b. Such interfaces make it impossible to analyze the inelastic behavior of the composite.

The second one is the resulting size of the model. For example, in our case the CT datafiles of the sample have sizes of $800 \times 800 \times 512$ and 512^3 voxels, which is a tremendous amount in terms of finite elements. Even after considering only a sub-volume of it, say of size $400 \times 400 \times 400$, it sums to $64e + 6$ elements (i.e. about $200e + 6$ DOFs for simple 8-node brick elements).

Although it might not be possible to analyze the whole sample at once on an average workstation, a partition into sub-volumes makes it feasible to obtain an approximation for the whole sample by averaging the results of all the sub-volumes. Figure 4.17 illustrates the effect of the partition of the same sample into sub-volumes of different sizes

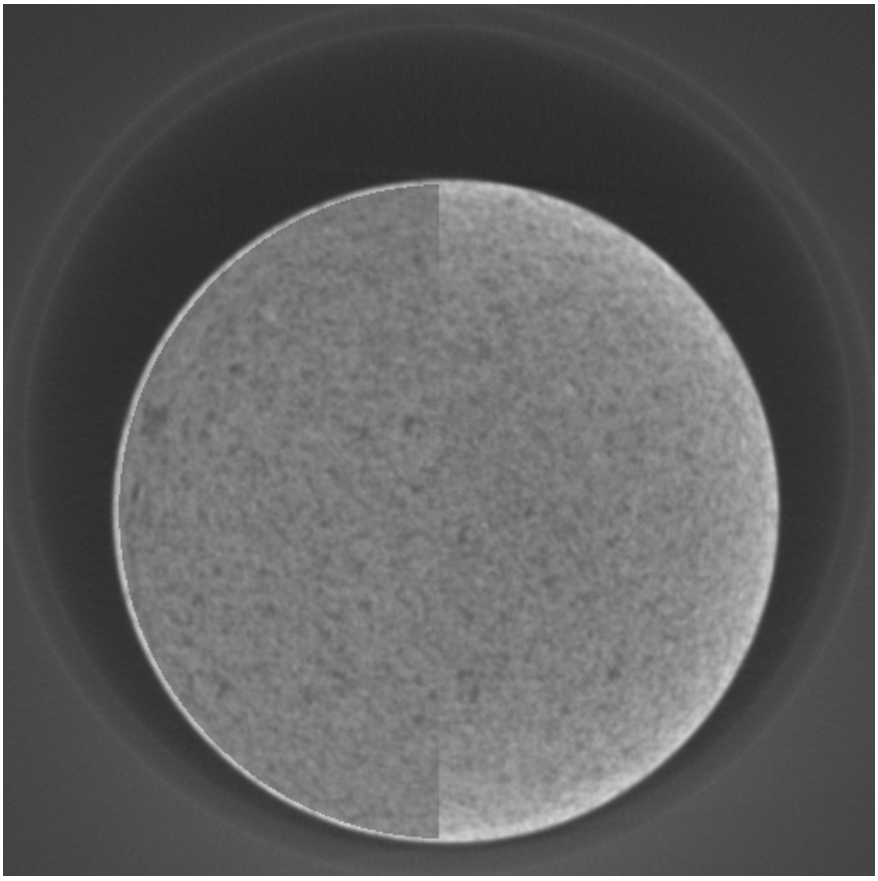

Figure 4.14: Before and after the correction (the left half of the corrected image superimposed on the original one)

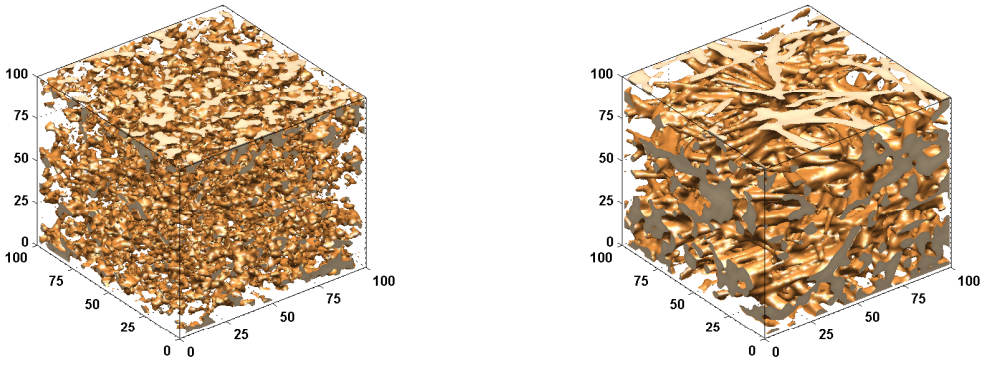

(a) Starch-based **(b)** Felt-based

Figure 4.15: Metal phase of reconstructed from the CT scans of starch-based and felt-based composites

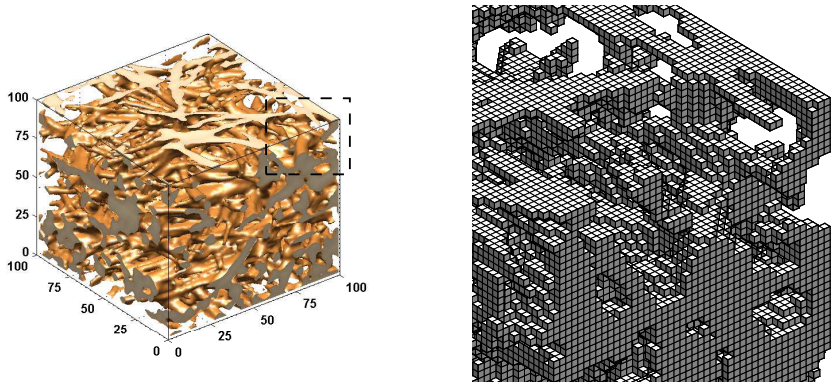

(a) The full sample **(b)** Zoom: upper right corner

Figure 4.16: Voxel-based mesh of the metal phase shown in Figure 4.15b

(foam-based alumina-copper composite). Note that although the size of 100^3 voxels is

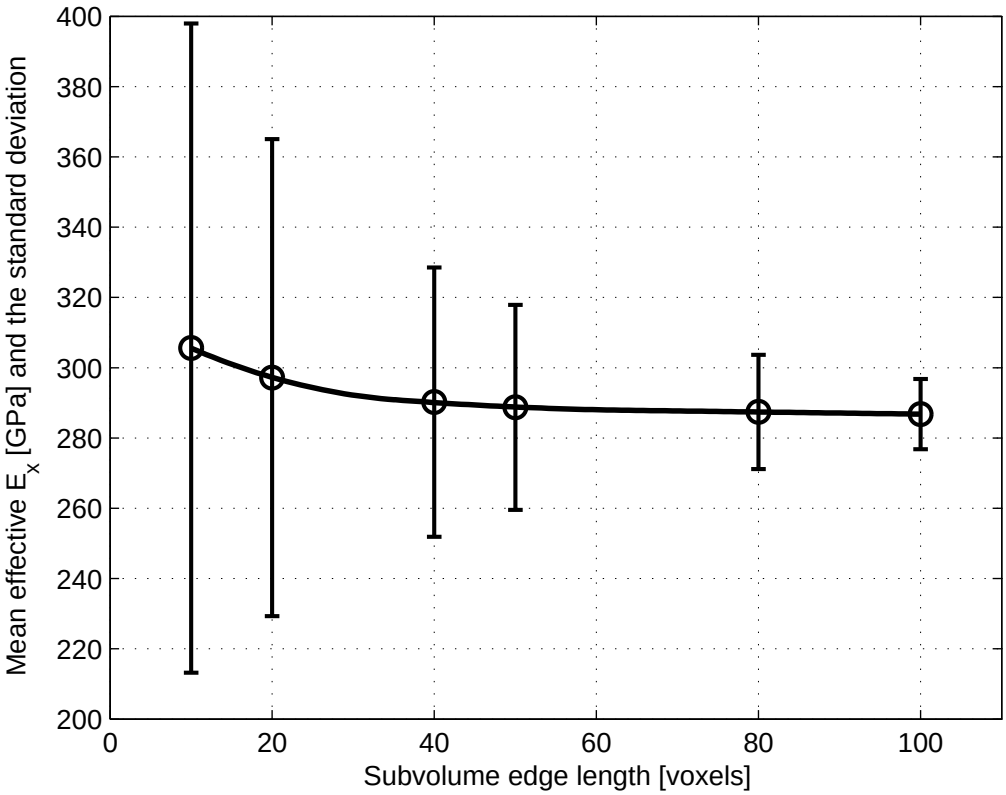

Figure 4.17: Dependence of the mean Young's modulus of the foam based composite (Figure 4.11a) on the sub-volume size

still smaller than the RVE (the scatter is still present), the average value can be considered as converged already at the size of 50^3 voxels. Below that size the accuracy of the approximation reduces with the decreasing size of the sub-volumes.

4.2.2.6 CT data reuse

Numerical analysis often raises the need for parametric studies, where only one parameter is allowed to change. With regard to the homogenization, the single most important parameter is the volume fraction. Basically, to perform such study, one would need to manufacture and scan a batch of samples. However, the process is long, numerically expensive and, most important, there is absolutely no way to make sure that the samples will differ in their volume fractions only.

Fortunately, there is a very simple solution. The volume fractions of the reconstructed phases are direct functions of the threshold value, used during the segmentation. It follows that by changing the threshold, one can obtain many digital samples with varying volume fractions from a single CT scan. Of course, a threshold that differs too much will cause many structural features to disappear. Small variations, however, will only slightly move the interfaces back and forth without changing their shape. For small variations in threshold value, the volume fraction is the only affected parameter. Figure 4.18 illustrates the results of the threshold variation within ±10% of the nominal value Figure 4.19 for the foam based composite, shown in Figure 4.11a. It shall be noted that in case the

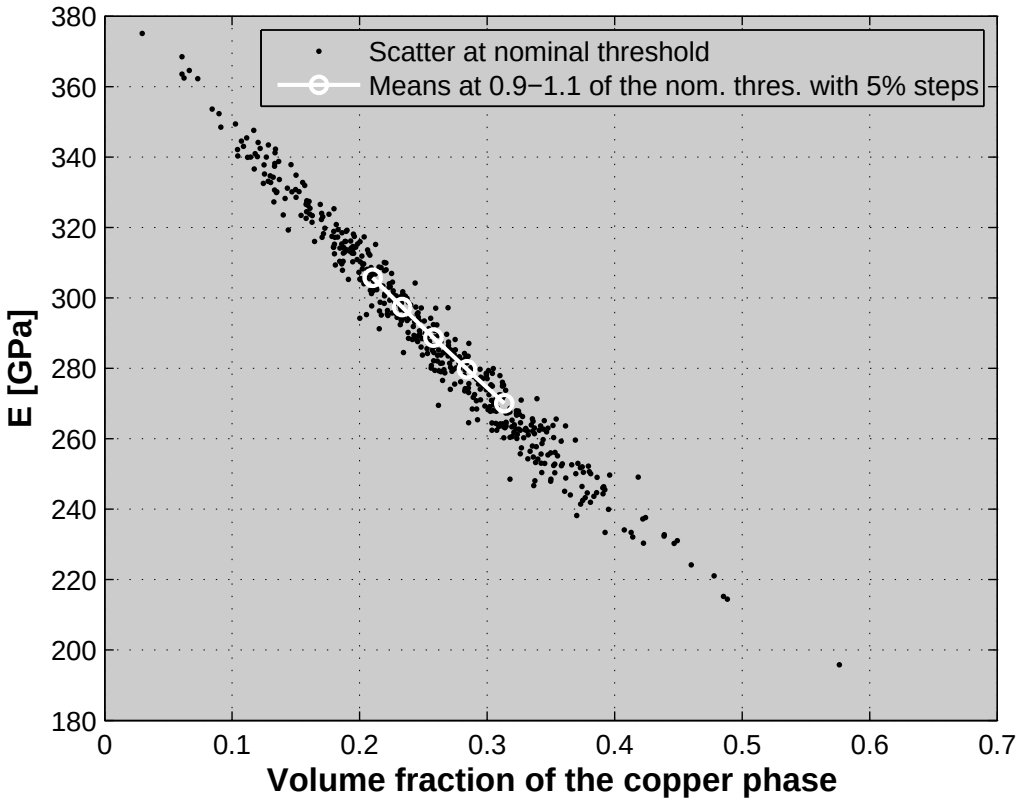

Figure 4.18: The effect of the threshold value variation

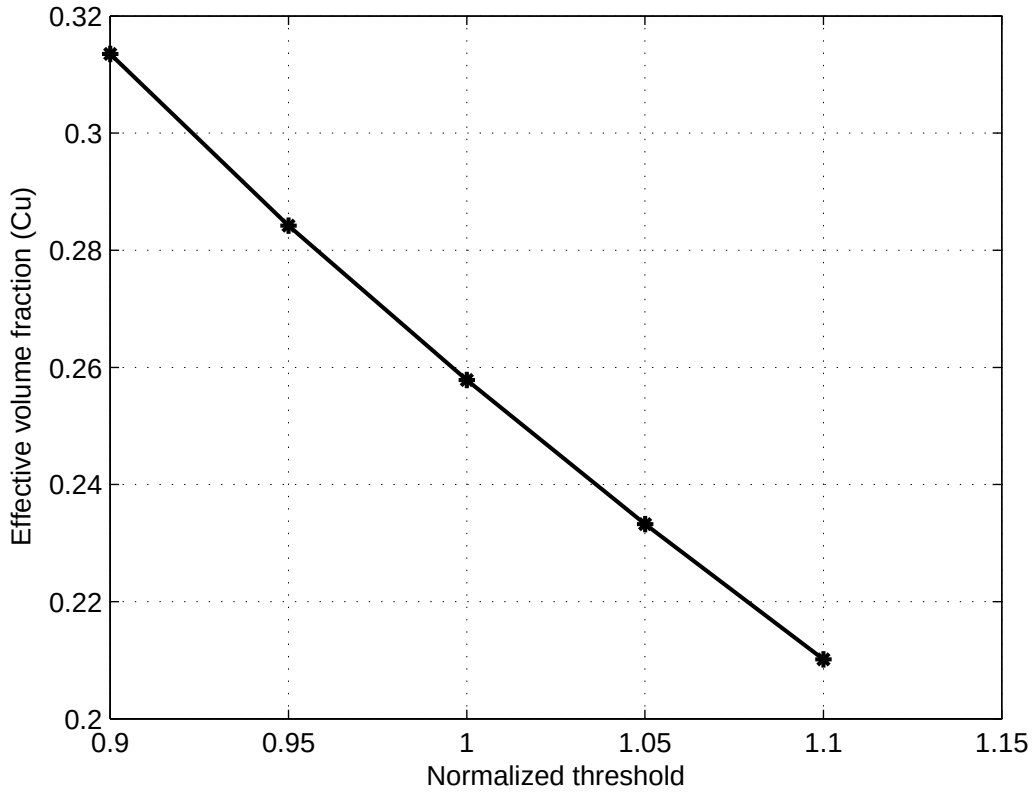

Figure 4.19: The change of the effective volume fraction due to the threshold value variation

vertical scatter of the sub-volumes reduces to a line, one can assume that statistically, volume fraction is the only parameter that varies between the sub-volumes. This is the case shown in Figure 4.20, where due to a bigger sub-volume size (64^3 vx) and better resolution (4.85 μm instead of 10 μm) the vertical scatter is almost zero. This figure compares the results of the scanned corn starch based and wool felt based composites with the experimental values of the wool & polypropylene felt based and corn & rice starch based composites with interpenetrating phases. In general, most of the experimental values do not match the finite element analysis due to the discussed earlier manufacturing defects, present in the bigger experimental samples and excluded from the reconstructed images.

4.3 Treatment of the materials' interface

The voxel-based approach, discussed above, places strong limitations with regard to the mesh generation and to the study of the interface-related problems. It is practically impossible to perform mesh convergence studies, since the size and the shape of the

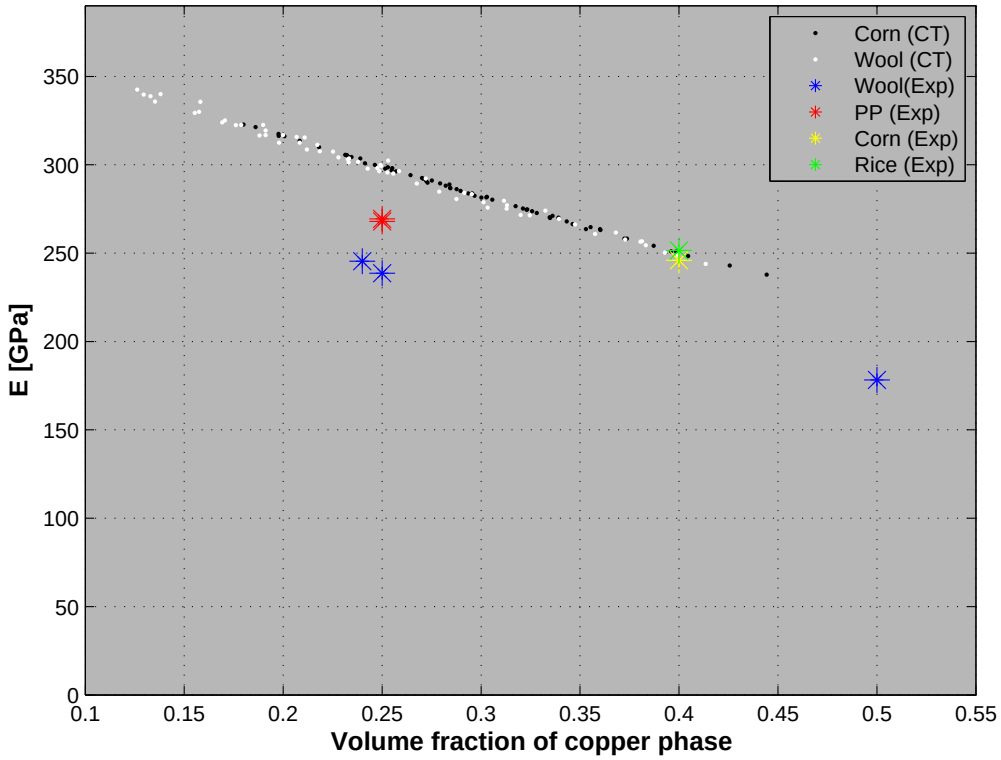

Figure 4.20: Starch (corn, rice)and felt (wool, polypropylene) based composites - FE vs. experiment (experimental values were obtained using the impulse excitation technique [53], data source: J. Winzer, NAW, Materialwissenschaften, TU Darmstadt)

elements are hardwired to the scan grid. It is also impossible to study the interface damaging processes and phases separation. To resolve these limitations, one has to either create an interface-conforming mesh, or to change the formulation of the finite element.

4.3.1 Interface conforming mesh

The threshold, used to separate the phases, defines actually an isosurface in a scalar-valued volumetric data-set. This surface (the material interface) can be easily extracted with the aid of the 'marching cubes' algorithm [54], [55], widely used in the graphics industry. It can then be used to create the finite element mesh. As an alternative, one can implement the algorithm as an additional step after the creation of the voxel-based mesh Figure 4.21. The problem with this approach is the inherently low quality of some elements as seen in the Figure 4.22. The marching cubes algorithm checks every single voxel by comparing the values at its vertices with the threshold defining the isosurface. For any two vertices connected by an edge, if both values are above or below the threshold —- there is no intersection with the surface. However if one value above and the other one below the

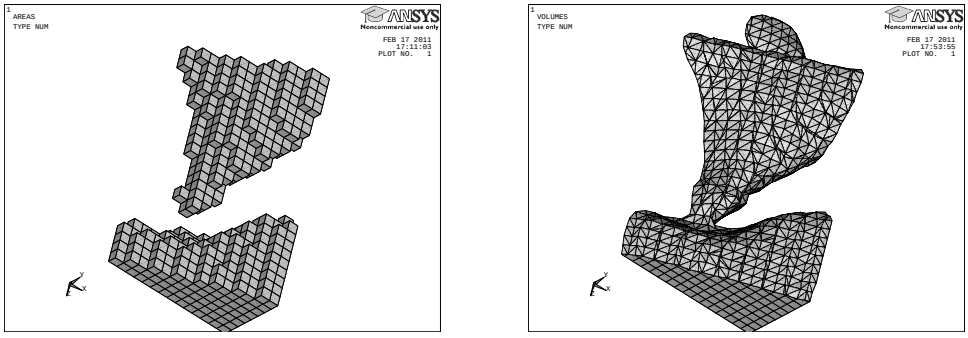

(a) Step-wise interface **(b)** Smoothed interface

Figure 4.21: The marching cubes algorithm applied to voxel-based mesh

threshold —- there is an intersection. The location of the intersection along the voxel edge is found by a linear interpolation. As soon as all such points are found, they are connected together to form triangular areas that define the isosurface. If the value of one of the vertices is very close to the threshold, the resulting intersection point is located near the voxel vertex and the resulting triangle base is very short. This is of course of no importance for graphical applications, but for finite element analysis one must then employ additional steps to remove or improve such elements.

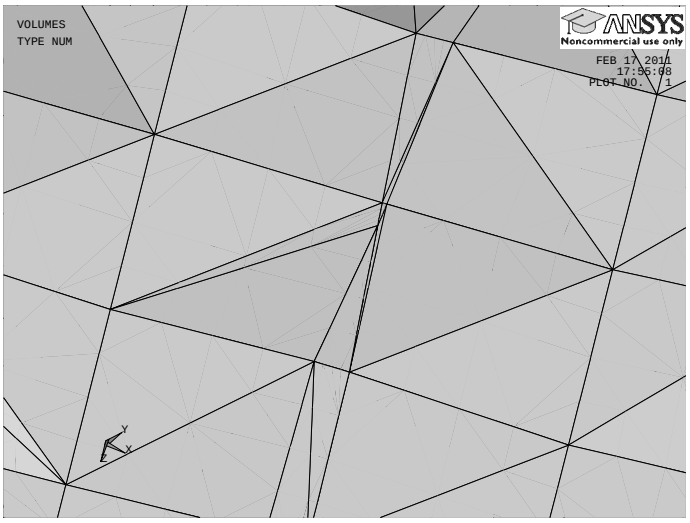

Figure 4.22: Elements with angles approaching 0^o and 180^o and with tiny areas

4.3.2 Intra-element phase separation

Another interesting possibility to account for the interface is to treat it at the element formulation level. Zohdi and Wriggers [27] have shown that a $5 \times 5 \times 5$ Gauss integration rule for a simple tri-linear element, integrates the elemental quantities with at most 2% integration error in the case that the material interface passes through the element. Accurate integration is, however, just one of the issues. Another issue is, for example, the fact that an interface must change the element stiffness to an anisotropic one. One can see the element with an interface as a bi-linear composite. Hence if for example the two phases are isotropic, the resulting element stiffness must possess transversal isotropy. This change from two isotropic stiffness matrices to one anisotropic can not be addressed by the integration alone. This aspect has not been treated yet.
A somewhat related, but actually much more advanced approach, is the so called FE^2, where each integration point is considered to represent a micromodel which must be separately homogenized [31]. FE^2 allows to incorporate for example a microstructural damage evolution into the macroscopic model. However, increased capabilities come at a price of increased computational effort, requiring parallel computing resources.

4.4 Iterative homogenization

To reduce the interaction between the boundary conditions and the analyzed microstructure, Dietrich et al [56] have developed the "embedded cell model" for microstructures which are periodic in loading direction. The model was subsequently extended to non-periodic two-dimensional [57–59] and three-dimensional composites [58]. In this model, the analyzed specimen (the cell) is surrounded by a layer of 'equivalent' material. The properties of the equivalent material are determined in an iterative self-consistent manner and as soon as these converge, the properties of the inner cell are obtained by averaging the stresses and strains in the cell.
Dong and Schmauder [60] observe later that "If the dimension of the embedding composite is sufficiently large compared to the embedded cell, the external geometry boundary conditions introduced around the embedding composite are almost without influence on the composite behavior of the inner embedded cell" and also "It has been found from systematic studies over a wide parameter range that convergence to the final stress strain curve of the composite is independent on the initial mechanical behavior of the embedding composite". In other words, the method should be insensitive neither to the initial guess, nor to the boundary conditions.
Since no analytic proof of the method convergence has been found in the corresponding

literature, and the terms "sufficiently large" and "almost without influence" need further clarification, we attempt to fill these gaps.

4.4.1 Algorithm

The embedded cell model Figure 4.23 is obtained by wrapping the original sample with a layer of some homogeneous material. It can be expected that in case the stiffness tensor

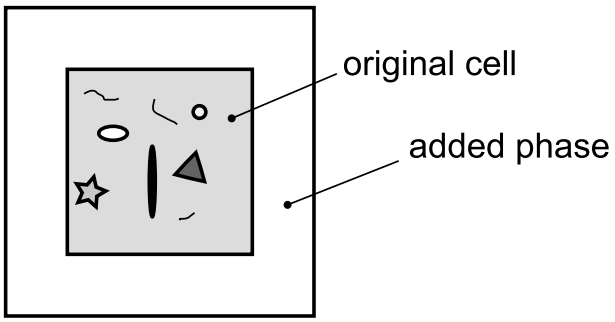

Figure 4.23: A unit cell surrounded by an additional phase

of the wrapping material $\mathbb{C}^{added}$ is exactly the same as the effective stiffness of the original composite $\mathbb{C}^{\mathrm{C}}$, the wrapping material will not affect the overall behavior. In reality, the stiffness of the added phase differs, since the effective stiffness of the original composite is not known a priori. However, the resulting total effective stiffness (original + added) $\mathbb{C}^{total}$ will be always closer to $\mathbb{C}^{\mathrm{C}}$ than $\mathbb{C}^{added}$ to $\mathbb{C}^{\mathrm{C}}$ i.e.

$$\|\mathbb{C}^{added} - \mathbb{C}^{\mathrm{C}}\| > \|\mathbb{C}^{total} - \mathbb{C}^{\mathrm{C}}\| \tag{4.11}$$

For the purpose of measuring the 'distance' between the matrices we use the Frobenius norm [61], defined as

$$\|A\| = \sqrt{Tr\, AA^T} \tag{4.12}$$

According to the observation (4.11), each subsequent iteration improves the initial guess by substituting the result of the previous step in to the guess of the next one. The iterative procedure can be outlined as: The first three iterations are illustrated in Figure 4.24 for the case $\|\mathbb{C}^{\mathrm{C}}\| > \|\mathbb{C}^{added}\|$.

Algorithm 2 Iterative homogenization procedure

Step 1: guess the initial stiffness tensor for the added phase ($\mathbb{C}_0^{added}$)

Step 2: find the effective stiffness of the resulting three-phase composite ($\mathbb{C}_i^{total}$)

Step 3: if the stopping criterion is fulfilled - stop. Else,

Step 4: update the guess ($\mathbb{C}_i^{added} = \mathbb{C}_{i-1}^{total}$)

Step 5: repeat steps 2-4 until the stopping criterion is fulfilled.

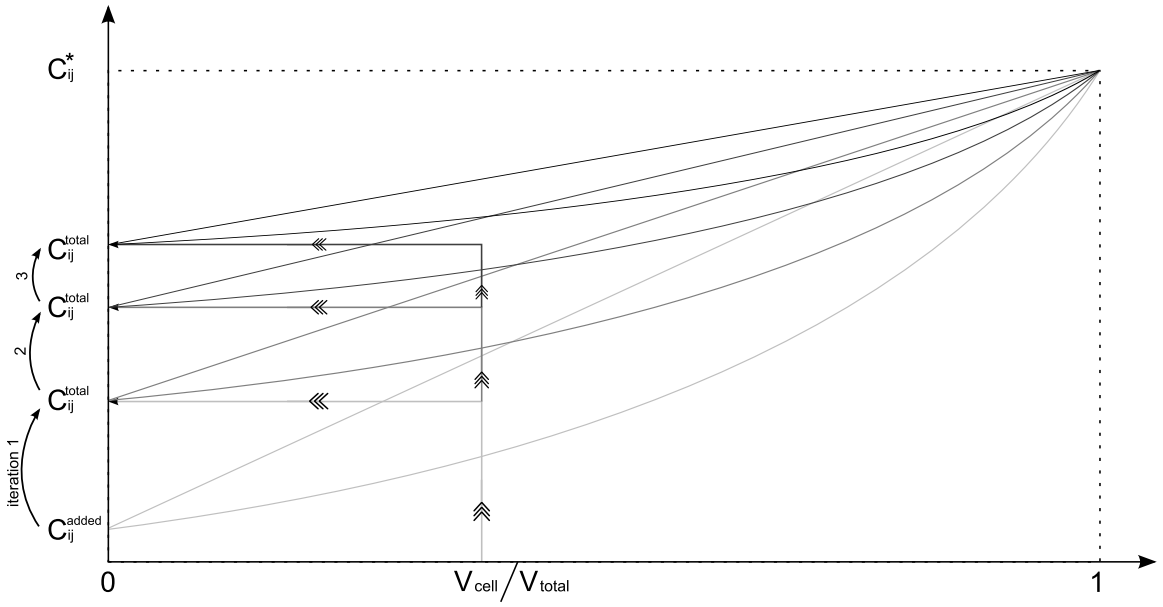

Figure 4.24: Schematic representation of the iterative process where the result of the next iteration is the homogenized property of the unit cell from the previous iteration for the case $\|\mathbb{C}^C\| > \|\mathbb{C}^{added}\|$. Continuous lines are the Voigt and Reuss bounds

4.4.2 Convergence proof

Since Voigt and Reuss bounds, depicted as continuous lines in Figure 4.24, are absolute bounds for both analytical homogenization and numerical alike, any homogenization result must lie within these bounds. Clearly, the closer the results of each iteration to the 'target' value, the faster and the easier the convergence. It follows that most unfavorable (conservative) situation is when the iteration results stay always on one of the bounds. Thus, to prove that these iterations converge, we need to show that (i) iterations, resulting in values on Voigt bound, and (ii) iterations, resulting in values on Reuss bound, both converge. Finally it is necessary to show that both (i) and (ii) converge to exactly the

same result. Let's start with the (i) - the Voigt bound. The first iteration is given by

$$\mathbb{C}_1 = v^{\mathrm{C}}\mathbb{C}^{\mathrm{C}} + v\mathbb{C}_0^{\mathrm{E}} \tag{4.13}$$

where the zero index denotes the initial guess for the equivalent phase, and $0 < v < 1$ is the volume fraction, defined as the ratio between the volume of the phase and the total volume of the sample. Consequently,

$$v^{\mathrm{C}} + v = 1 \tag{4.14}$$

Volume fractions of the phases do not change during the iterations. The k-th iteration is then

$$\mathbb{C}_k = v^{\mathrm{C}}\mathbb{C}^{\mathrm{C}} + v\mathbb{C}_{k-1} \tag{4.15}$$

By substitution of the $k-1$ first iterations into the k-th iteration, (4.15) can be written as

$$\mathbb{C}_k = v^{\mathrm{C}}\mathbb{C}^{\mathrm{C}} \sum_{n=0}^{k-1} v^n + v^k\mathbb{C}_0 \tag{4.16}$$

where an upper index denotes power. To complete the proof we find $\mathbb{C}_\infty$:

$$\lim_{k\to\infty} \mathbb{C}_k = v^{\mathrm{C}}\mathbb{C}^{\mathrm{C}} \lim_{k\to\infty} \left(\sum_{n=0}^{k-1} v^n \right) + \mathbb{C}_0 \lim_{k\to\infty} v^k \tag{4.17}$$

However, since $\forall v \in [0,1]$, $\lim\limits_{x\to\infty} v^x = 0$ and $\lim\limits_{x\to\infty} \left(\sum\limits_{n=0}^{x} v^n \right) = \frac{1}{1-v}$, equation (4.17) simplifies to

$$\lim_{k\to\infty} \mathbb{C}_k = \frac{v^{\mathrm{C}}\mathbb{C}^{\mathrm{C}}}{1-v} \tag{4.18}$$

Recalling that $1 - v = v^{\mathrm{C}}$, we complete the first part of the proof:

$$\lim_{k\to\infty} \mathbb{C}_k = \mathbb{C}^{\mathrm{C}} \tag{4.19}$$

A proof for the (ii) - the Reuss bound, is identical, if one uses compliance instead of stiffness. Since

$$\mathbb{C}^{-1} \equiv \mathbb{S} \tag{4.20}$$

the Reuss bound for the first iteration can be written as

$$\mathbb{S}_1 = v^{\mathrm{C}}\mathbb{S}^{\mathrm{C}} + v\mathbb{S}_0 \tag{4.21}$$

and the rest of the proof follows equations (4.15)-(4.18). For this reason, we show only the end result:

$$\lim_{m\to\infty} \mathbb{S}_m = \mathbb{S}^{\mathrm{C}} \tag{4.22}$$

Note that we have made no assumptions regarding the nature of the initial guess. It means the convergence is guaranteed for any guess no matter whether it's isotropic or anisotropic and no matter how 'far' it is from the final value. Note also that there are also no restrictions on the amount of the added wrapping layer.
Since the right hand side (RHS) of both equations (4.19) and (4.22) denote the macroscopic properties of the original composite, we have

$$\lim_{m\to\infty} \mathbb{S}_m = \mathbb{S}^{\mathrm{C}} \equiv \left(\mathbb{C}^{\mathrm{C}}\right)^{-1} = \left(\lim_{k\to\infty} \mathbb{C}_k\right)^{-1} \tag{4.23}$$

which identically finalizes the proof.
In other words, the iterative embedded cell method guaranties convergence to the macroscopic value (within the convergence tolerance used) regardless of the boundary conditions, thickness of the surrounding layer and the initial guess.

4.4.3 Convergence speed

Convergence is achieved when the absolute difference of the results in two consecutive iterations becomes smaller than some small number ϵ, which is called the convergence tolerance. In our case we can express this condition as

$$\|\mathbb{C}_k - \mathbb{C}_{k-1}\| \leq \epsilon \tag{4.24}$$

Substituting (4.16) with appropriate indices into the LHS of the above condition we obtain

$$\left\| \left(v^{\mathrm{C}}\mathbb{C}^{\mathrm{C}} \sum_{n=0}^{k-1} v^n + v^k \mathbb{C}_0 \right) - \left(v^{\mathrm{C}}\mathbb{C}^{\mathrm{C}} \sum_{n=0}^{k-1} v^n + v^k \mathbb{C}_0 \right) \right\| = \|v^{\mathrm{C}}\mathbb{C}^{\mathrm{C}} v^{k-1} + \mathbb{C}_0 v^{k-1} v - 1\| \leq \epsilon \tag{4.25}$$

Using (4.14), inequality (4.25) finally transforms to

$$v^{\mathrm{C}} v^{k-1} + \|\mathbb{C}^{\mathrm{C}} - \mathbb{C}_0\| \leq \epsilon \tag{4.26}$$

Clearly, the better the initial guess, the faster the convergence. In case the initial guess is not that good, the only way to achieve the convergence is to make the v^{k-1} sufficiently small. However the amount of iterations, k, will be different for different values of the wrapping layer volume fraction v.
As already mentioned, the composite response always lies between the corresponding

Voigt and Reuss bounds. Thus it is advisable to choose an initial guess also between these bounds. The difference will be then

$$\|\mathbb{C}^{\mathrm{C}} - \mathbb{C}_0\| \leq \|\mathbb{C}_V - \mathbb{C}_R\| \tag{4.27}$$

And if one will choose the average of the two bounds,

$$\mathbb{C}_0 = \frac{1}{2}\left(\mathbb{C}_V + \mathbb{C}_R\right) \tag{4.28}$$

the difference will be halved

$$\|\mathbb{C}^{\mathrm{C}} - \mathbb{C}_0\| \leq \frac{1}{2}\|\mathbb{C}_V - \mathbb{C}_R\| \tag{4.29}$$

Solving now inequality (4.26) for k, it is possible to estimate the upper bound of the required iterations number:

$$k \leq \frac{\ln \epsilon - \ln v^{\mathrm{C}}\|\mathbb{C}_V - \mathbb{C}_R\|/2}{\ln v} + 1 \tag{4.30}$$

Figure 4.25 depicts the convergence curves of the 3D cross model, shown in Figure 4.6, for different values of the wrapping layer thickness. The inclination of the convergence curves corresponds directly to the rate of convergence. Although it will be shown in the next

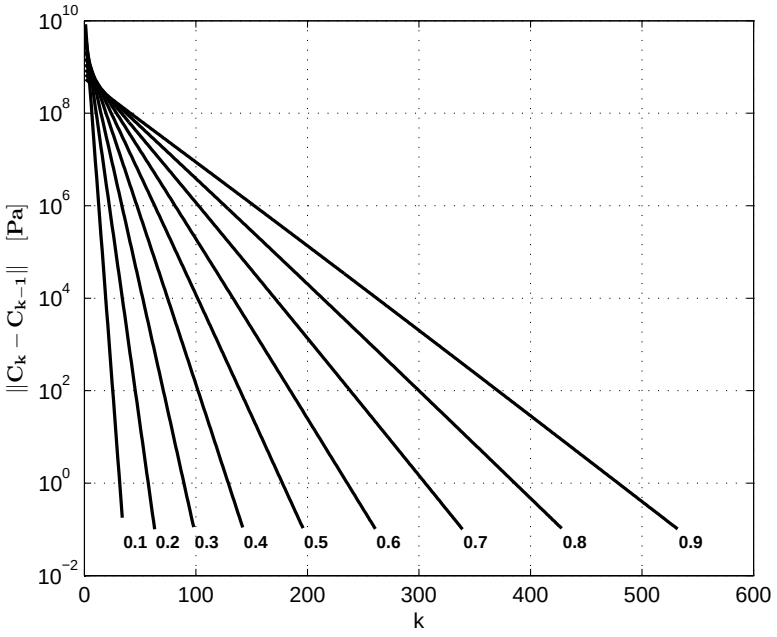

Figure 4.25: Convergence rates for different thickness of the wrapping layer (copper $^{7}/_{27}$, alumina $^{20}/_{27}$)

subsection that the above proof is slightly flawed, the agreement between the estimate given by equation (4.30) and the actual number of iterations with convergence tolerance of 0.1 Pa is remarkable, Figure 4.26. It must be noted however that with an increase in the materials' "contrast", the accuracy of the approximation may decrease.

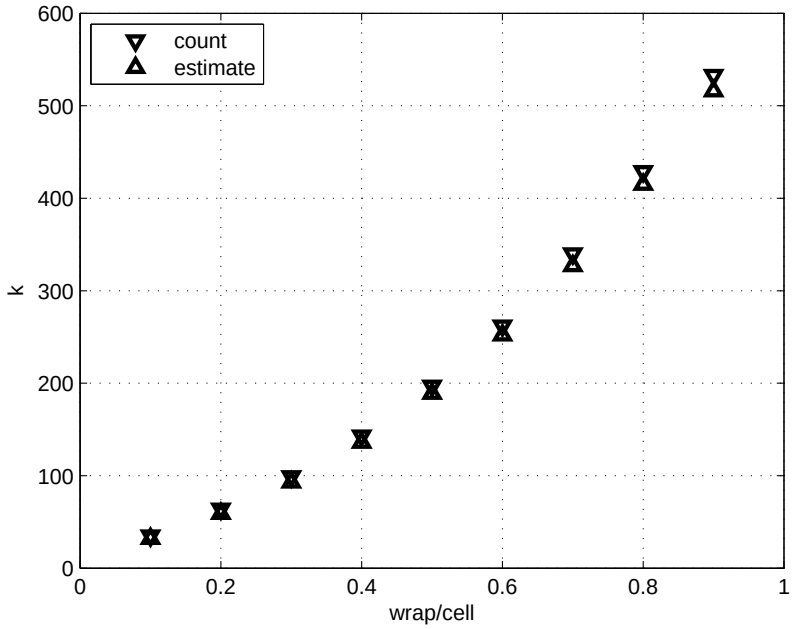

Figure 4.26: Total number of iterations till absolute convergence of $\delta = 0.1\,\mathrm{Pa}$

Remarks:

- The original procedure, as described for example in [59], contains two subparts - 1) the iterative determination of the properties of the effective medium and after the iterations converge 2) determination of the embedded cell properties. However, when the iterations converge, the properties of the effective medium, of the embedded cell and of the overall composite are all equal to each other (up to the convergence tolerance). Thus the latter subpart is not needed.

- Some works state a few optimistic estimates of the amount of iterations needed: 4-5 iterations [60, 62], 5-10 iterations [57]. There appear to be no details of the convergence tolerance used in either of the cited works but in view of the above analysis it is important to point out that there is no 'rule of thumb' here. The amount of iterations can be much higher than what is stated depending on the layer thickness, initial guess and the convergence tolerance.

4.4.4 Interface Affected Zone hypothesis

A single contradicting example should suffice to disprove a theory. In this case, two different unit cells, isotropic spherical composite, Figure 4.27a, and an interpenetrating 3-D cross, Figure 4.27b, both show that something was overlooked in the above convergence proof. Both models show wrapping layer thickness - dependent and boundary conditions

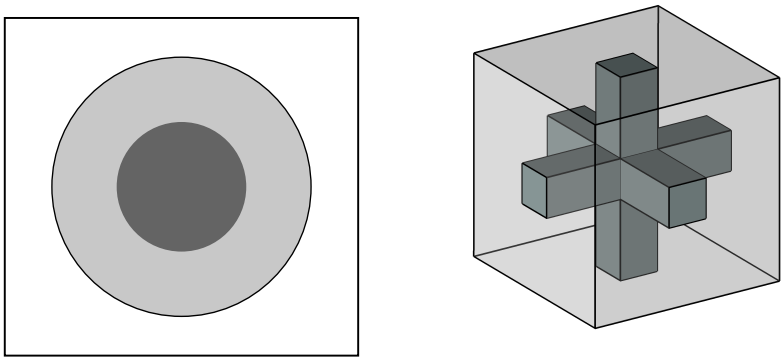

(a) spherical composite model **(b)** 3D cross

Figure 4.27: Test models

- dependent results Figure 4.28. Moreover, for some sizes the stiffness hierarchy is lost, i.e $\mathbb{C}_{KUBC} < \mathbb{C}_{SUBC}$

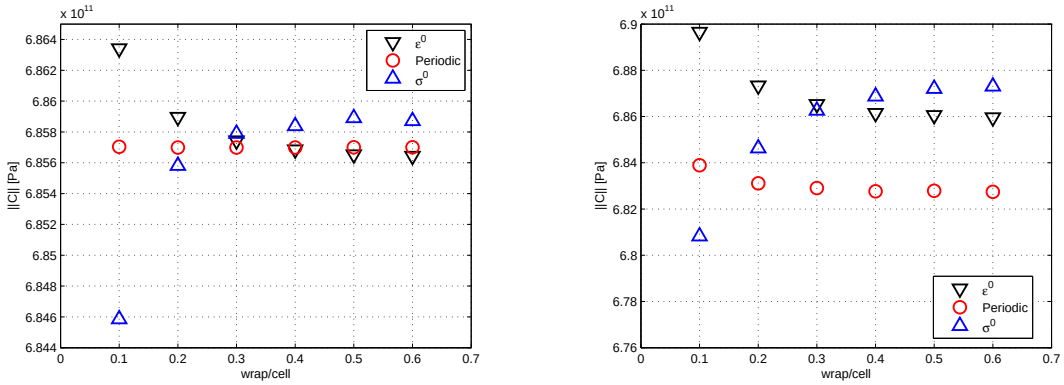

(a) spherical composite **(b)** 3D cross

Figure 4.28: Boundary conditions and wrapping layer thickness influence; $\boldsymbol{\varepsilon}^0$ denotes displacement BC, $\boldsymbol{\sigma}^0$ denotes traction BC

4.4.4.1 The interface influence

A critical look into the embedded-cell model reveals only one feature that is present in the model and does not exist in the reality — an artificial interface between the unit cell and

the effective medium. The interfaces inside the unit cell should not make any difference, since all the existing interfaces and their effects (if any) are already accounted for, by the use of the Voigt and Reuss bounds. The 'everything inside' was the main reason to use the absolute bounds. However, by direct coupling of the micro and macro worlds in the same model an additional explicit interface is created between the constituent phases and the effective medium Figure 4.29. This interface does not exist in the reality and it is not accounted for in the above proof.

Let's now imagine an infinite bi-material composite sample with a planar interface be-

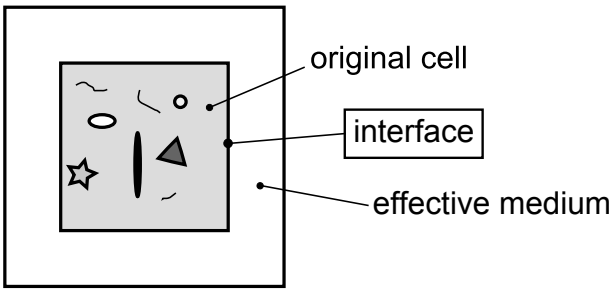

Figure 4.29: An interface between the unit cell and the effective medium

tween homogeneous isotropic phases Figure 4.30 with an applied load, say tensile. Since the constituents are homogeneous, a disturbance to the internal stress, strain and displacements fields can occur in the vicinity of the interface only. The influence of the interface on the internal fields must vanish at some normal distance d_i, where the index corresponds to the considered phase. Let's now make imaginary cuts on both sides of the interface at these distances and consider the region between the cuts as a third material - an 'interphase'.

Let's now consider again the iterative procedure and its proof. The first iteration must

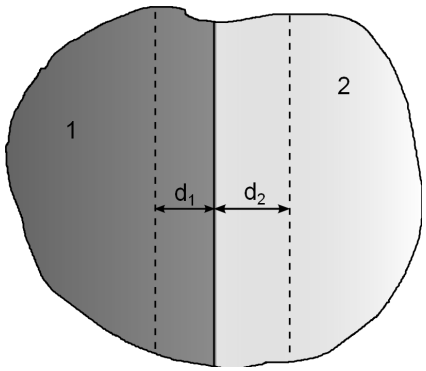

Figure 4.30: An infinite bi-material composite with a planar interface

be accordingly rewritten:

$$\mathbb{C}_1 = (v^{\mathrm{C}} - v^{\mathrm{IC}})\mathbb{C}^{\mathrm{C}} + (v^{\mathrm{E}} - v^{\mathrm{IE}})\mathbb{C}_0^{\mathrm{E}} + (v^{\mathrm{IC}} + v^{\mathrm{IE}})\mathbb{C}_0^{\mathrm{I}} \tag{4.31}$$

where the zero index denotes the initial guess for the effective medium, denoted with 'E', 'C' denotes quantities of the original unit cell and 'I' - the interphase material, 'IE' and 'IC' denote the partial effective medium and cell volumes occupied by the 'interphase'. Note that since the interphase partially consists of the effective medium, its properties will likewise change.
The k-th iteration is then

$$\mathbb{C}_k = (v^{\mathrm{C}} - v^{\mathrm{IC}})\mathbb{C}^{\mathrm{C}} + (v^{\mathrm{E}} - v^{\mathrm{IE}})\mathbb{C}^{\mathrm{E}}_{k-1} + v^{\mathrm{I}}\mathbb{C}^{\mathrm{I}}_{k-1} \tag{4.32}$$

where $v^{\mathrm{I}} = v^{\mathrm{IC}} + v^{\mathrm{IE}}$. By substitution of the $k-1$ first iterations into the k-th iteration, (4.32) can be written as

$$\mathbb{C}_k = (v^{\mathrm{C}} - v^{\mathrm{IC}})\mathbb{C}^{\mathrm{C}} \sum_{n=0}^{k-1} (v^{\mathrm{E}} - v^{\mathrm{IE}})^n + (v^{\mathrm{E}} - v^{\mathrm{IE}})^k \mathbb{C}^{\mathrm{E}}_0 + v^{\mathrm{I}} \sum_{m=0}^{k-1} \mathbb{C}^{\mathrm{I}}_m (v^{\mathrm{E}} - v^{\mathrm{IE}})^m \tag{4.33}$$

Finally, we find the limit $\mathbb{C}_\infty$:

$$\begin{aligned}\lim_{k\to\infty} \mathbb{C}_k = (v^{\mathrm{C}} - v^{\mathrm{IC}})\mathbb{C}^{\mathrm{C}} \lim_{k\to\infty} \left(\sum_{n=0}^{k-1} (v^{\mathrm{E}} - v^{\mathrm{IE}})^n \right) + \mathbb{C}^{\mathrm{E}}_0 \lim_{k\to\infty} (v^{\mathrm{E}} - v^{\mathrm{IE}})^k \\ + v^{\mathrm{I}} \lim_{k\to\infty} \left(\sum_{m=0}^{k-1} \mathbb{C}^{\mathrm{I}}_m (v^{\mathrm{E}} - v^{\mathrm{IE}})^m \right)\end{aligned} \tag{4.34}$$

The first term converges to

$$(v^{\mathrm{C}} - v^{\mathrm{IC}})\mathbb{C}^{\mathrm{C}} \lim_{k\to\infty} \left(\sum_{n=0}^{k-1} (v^{\mathrm{E}} - v^{\mathrm{IE}})^n \right) = \frac{(v^{\mathrm{C}} - v^{\mathrm{IC}})\mathbb{C}^{\mathrm{C}}}{1 - (v^{\mathrm{E}} - v^{\mathrm{IE}})} = \frac{(v^{\mathrm{C}} - v^{\mathrm{IC}})\mathbb{C}^{\mathrm{C}}}{v^{\mathrm{C}} + v^{\mathrm{IE}}} \tag{4.35}$$

The second term vanishes

$$\mathbb{C}^{\mathrm{E}}_0 \lim_{k\to\infty} (v^{\mathrm{E}} - v^{\mathrm{IE}})^k = 0 \tag{4.36}$$

and since $(v^{\mathrm{E}} - v^{\mathrm{IE}})^m$ tends to zero, the last term is finite as well. With the definition

$$v^{\mathrm{I}} \lim_{k\to\infty} \left(\sum_{m=0}^{k-1} \mathbb{C}^{\mathrm{I}}_m (v^{\mathrm{E}} - v^{\mathrm{IE}})^m \right) = \mathbb{C}^{\mathrm{I}}_\infty \tag{4.37}$$

and the results from (4.35) and (4.36), $\mathbb{C}_\infty$ is given by

$$\mathbb{C}_\infty = \frac{v^{\mathrm{C}} - v^{\mathrm{IC}}}{v^{\mathrm{C}} + v^{\mathrm{IE}}} \mathbb{C}^{\mathrm{C}} + v^{\mathrm{I}} \mathbb{C}^{\mathrm{I}}_\infty \tag{4.38}$$

The value of the second term of (4.38) depends on the total volume and provides an explanation for the observed dependence of the results on the wrapping layer thickness. The expression for the compliance is similar:

$$\mathbb{S}_\infty = \frac{v^{\mathrm{C}} - v^{\mathrm{IC}}}{v^{\mathrm{C}} + v^{\mathrm{IE}}}\mathbb{S}^{\mathrm{C}} + v^{\mathrm{I}}\mathbb{S}^{\mathrm{I}}_\infty \tag{4.39}$$

Note that although the iterations still converge, (4.23) does not hold anymore, i.e

$$\mathbb{S}_\infty \neq \mathbb{C}_\infty \tag{4.40}$$

Consequently, interface affected zone hypothesis provides also an explanation to the dependence of the results on the applied boundary condition. Finally, since the coefficient of the first term in both equations (4.38) and (4.39) is always smaller than 1, one can expect $\mathbb{C}_\infty < \mathbb{C}^{\mathrm{C}}$ and $\mathbb{S}_\infty < \mathbb{S}^{\mathrm{C}}$, resulting in a reversed stiffness hierarchy in some cases.

4.4.4.2 The influence of the mesh size

The value of the first term coefficient depends on the ratio $\frac{v^{\mathrm{IC}}}{v^{\mathrm{C}}}$. For a cubic unit cell with edge length a and total (including wrapping layer) edge b, its volume fraction is given by

$$v^{\mathrm{C}} = \frac{a^3}{b^3} \tag{4.41}$$

whereas the volume fraction of the interface affected zone is given by

$$v^{\mathrm{IC}} = \frac{a^3 - (a - d_c)^3}{b^3} \tag{4.42}$$

where d_c is the depth of the interface affected zone.
Their ratio is then

$$\frac{v^{\mathrm{IC}}}{v^{\mathrm{C}}} = 3\frac{d}{a} + 3\left(\frac{d}{a}\right)^2 - \left(\frac{d}{a}\right)^3 \tag{4.43}$$

While the real depth of the IAZ is not known, it is a function of the materials contrast. For the embedded cell model, this contrast is limited by the difference between the true effective cell stiffness and the approximated one. However, no matter how small this contrast and consequently the depth of the IAZ is, in numerical environment it can not be smaller than the size of the elements adjacent to the interface. In other words, the influence of the interface propagates to the depth of at least one element. Results, shown in Figure 4.31a correspond to a very coarse mesh — only six elements per unit cell edge. Refining the mesh to only 12 elements per edge results already in a significant improvement, Figure 4.31b.

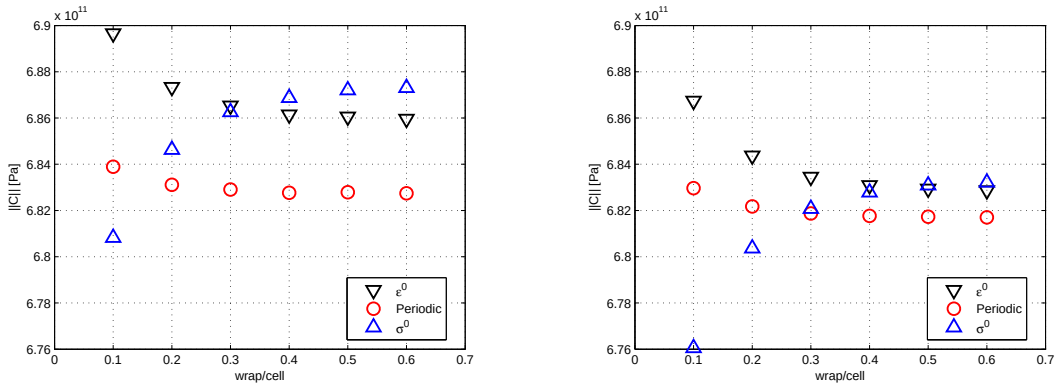

(a) 6 elements per cell edge **(b)** 12 elements per cell edge

Figure 4.31: Influence of the mesh size on the homogenization results

4.4.5 Method summary

The recently developed iterative self-consistent embedded cell method for the determination of the effective properties of composite materials [56–58], can be particularly appealing to the engineering community since it can be readily implemented in any existent commercial FE code without the need of programming new elements or subroutines.
In the previous subsections this method was shown to be unconditionally stable, however due to the direct coupling of the micro and macro worlds within the same model, the resulting artificial interface drives the properties off of their target values. The most serious issue arising from this interface is the broken stiffness hierarchy with respect to various boundary conditions. It shall be noted, however, that the overall negative effects are relatively small even for a very coarse mesh - less than 1% worse difference for both used models. This is due to the fact that the assumed interface stiffness is tightly bounded by the true effective cell stiffness and the approximated one.
The upper bound of the amount of iterations till convergence that was derived without the influence of the artificial interface, can not be easily adjusted and can be considered as a rough estimate only.
Despite the discovered issues, the iterative method can be considered as a reliable numerical homogenization procedure, which is equally well suited for synthetic unit cell models and the 3D images of a real microstructure.

Chapter 5

Summary

The development of homogenization models and solutions, either analytic or numerical, is an extremely difficult task. It was mentioned in the introduction that it is one of the nature's survival mechanisms. This mechanism, averaging, smoothes local variations and reduces the influence of single defects. Its mathematical counterpart exhibits exactly the same property - the influence of local variations or single defects vanishes due to the integral nature of the averaging equations. As an illustration, one can consider the Alumina-Copper composite with almost 80% difference in bulk moduli, which reduces to about 9% between the Voigt and Reuss bounds at their widest difference!
Unfortunately, the single defects can be not only structural, but also wrong assumptions, incorrect boundary conditions or bugs in a source code. However, due to the said nature of equations, the result has a good chance to fall within the Voigt-Reuss bounds and as long as it is there - there might be no indication for a mistake. The difficulty of the homogenization stems not from the involved mathematical concepts, but rather from the little, to at times, no difference between something correct and something that just happens to look plausible.
This difficulty leads to a confusion between the concept of bounds and the concept of boundaries of a surface in a multidimensional space. Till now the Hashin-Shtrikman expressions were regarded as bounds for the isotropic composites. Consequently, any expression, whose result falls within these 'bounds' is considered as a legitimate model for such composites. However, the properties of any composite are multivariate functions (hypersurfaces) in which the volume fractions of the phases are not the only variables. Consequently, there can be no single model that can fit all, even just all the isotropic, composites with volume fraction being the only variable.
Using the concept of surface boundaries, supported by the works on the higher-order bounds, one arrives at a general expression for the macroscopic behavior of the isotropic composites as a function of the morphological descriptors. It seems that the main chal-

lenges for the analytical homogenization field can be formulated as

- to determine the minimum number of independent morphological variables for each material constant,
- to find the exact expressions of the hypersurfaces,
- to find an inexpensive way to extract the morphological values of the morphological variables from a given microstructure

Using a few simple homogenization concepts, it has been possible to derive a system of equations, describing the macroscopic behavior of heterogeneous materials as a function of a single parameter. This parameter can be linked to the structural damping phenomenon and thus can be determined experimentally. This system of equations possesses a simple solution in the isotropic case.

The challenge of the numerical homogenization, though, does not differ from any other numerical treatment - assurance of the validity of the results. Here, the analytical consideration of the convergence of one of the existing methods, brings in the much needed confidence in using it. The simplicity of the iterative homogenization method, together with the added confidence in its results makes it a very strong tool.

List of Figures

List of Tables

Bibliography

[1] D. Raabe, P. Romano, C. Sachs, H. Fabritius, A. Al-Sawalmih, S.-B. Yi, G. Servos, and H. Hartwig, "Microstructure and crystallographic texture of the chitin-protein network in the biological composite material of the exoskeleton of the lobster Homarus americanus," *Materials Science and Engineering: A*, vol. 421, no. 1-2, pp. 143 – 153, 2006.

[2] A. Matthiessen, "Ueber die elektrische Leitungsfaehigkeit der Metalle," *Annalen der Physik*, vol. 103, pp. 428–434, 1858.

[3] C. Maxwell, J., *A Treatise on Electricity and Magnetism*, vol. 1. MACMILLAN & Co, 1873.

[4] K. Lichtenecker, "Zur Widerstandsberechnung mischkristallfreier Legierungen," *Physikalische Zeitschrift*, vol. 10, pp. 1005–1008, 1909.

[5] G. S. son Frey, "Ueber die elektrische Leitfaehigkeit binaerer Aggregate," *Zeitschrift fuer Elektrochemie und angewandte physikalische Chemie*, vol. 38, no. 5, pp. 260–274, 1932.

[6] K. Lichtenecker, "Der elektrische Leitungswiderstand künstlicher und natürlicher Aggregate.," *Physikalische Zeitschrift*, vol. 8,9, pp. 169–181,193–204, 1924.

[7] L. I. Tuchinskii, "Elastic constants of pseudoalloys with a skeletal structure," *Powder Metallurgy and Metal Ceramics*, vol. 22, no. 7, pp. 588–595, 1983. 10.1007/BF00805660.

[8] L. I. Tuchinskii, "Thermal expansion of composites with a skeletal structure," *Powder Metallurgy and Metal Ceramics*, vol. 22, no. 8, pp. 659–664, 1983.

[9] X.-Q. Feng, Z. Tian, Y.-H. Liu, and S.-W. Yu, "Effective Elastic and Plastic Properties of Interpenetrating Multiphase Composites," *Applied Composite Materials*, vol. 11, no. 1, pp. 33–55, 2004.

[10] J. F. Wang, J. K. Carson, J. Willix, M. F. North, and D. J. Cleland, "A symmetric and interconnected skeleton structural (SISS) model for predicting thermal and electrical conductivity and Young's modulus of porous foams," *Acta Materialia*, vol. 56, no. 18, pp. 5138–5146, 2008.

[11] W. Voigt, "Ueber die Beziehung zwischen den beiden Elastizitaetskonstanten isotroper Koerper," *Wied. Ann.*, vol. 38, pp. 573–587, 1889.

[12] A. Reuss, "Berechnung der Fliessgrenze von Mischkristallen auf Grund der Plastizitätsbedingung für Einkristalle," *Z. Angew. Math. Mech*, vol. 9, pp. 49–58, 1929.

[13] R. Hill, "Elastic properties of reinforced solids: Some theoretical principles," *Journal of the Mechanics and Physics of Solids*, vol. 11, no. 5, pp. 357 – 372, 1963.

[14] Z. Hashin and S. Shtrikman, "On some variational principles in anisotropic and nonhomogeneous elasticity," *Journal of the Mechanics and Physics of Solids*, vol. 10, no. 4, pp. 335 – 342, 1962.

[15] Z. Hashin and S. Shtrikman, "A variational approach to the theory of the elastic behaviour of multiphase materials," *Journal of the Mechanics and Physics of Solids*, vol. 11, no. 2, pp. 127–140, 1963.

[16] J. D. Eshelby, "The elastic field of an ellipsoidal inclusion, and related problems," *Proc. Roy. Soc. A*, vol. 241, pp. 376–396, 1957.

[17] R. Hill, "A self consistent mechanics of composite materials," *Journal of the Mechanics and Physics of Solids*, vol. 13, pp. 213–222, 1965.

[18] T. Mori and K. Tanaka, "Average stress in matrix and average elastic energy of materials with misfitting inclusions," *Acta Metallurgica*, vol. 21, no. 5, pp. 571 – 574, 1973.

[19] D. A. G. Bruggeman, "Berechnung verschiedener physikalischer Konstanten von heterogenen Substanzen. I. Dielektrizitätskonstanten und Leitfähigkeiten der Mischkörper aus isotropen Substanzen," *Annalen der Physik*, vol. 416, no. 8, pp. 636–679, 1935.

[20] D. A. G. Bruggeman, "Berechnung verschiedener physikalischer Konstanten von heterogenen Substanzen. II. Dielektrizitätskonstanten und Leitfähigkeiten von Vielkristallen der nichtregulären Systeme," *Annalen der Physik*, vol. 417, no. 7, pp. 645–672, 1936.

[21] D. A. G. Bruggeman, "Berechnung verschiedener physikalischer Konstanten von heterogenen Substanzen. III. Die elastischen Konstanten der quasiisotropen Mischkörper aus isotropen Substanzen," *Annalen der Physik*, vol. 421, no. 2, pp. 160–178, 1937.

[22] M. Beran and J. Molyneux, "Use of classical variational principles to determine bounds for the effective bulk modulus in heterogeneous media," *Q. Appl. Math.*, vol. 24, pp. 107–118, 1965.

[23] J. J. McCoy, "On the displacement field in an elastic medium with random variations of material properties," in *Recent Advances in Engineering Sciences 5*, pp. 235–254, New York: Gordon and Breach, 1970.

[24] G. Milton, "Bounds on the elastic and transport properties of two-component composites," *Journal of the Mechanics and Physics of Solids*, vol. 30, no. 3, pp. 177 – 191, 1982.

[25] F. Lado and S. Torquato, "Effective properties of two-phase disordered composite Media. I. Simplification of bounds on the conductivity and bulk modulus of dispersions of impenetrable spheres," *Phys. Rev. B*, vol. 33, pp. 3370–3378, Mar 1986.

[26] L. V. Gibiansky and S. Torquato, "Phase-interchange relations for the elastic moduli of two-phase composites," *International Journal of Engineering Science*, vol. 34, no. 7, pp. 739 – 760, 1996.

[27] T. I. Zohdi and P. Wriggers, *Introduction to Computational Micromechanics*. Lecture Notes in Applied and Computational Mechanics, New York: Springer, 2005.

[28] C. Huet, "Application of variational concepts to size effects in elastic heterogeneous bodies," *Journal of the Mechanics and Physics of Solids*, vol. 38, no. 6, pp. 813–841, 1990.

[29] S. Hazanov and C. Huet, "Order relationships for boundary conditions effect in heterogeneous bodies smaller than the representative volume," *Journal of the Mechanics and Physics of Solids*, vol. 42, no. 12, pp. 1995–2011, 1994.

[30] C. Dietrich, *Mechanisches Verhalten von Zweiphasengefügen: Numerische und experimentelle Untersuchungen zum Einfluß der Gefügegeometrie*, vol. 128 of *VDI-Fortschrittsberichte*. Düsseldorf: Vor-Verlag, Germany, 1993.

[31] V. Kouznetsova, *Computational homogenization for the multi-scale analysis of multi-phase materials*. PhD thesis, Eindhoven University of Technology, 2002.

[32] Y. C. Fung, *A First Course In Continuum Mechanics*. Englewood, NJ: Prentice-Hall, 1969.

[33] "deformation." http://www.merriam-webster.com/dictionary/deformation, 2010. Retrieved July 11, 2010.

[34] T. Belytschko, W. K. Liu, and B. Moran, *Nonlinear Finite Elements for Continua and Structures*. John Wiley & Sons Ltd, 2000.

[35] D. Gross and T. Seelig, *Fracture Mechanics: With an Introduction to Micromechanics*. Mechanical Engineering Series, Springer-Verlag, 2006.

[36] S. Torquato and F. Lado, "Effective properties of two-phase disordered composite media: 2. Evaluation of bounds on the conductivity and bulk modulus of dispersions of impenetrable spheres," *Phys. Rev. B*, vol. 33, pp. 6428–6435, May 1986.

[37] S. Torquato, "Morphology and effective properties of disordered heterogeneous media," *International Journal of Solids and Structures*, vol. 35, no. 19, pp. 2385 – 2406, 1998.

[38] L. Walpole, "On bounds for the overall elastic moduli of inhomogeneous systems–1," *Journal of the Mechanics and Physics of Solids*, vol. 14, no. 3, pp. 151 – 162, 1966.

[39] A. Helte, "Fourth-Order Bounds on the Effective Bulk and Shear Moduli of Random Dispersions of Penetrable Spheres," *Proceedings: Mathematical and Physical Sciences*, vol. 450, pp. 651–665, Sept. 1995.

[40] G. W. Milton and N. Phan-Thien, "New Bounds on Effective Elastic Moduli of Two-Component Materials," *Proceedings of the Royal Society of London. A. Mathematical and Physical Sciences*, vol. 380, no. 1779, pp. 305–331, 1982.

[41] K. Lichtenecker, "Über die elektrische Leitfähigkeit und andere Körpereigenschaften desselben Typus bei binären Aggregaten.," *Zeitschrift fuer Elektrochemie und angewandte physikalische Chemie*, vol. 40, pp. 11–14, 1934.

[42] Z. Poniznik, V. Salit, M. Basista, and D. Gross, "Effective elastic properties of interpenetrating phase composites," *Computational Materials Science*, vol. 44, no. 2, pp. 813–820, 2008.

[43] J. Mishnaevsky, L., *Numerical Experiments in the Mesomechanics of Materials*. TU Darmstadt, 2005.

[44] N. Maron and O. Maron, "Criteria for mixing rules application for inhomogeneous astrophysical grains," *Monthly Notices of the Royal Astronomical Society*, vol. 391, no. 2, pp. 738–764, 2008.

[45] W. Research, *Mathematica*. Wolfram Research, Inc., version 7.0 ed., 2008.

[46] S. Newmark, "Concept of Complex Stiffness Applied to Problems of Oscillations with Viscous and Hysteretic Damping," *AERONAUTICAL RESEARCH COUNCIL REPORTS AND MEMORANDA*, vol. 2369, 1957.

[47] M. Gottlieb, "Effektive Eigenschaften von Füllstoff verstärkten Elastomeren," Master's thesis, TU Darmstadt, 2006.

[48] H. Prielipp, M. Knechtel, N. Claussen, S. Streiffer, H. Müllejans, M. Rühle, and J. Rödel, "Strength and Fracture-Toughness of Aluminum Alumina Composites with Interpenetrating Networks, , 197 (1995) 19-30," *Materials Science and Engineering: A*, vol. 197, pp. 19–30, 1995.

[49] M. Hoffman, S. Skirl, W. Pompe, and J. Rödel, "Thermal residual strains and stresses in Al2O3/Al composites with interpenetrating networks," *Acta Materialia*, vol. 47, no. 2, pp. 565 – 577, 1999.

[50] A. R. Studart, U. T. Gonzenbach, E. Tervoort, and L. J. Gauckler, "Processing Routes to Macroporous Ceramics: A Review," *J. Am. Ceram. Soc.*, vol. 89, pp. 1771–1789, 2006.

[51] G. R. Davis and J. C. Elliott, "Artefacts in X-ray microtomography of materials," *Materials Science and Technology*, vol. 22, pp. 1011–1018, 2006.

[52] MATLAB, *version 7.5 (R2007b)*. Natick, Massachusetts: The MathWorks Inc., 2007.

[53] ASTM-E1876-99, "Standard Test Method for Dynamic YoungŠs Modulus, Shear Modulus, and PoissonŠs Ratio by Impulse Excitation of Vibration," 2001.

[54] W. E. Lorensen and H. E. Cline, "Marching cubes: A high resolution 3D surface construction algorithm," *SIGGRAPH Comput. Graph.*, vol. 21, pp. 163–169, August 1987.

[55] E. V. Chernyaev, "Marching Cubes 33: Construction of Topologically Correct Isosurfaces," tech. rep., 1995.

[56] C. Dietrich, M. Poech, S. Schmauder, and H. Fischmeister, "Numerische Modellierung des mechanischen Verhaltens von Faserverbundwerkstoffen unter transversaler Belastung," in *Verbundwerkstoffe und Werksloffverbunde*, pp. 611–618, DGM-Informationsgesellschaft mbH, Oberursel, 1993.

[57] D. B. Zahl and S. Schmauder, "Transverse strength of continuous fiber metal matrix composites," *Computational Materials Science*, vol. 3, no. 2, pp. 293–299, 1994.

[58] M. Sautter, *Modellierung des Verformungsverhaltens mehrphasiger Werkstoffe mit der Methode der finiten Elemente.* Dissertation, University of Stutgart, Germany, 1995.

[59] M. Dong and S. Schmauder, "FE modeling of continuous fiber and particle reinforced composites by self-consistent embedded cell models," in *Computational Methods in Micromechanics*, vol. 62, ASME, 1995.

[60] M. Dong and S. Schmauder, "Modeling of metal matrix composites by a self-consistent embedded cell model," *Acta Materialia*, vol. 44, no. 6, pp. 2465–2478, 1996.

[61] E. W. Weisstein, "Frobenius Norm." MathWorld–A Wolfram Web Resource.

[62] S. Schmauder and L. Mishnaevsky, *Micromechanics and Nanosimulation of Metals and Composites: Advanced Methods and Theoretical Concepts.* Springer, 2009.

Bisher sind in dieser Reihe erschienen

Band 1
Zur mikrorissinduzierten Schädigung spröder Materialien
B. Lauterbach, Dissertation 2001, ISBN 3-935868-01-4

Band 2
3D-Simulation der Mikrostrukturentwicklung in Zwei-Phasen-Materialien
R. Müller, Dissertation 2001, ISBN 3-935868-02-2

Band 3
Zur numerischen Simulation von Morphologieänderungen in mikroheterogenen Materialien
S. Kolling, Dissertation 2001, ISBN 3-935868-03-0

Band 4
Theoretische und numerische Untersuchung von Versagensmechanismen in Metall-Keramik-Verbundwerkstoffen
T. Emmel, Dissertation 2002, ISBN 3-935868-04-9

Band 5
On microcrack dominated problems in dynamics and statics of brittle fracture: a numerical study by boundary element techniques
S. Rafiee, Dissertation 2002, ISBN 3-935868-05-7

Band 6
Kontinuumsmechanik anisotroper Festkörper und Fluide
H. Ehrentraut, Habilitationsschrift 2002, ISBN 3-935868-06-5

Band 7
Plane unsteady inviscid incompressible hydrodynamics of a thin elastic profile
N. Blinkova, Dissertation 2002, ISBN 3-935868-07-3

Band 8
Anmerkungen zur Simulation von entfestigendem Materialverhalten
H. Baaser, Habilitationsschrift 2004, ISBN 3-935868-08-1

Band 9
Orts- und zeitadaptive DAE-Methoden zur Beschreibung elastisch-plastischen Materialverhaltens innerhalb der FEM
S. Eckert, Dissertation 2005, ISBN 3-935868-09-X

Band 10
Simulations of the Flow of the Ross Ice Shelf, Antarctica: Parameter Sensitivity Tests

and Temperature-Dependent Rate Factor
A. Humbert, Dissertation 2005, ISBN 3-935868-10-3

Band 11
A Thermo-mechanical Continuum Theory with Internal Length of Cohesionless Granular Materials
Chung Fang, Dissertation 2006, ISBN 3-935868-11-1

Band 12
Modeling Dry Granular Avalanches past Different Obstructions: Numerical Simulation and Laboratory Analyses
Chiou Min-Ching, Dissertation 2006, ISBN 3-935868-12-X

Band 13
Configurational forces in defect mechanics and in computational methods
R. Müller, Habilitationsschrift 2005, ISBN 3-935868-13-8

Band 14
Hyperelastic dynamics in physical and material space
S. Kolling, Habilitationsschrift 2007, ISBN 978-3-935868-14-3

Band 15
Phenomenological modeling of ferroelectric material behavior
V. Mehling, Dissertation 2007, ISBN 978-3-935868-15-0

Band 16
Ein mischungsbasiertes Materialmodell zum Knochenumbau
R.-R. Kühn, Dissertation 2006, ISBN 978-3-935868-16-7

Band 17
Einige Erweiterungen der Rand-Finite-Elemente-Methode und deren Anwendung auf Randeffekte in ebenen Laminaten
J. Artel, Dissertation 2007, ISBN 978-3-935868-17-4

Band 18
Spannungskonzentrations-Effekte an Verstärkungspflaster-Ecken
H. Wigger, Dissertation 2008, ISBN 978-3-935868-18-1

Band 19
Rotationseffekte in der Kristallplastizität
C. Bröse, Dissertation 2007, ISBN 978-3-935868-19-8

Band 20
Finite-Element-Modelle zur Simulation von Delaminationen dünner Filme auf Substraten
V. D. Pham, Dissertation 2010, ISBN 978-3-935868-20-4

Band 21

Asymptotische Nahfeldanalysen ebener Multi-Materialverbindungsstellen mit der Methode komplexer Potentiale

C. Sator, Dissertation 2010, ISBN 978-3-935868-21-1

Band 22

Modellierung spröder Rissbildung an Spannungskonzentrationen mit der Bruchmechanik finiter Risse

J. Hebel, Dissertation 2010, ISBN 978-3-935868-22-8

The development of the homogenization models and solutions, either analytic or numerical, is a difficult task. Due to the integral nature of equations, the result has a good chance to fall within the theoretical bounds and as long as it is there - there might be no indication for any mistake. The difficulty of the homogenization stems not from the involved mathematical concepts, but rather from the little, to at times, no difference between something correct and something that just happens to look plausible.

In this work it is argued that the Hashin-Shtrikman expressions are not bounds, but rather boundaries of the solution (hyper)surface. It is also shown that the well known Hill condition is not a necessary ingredient for the homogenization. Using a few homogenization concepts, a complete system of equations describing the macroscopic behavior of the heterogeneous materials has been derived. This system possesses a simple solution in the isotropic case.

ISBN 978-3-935868-23-5